Renewable methane production from the catalytic reduction of CO2 using solar light

Martin Kientz

Université de Paris

Ecole Doctorale 388 - Chimie Physique et de Chimie Analytique de Paris Centre

Laboratoire d'Electrochimie Moléculaire

Renewable methane production from the catalytic reduction of CO_2 using solar light

Par **Martin Kientz**

Thèse de Doctorat de Chimie, spécialité Chimie, énergie, nanosciences, surface

Dirigée par **Dr. Julien Bonin**

Présentée et soutenue publiquement le 10 Février 2022

Devant un jury composé de :

Pr. Anne-Cécile Roger	Université de Strasbourg	Rapportrice
Dr. Jérôme Fortage	Université Grenoble-Alpes	Rapporteur
Dr. Anne Dolbecq	Université de Versailles Saint-Quentin-en-Yvelines	Examinatrice
Pr. Jean-Luc Renaud	Université Caen Normandie	Examinateur
Dr. Julien Bonin	Université de Paris	Directeur de thèse
Pr. Marc Robert	Université de Paris	Co-encadrant, invité
Dr. Sylvain Frédéric	GRDF	Membre invité
Dr. Guilhem Caumette	Teréga	Membre invité

“*May it be a light to you in dark places when all other lights go out* “

J.R.R. Tolkien

Acknowledgments

The present thesis was possible by financial support of the MARS consortium composed of: Terega, GRTgaz and GRDF I would like to thank them and especially Guilhem Caumette, Corentin Dussene and Sylvain Frederic for their personal support.

I would like to thank my supervisor Julien Bonin for his everyday support and for trusting me even when nothing made sense. He was always here for giving me oxygen when I couldn't breathe. He was the very first and the last teacher I had during my 8 years studying chemistry I owe him a lot and I couldn't think of a better supervisor.

Thank you to Marc Robert for believing in me from the beginning by sending me to Denmark before giving me the opportunity of doing my thesis in his team and thank you for the scientific supervision.

A special thank you to my two coworkers and friends Marie and Dorian, we helped each other a lot and working with close friends doesn't really seems like working anymore. Thank you for all the βοήθεια and thank you for helping me with my compulsive cleaning every now and then.

I would like to thank Nikos for being so calm and not getting angry whenever a machine was not working and thank you for the bake rolls every time you went back to Greece.

A special thank you for my labmate Bing the sweetest person you can hope to work with. Thank you for all the help and the songs.

I would like to thanks all the phD students and post-doc I had the chance to work with: Etienne, Célia, Justine, Daniela, Ruwen, Julian, Thomas, Tamal, Orestes, Jaya, Aude, Tamires.

Thank you to all the technicians for their help especially Esther and Alexandra. A special thank to tata Sihem for being so helpful and so kind everyday it's a real pleasure working with you.

Thank you to all the researchers I had the chance to work with in and outside the lab.

Finally, I would like to thanks my friends and my family for their support and above all Joséphine for asking me about my work even if you understood half of it.

Table of contents

List of acronyms

9CNA	9-Cynaoanthracene
ACN	Acetonitrile
AQY	Apparent quantum yield
BIH	1,3-dimethyl-2-phenyl-2,3-dihydro-1H-benzo[d]imidazole
BNAH	1-Benzyl-1,4-dihydronicotinamide
C_3N_4	Carbon nitride
CAES	Compressed air energy storage
CAT	Catalyst
CNG	Compressed natural gas
Cs	Catalytic selectivity
CV	Cyclic voltammetry or voltammogram
DMF	Dimethylformamide
EA	Electron acceptor
EXAF	Extended X-Ray Absorption Fine Structure
FE	Faradaic efficiency
Fe-*p*-TMA	chloro iron(III) 5,10,15,20-tetra(4'-N,N,N-trimethylanilinium)porphyrin
GC	Gas chromatography
HER	Hydrogen evolution reaction
IQY	Internal quantum yield
$Ir(ppy)_3$	Tris[2-phenylpyridinato-C2,N]iridium(III)
MOF	Metal organic framework
MS	Mass spectrometry
NHE	Normal hydrogen electrode
PS	Photosensitizer
PSH	Pumped storage hydroelectricity
PV	Photovoltaic
RHE	Reversible hydrogen electrode
$Ru(bpy)_3^{2+}$	Tris(bipyridine)ruthenium(II)
SCE	Saturated calomel electrode
SD	Sacrificial electron donor
SMES	Superconduction magnetic energy storage
TEA	Triethylamine
TEOA	Triethanolamine
TFE	Trifluoroethanol
TOF	Turnover frequency
TON	Turnover number
XANES	X-ray Absorption Near Edge Structure

Résumé

La production de carburant renouvelable est un enjeu majeur de la transition énergétique et la source d'énergie permettant de le faire est un élément primordial. De précédents travaux menés au laboratoire ont conduit à proposer un système chimique comprenant un catalyseur à base de fer et utilisant la lumière du soleil comme source principale d'énergie pour la réduction du dioxyde de carbone en méthane, et les travaux de cette thèse en sont le prolongement. Les différents intermédiaires possibles entre le CO_2 et le méthane ont tout d'abord été étudiés. Le monoxyde de carbone a été identifié comme étant un intermédiaire clé dans des travaux antérieurs. Parmi les autres intermédiaires envisageables, le méthanol et le formaldéhyde sont les deux molécules les plus probables. Nous avons pu montrer que notre système standard était capable de réduire le méthanol en méthane, mais que ce n'était pas le cas pour le formaldéhyde. Ceci ne prouve cependant pas l'existence d'un intermédiaire méthanol mais semble exclure l'intermédiaire formaldéhyde, ajoutant ainsi des éléments de réponse au mécanisme complet de la réaction. Le remplacement d'un des composants du système, le photosensibilisateur, jusqu'alors un complexe d'iridium, a fait l'objet d'une attention particulière. Deux classes de molécules totalement organiques ont été évaluées dans ce but, une coumarine et plusieurs phenoxazines. Pour ces dernières, la variation structurale et donc de propriétés électroniques ont permis de mettre en évidence le fait que le système était limité par la régénération du photosensibilisateur par le donneur d'électron présent en solution et non pas par l'étape d'activation du catalyseur contrairement à ce qui était supposé. En modifiant la cellule photochimique dans laquelle est menée la réaction, un effet inattendu de la présence de dioxygène dans la solution de réaction a été mis en évidence. O_2 influence les performances globales du système et en particulier son absence totale empêche la production de méthane à partir du CO_2. Aussi, son influence sur les différentes molécules présentes en solution a été étudiée. Le photosensibilisateur et le donneur de protons se sont montrés insensibles à la présence de dioxygène. En revanche, le donneur d'électrons est particulièrement sensible à la présence de dioxygène dans nos conditions photochimiques et son oxydation en un bouquet de composés a pu être mis en évidence. Enfin, le catalyseur à base de fer est également sensible à l'oxygène mais aucun mécanisme n'incluant sa présence n'a pu être mis en évidence et en particulier permettant d'expliquer son rôle dans la production de méthane. Nous avons en parallèle développé une cellule dans laquelle il est possible d'associer l'électrochimie et la photochimie afin de nous permettre d'analyser et de mieux comprendre le mécanisme global de la réaction par des mesures *operando*. Cette cellule permet d'effectuer à la fois des mesures de voltamétrie cyclique ou des électrolyses, tout en irradiant la solution et ainsi déclenchant les processus photochimiques impliqués.

Mots clés : dioxyde de carbone, méthane, catalyse moléculaire, photochimie, porphyrines.

Summary

The production of renewable fuel is a major issue in the energy transition and the source of energy to do so is also essential. A chemical system composed of an iron-based catalyst and using sunlight as the main source of energy was previously proposed for the reduction of carbon dioxide to methane, and the work of this thesis is the continuation of it. The various possible intermediates between CO_2 and methane were first studied. Carbon monoxide was the only one identified as a key intermediate in a previous work. Among the other possible intermediates, methanol and formaldehyde are the two most probable molecules. We have shown that our standard system was able to reduce methanol to methane, but it was not the case for formaldehyde. Even if it does not constitute of proof that methanol is indeed a reaction intermediate, it seems to exclude formaldehyde as a possible one. The replacement of one of the components of the system, the photosensitizer, based on an iridium complex, has been also investigated. Two classes of fully organic molecules have been evaluated for this purpose, a coumarin and several phenoxazines. For the latter, the structural variation and therefore of their electronic properties made it possible to highlight the fact that the system was limited by the regeneration of the photosensitizer by the electron donor present in solution and not by the step of activation of the catalyst, contrary to what was supposed. By changing the design of photochemical cell in which the reaction takes place, an unexpected effect of the presence of dioxygen in the reaction has been demonstrated. This influences the overall performances of the system by increasing it and the complete absence of dioxygen does not allow the production of methane from CO_2 photochemically. The effect of O_2 on the different molecules present in solution has been studied. The photosensitizer and proton donor were shown to be insensitive to the presence of molecular oxygen. On the other hand, the electron donor is particularly sensitive to the presence of dioxygen under our photochemical conditions and its oxidation into a bunch of compounds has been demonstrated. Finally, the iron-based catalyst is also sensitive to oxygen, but no mechanism including its presence has been demonstrated and in particular that would allow to explain its role in the production of methane. At the same time, we have developed a cell in which it is possible to combine electrochemistry and photochemistry in order to allow us to analyze and to better understand the global mechanism of the reaction through *operando* measurements. This cell makes it possible to perform both cyclic voltammetry measurements or electrolysis, while irradiating the solution and thus triggering the photochemical processes involved.

Keywords: carbon dioxide, methane, molecular catalysis, photochemistry, porphyrins.

Chapter 1 - Introduction

1.1 General context

Since the beginning of the industrial age in the end of the 19th century, the world energy consumption has been continuously rising to reach today more than 1.3×10^8 GWh per year.[1] The industrial revolution marked an important and radical change regarding the source of energy used. Before 1850, primary energy sources were wood and crop residues which could be considered as biofuels. However, after 1850 both were replaced by oil and coal, two fossil fuels. These fuels have several advantages that explain their massive use since that time such as abundance, availability, storability, easily transportable, and their important calorific power. However, because fossil fuels are hydrocarbon-containing materials, their use causes massive emissions of gases in the atmosphere and particularly carbon dioxide. In the 20th century, other sources of energy have emerged such as natural gas, nuclear or renewable energies like wind, solar or hydraulic. However, these sources also have drawbacks in terms of environmental footprint. First, even if natural gas is a cleaner fuel than oil in the sense that it does not (or very few) reject small particles during its (total) combustion, it is still a fossil fuel that, upon combustion, rejects CO_2 in the atmosphere. Second, regarding nuclear energy, a major advantage compare to fossil fuels is that it does not emit directly CO_2 for generating electricity. However, the extraction of the uranium based fuel, its transport, the construction and demolition of a nuclear power plant are factors contributing to CO_2 emissions and it was estimated that a nuclear power plant generates 66 gCO2e/kWh compare to 443 for natural gas, 10 for wind and 32 for photovoltaic.[2] Due to the very nature of the radioactive material employed, other issues should be emphasized: the radioactive fuel once used need to be treated and sealed in dedicated places to avoid contaminations, those actions once again participating to CO_2 emissions related to the nuclear energy. Regarding other sources of energy, the growth rate of renewable and nuclear is the fastest in the world energy mix among all sources of energy, which could then imply a change in the CO_2 emissions. However, based on projections, in 2040 fossil fuels will still represented 77% of the world energy consumption.[1] It is then crucial to find other sources of sustainable energy to contribute to mitigate climate change.

On Earth, it exists several cycles that allow life to develop, the three mains being water, nitrogen and carbon cycles. Regarding the latter, carbon can be found in various forms on Earth (Figure 1.1). In the atmosphere, it mainly exists in the form of gaseous CO_2, whereas on land, it can be

found in all living organism and in carbon containing minerals. Finally, one of the biggest carbon reservoirs is the oceans, in which an equilibrium exists between gaseous CO_2, bicarbonate and carbonate. However, this cycle has been perturbed by human activity, mainly because of massive CO_2 emissions in the last 150 years, but also by deforestation which prevent CO_2 sequestration by trees, accentuating even more the greenhouse effect. As an example of the impact of deforestation, pre-industrial deforestation alone is estimated to have contributed to 24 ppm of CO_2 increased in the atmosphere.[3]

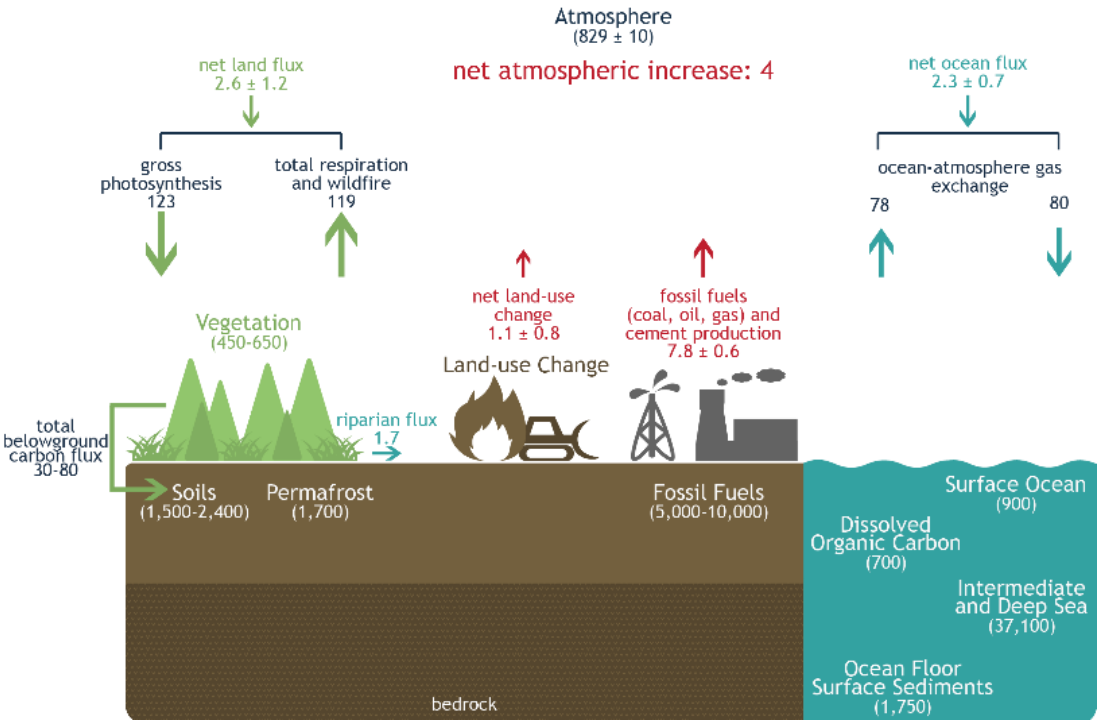

Figure 1.1: Global carbon cycle. Carbon pool numbers (GtC) are denoted in (parentheses), and flux numbers (GtC per year) are associated with arrows.[4]

Since the origin of the Earth, CO_2 concentration in the atmosphere has been fluctuating between periods of high and low concentrations corresponding to the different ice age periods, as demonstrated by the analysis of coral ice core data on more than 800 thousand years (Figure 1.2). On a shorter timescale, seasonal variations can also be observed. Since the last ice age, *ca.* 15000 years ago, Earth is on a rising period regarding CO_2 concentration, following a natural cycle trend. However, since 1800, atmospheric CO_2 has been rising drastically, and especially in the 20th century during which it increased by 45% reaching unprecedented level of 413.78 ppm in October 2021. It is then undeniable that this straight increase is due to human activities and it is our role to lower CO_2 emission and bring back the carbon cycle to a neutral state.[5] This could be achieved by

two major pathways: a radical change in the global energy consumption -even if this falls into the political/social domain which will not be treated here- and another radical change in the production of energy, to make it (more) carbon neutral.

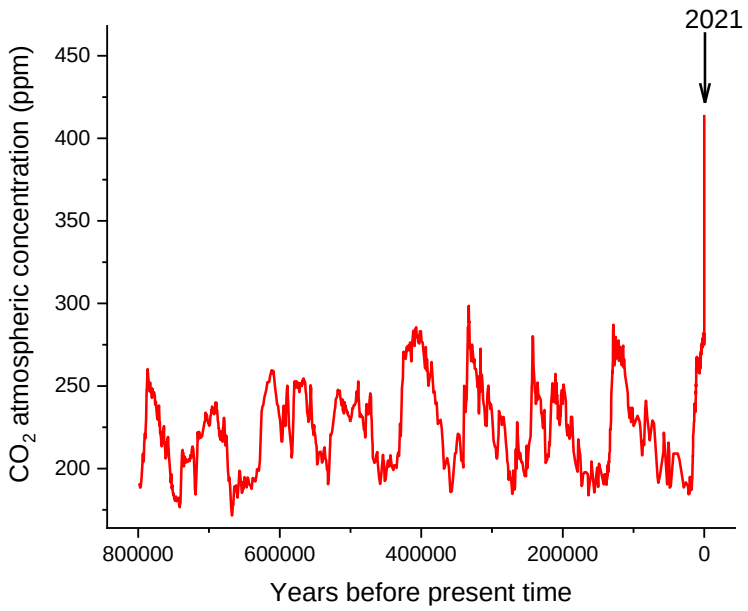

Figure 1.2: Evolution of CO_2 concentration in the atmosphere over the last 800 thousand years[5]

The second objective could be achieved with a circular energy production. Right now, our societies use fossil fuels to produce energy which rejects CO_2 in the atmosphere. In this situation, CO_2 is a waste and is not used or valued afterwards: this is a linear consumption of energy. In a circular production, CO_2 is not treated as a waste but as a feedstock for further energy production. We will focus on this approach in the following sections.

Among the C1 products (*i.e.*, not considering C-C coupling processes) which can be obtained from CO_2 reduction, two are particularly good candidates as renewable fuels. The first one, methanol (CH_3OH), is obtained through a 6 electrons and 6 protons reduction process (Table 1.2) and is currently used in small proportions in petrol for internal combustion engines. Despite a niche in car racing competition, the massive use of pure methanol in common car engine is still not possible due to some limitations such as the formation of acidic products during combustion that could damage the valves and the cylinders of the engine.[6] The second fuel that can be formed from CO_2 is methane (CH_4), which required a total reduction of CO_2 by 8 electrons and concomitant 8 protons transfers (Table 1.2). Methane presents a lot of advantages and its uses are not limited to a fuel for

internal combustion engine even though it can be used as such in the form of compressed natural gas (CNG). First, it is important to emphasize the fact that a classic car engine can run on methane with only a minor modification (addition of a pressure valve) unlike methanol that would require a complete change of the material used to avoid corrosion. Second, if we compare with unleaded gasoline, the combustion of methane is "cleaner" in different aspects. Thanks to its total combustion, methane rejects 20% less CO_2 than gasoline and 80% less nitrogen oxide, but also less carbon monoxide, less sulfur oxides and almost no particles. Methane can also be directly used in gas pipelines to feed both industry and domestic needs for heating and cooking. If we compare the two C1 fuels that can be generated from CO_2 (methanol and methane) the latter has a clear advantage both in terms of calorific value (15.4 kWh kg^{-1} compare to 6.39 kWh kg^{-1} for methanol) and in terms of existing or easily adaptable infrastructures. All in all, methane is a strategic target since the whole chain, from transportation to the final use, is already existing and does not require any extra investment to be operational. However, these considerations only make sense as a sustainable alternative energy if the fuel in question is produced renewably. Today in France, 99.97% of the gas consumption comes from fossil sources (mainly from Norway, Russia and Algeria) leaving a lot of room for renewable sources to emerge.[7]

1.2 Solar energy

Life as we know is possible because millions of years ago, some small organisms started to absorb light, through chlorophyll molecules, and used it to convert water and carbon dioxide into energy, *e.g.* carbohydrates, to grow. This process is called natural photosynthesis and it generates molecular oxygen as a byproduct which is one of the essential molecules for life. Solar energy is the main source of energy on Earth, with a total solar power reaching its surface estimated to four millions exajoules (EJ) per year, with only 5000 EJ which could be harvested if we consider only the continental lands as potential harvesting sites.[8] Thus, it is considered today as the only renewable source of energy able to address the world energy demand in a sustainable way in the future.[8]

Two major pathways exist to use solar light to generate electricity. The first and largely used is through a photovoltaic (PV) device. Since the discovery in 1839 by Alexandre Becquerel that light could induce an electrical current, PV effect has generated numbers of publications and is today the most developed technology to harvest sunlight.[9] The first PV cell developed 45 years ago had an efficiency of about 1%, but in 2021, the most efficient one can reach up to 47.1% (Figure 1.3).[10]

Taking into account the actual growth and improvement of PV cells, the total energy production using this technology should go from 585 TWh in 2018 to 3268 TWh in 2030.[11]

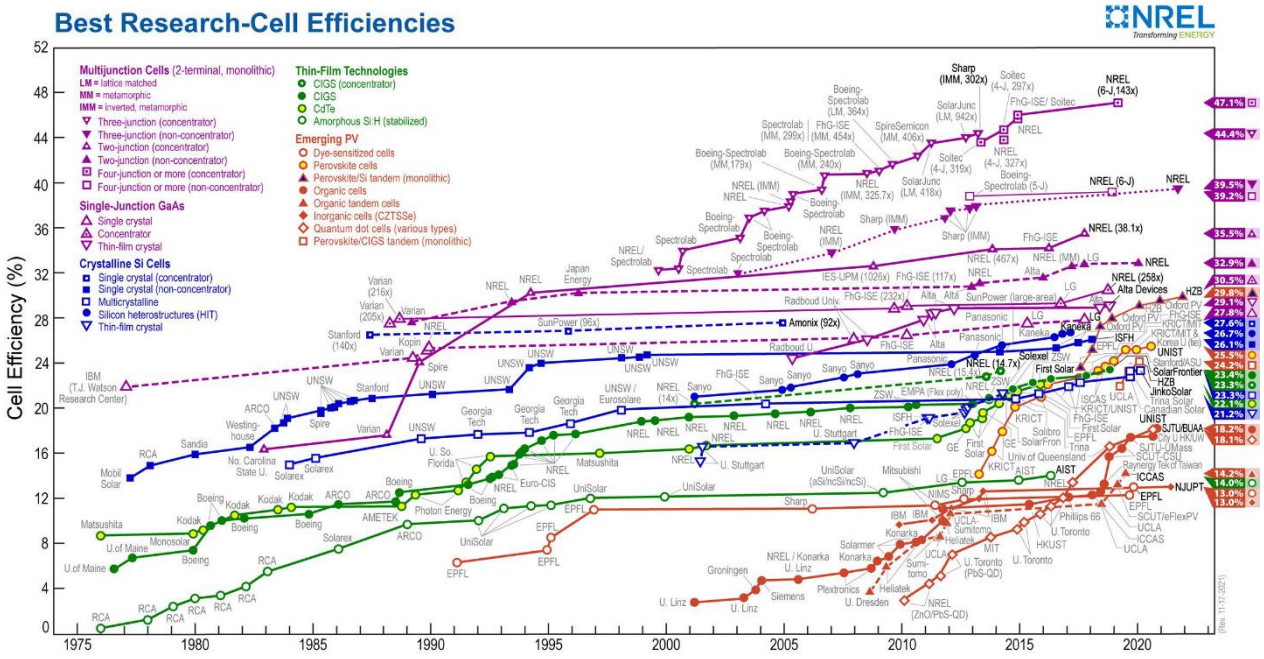

Figure 1.3: Highest conversion efficiencies for research cells for a range of photovoltaic technologies, plotted from 1976 (https://www.nrel.gov/pv/cell-efficiency.html).

The second way to produce energy from sunlight is through a solar thermal system. This technology was first demonstrated in 1869 by Augustin Mouchot, a French physicist, as an alternative heating source to coal.[12] The working principle is based on the thermal energy that can be harvested from sunlight: a mirror, usually circular, concentrates the beam of light on one spot, making the temperature rise rapidly. Even though the principle is the same, solar thermal can be used for producing either thermal or electrical energy (Figure 1.4). In the first case, small devices are used in houses or buildings for house or water heating. In the second case, a bigger facility is needed: hundreds or thousands of mirrors reflects the light into a specific spot, rising the temperature up to 500°C, thus flowing molten salts into a steam turbine which generates electricity. In 2017, solar thermal represented, in the world, a capacity of production of 472 MWth.[13]

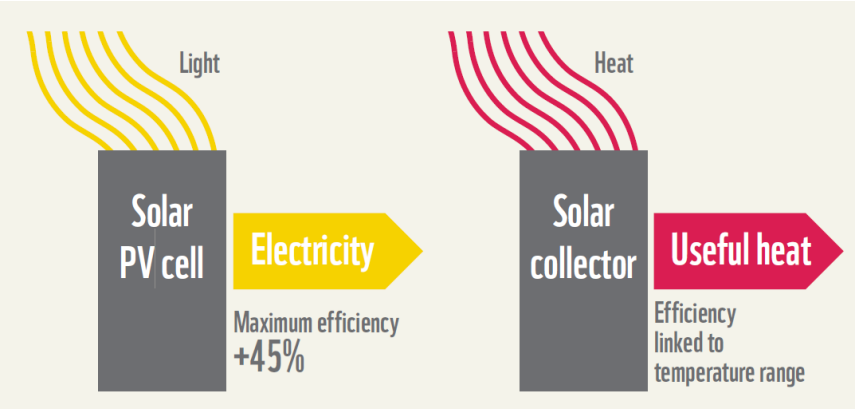

Figure 1.4: Comparison of solar PV and solar thermal.[14]

Like other renewable energy such as wind or tides, the major drawback of solar is its intermittency. Intrinsically, electricity can only be produced during the day and the production is highly depending on nebulosity. Moreover, unlike power plants based on coal or nuclear, the production of electricity based on solar energy cannot be regulated: it is either on or off. If the production of power exceeds the demand, the excess of electricity is either lost or need to be stored. Nowadays, several technologies exist to do so, and they can be classified in four categories. The first and probably the oldest way to store energy is through mechanical storage such as flywheels, compressed-air energy storage (CAES) or pumped-storage hydroelectricity (PSH) which has the advantage to allow long term storage but is of low energy density. The second category is electrical storage in super-capacitor or superconduction magnetic energy storage (SMES) which presents the advantage of very short response time but at the same time those technologies usually have a non-negligible self-discharge. The solution might come from electrochemical storage, *i.e.* in batteries, for which the response time is around the same as for electrical storage but with a higher energy density and a lower self-discharge. However, batteries have a relatively short lifetime that limits the storage over long periods of time.

To address this problem, the solution can come from an alternative way to produce energy from light: the generation of solar fuels in which energy is stored as chemical bonds. In this process, solar energy is used to synthesize fuel such as molecular hydrogen or methane (sometimes called synthetic natural gas or SNG) which are very stable molecules and will not alter over years. The details for producing solar fuels will be described later on this document. The lifetime limitation mainly come from leaks during the storage and is therefore not intrinsic to the compound itself.

Moreover, molecules present the highest energy density of all storage technologies: 1800 Wh L^{-1} for SNG compared to 400 Wh L^{-1} for Li-ion battery (see Table 1.1).

Technologies	Power rating (MW)	Storage duration (h)	Cycling or lifetime	Self-discharge (%)	Energy density (Wh L^{-1})	Power density(W L^{-1})	Efficiency (%)	Response time
Super-capacitor	0.01-1	ms-min	10,000-100,000	20-40	10-20	40000-120000	80-98	10-20ms
SMES	0.1-1	ms-min	100,000	10-15	~6	1000-4000	80-95	< 100ms
PHS	100-1,000	4-12 h	30-60 years	~0	0.2-2	0.1-0.2	70-85	sec-min
CAES	10-1,000	2-30 h	20-40 years	~0	2-6	0.2-0.6	40-75	sec-min
Flywheels	0.001-1	sec-hours	20,000-100,000	1.3-100	20-80	5000	70-95	10-20 ms
NaS battery	10-100	1 min-8 h	2,500-4,400	0.05-20	150-300	120-160	70-90	10-20 ms
Li-ion battery	0.1-100	1 min-8 h	1,000-10,000	0.1-0.3	200-400	1300-10000	85-98	10-20 ms
Flow battery	1-100	1-10h	12,000-14,000	0.2	20-70	0.5-2	60-85	10-20 ms
Hydrogen	0.01-1.000	min-weeks	5-30 yrs	0-4	600 (200 bar)	0.2-20	25-45	sec-min
SNG	50-1.000	hours-weeks	30 yrs	negligible	1,800 (200 bar)	0.2-2	25-50	sec-min

Electrical Mechanical Electrochemical Chemical

Table 1.1: Characteristics of energy storage technologies. [15]

This high density comes from the fact that chemical bonds contain a lot of energy and therefore are a great way to store it. For example, dissociation enthalpy for a C-H is *ca.* 410 kJ mol^{-1} and 345 kJ mol^{-1} for a C-C bond. This is why hydrocarbons are so efficient as fuels, and a reason to use them to store energy.

Solar energy reaching Earth surface could be classified in three different regions, depending on their energy/wavelength. UV domain is the most powerful part of the solar spectrum, with short wavelengths (~100 and 400 nm) and photons energy as high as 12.4 eV, but it only represents about

5% of the total solar irradiance. On the opposite side of the spectrum is the infrared domain, with wavelengths between 800 and 2500 nm, corresponding, respectively, to photons between 1.55 and 0.5 eV. This part of the solar spectrum, accounting for about 50% of the total, is however not energetic enough to activate most of the reported photocatalysts. Finally, the visible domain, with wavelengths between 400 and 800 nm, represents 45% of the total solar irradiance and is energetic enough to be used for photocatalysis, with photon energy ranging from 3.1 and 1.55 eV. A larger number of studies have been dedicated to the use of visible light at the main energy source in photocatalysis, as exposed later in the manuscript. This was also one of the mandatory parameters in this work.

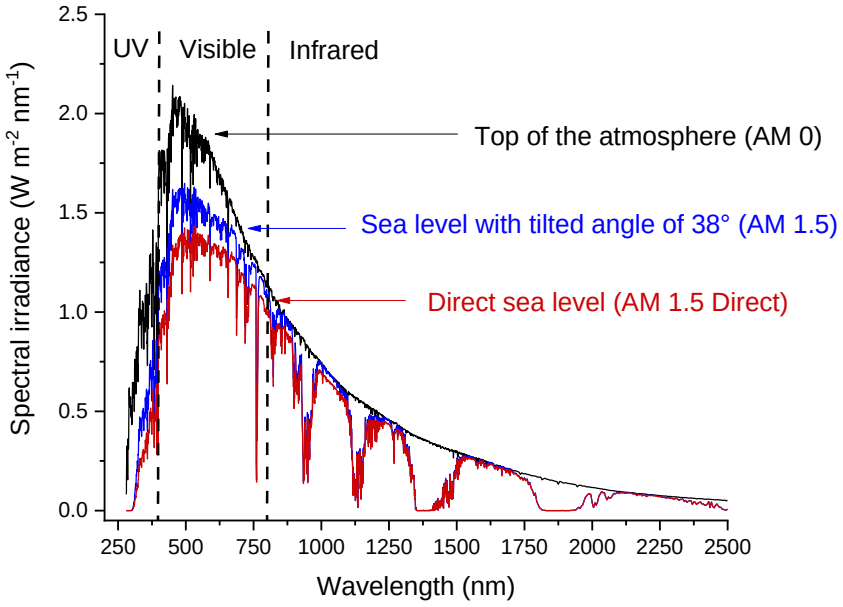

Figure 1.5: Mean solar irradiance for different standards.[16] AM stands for the Air Mass coefficient which defines the direct optical path length through the atmosphere and which correspond to a ratio relative to the zenith.

1.3 Thermodynamics of CO_2 reduction

CO_2 is a very stable molecule which stays in the atmosphere between 200 to 2000 years depending on the model used and is not easily degraded even by strong UV radiation.[17] This is due to the fact that CO_2 is a linear molecule and the orbitals of the carbon atom are sp hybridized which form two very stable σ bonds with the oxygen atoms. The two non-hybridized p orbitals of the carbon form the double bond with the p orbitals of the oxygen. The combination of these two molecular orbitals makes the C=O bonds extremely strong, with a dissociation energy about 750

kJ mol^{-1}. Carbon dioxide can however be reduced to various compounds, as depicted in Figure 1.6, but cannot be further oxidized, the carbon atom being in its most oxidized state.

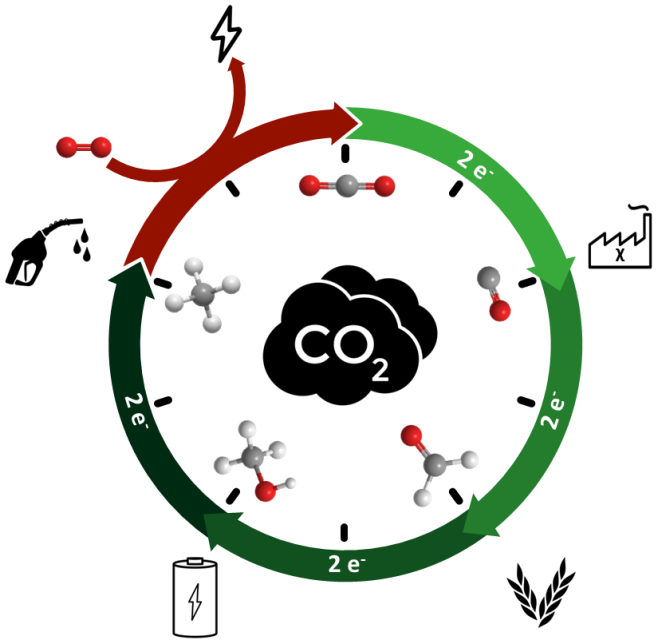

Figure 1.6: C1 reduction products from CO_2 depending on the number of electrons transferred ("the CO_2 clock").[18]

Among the variety of products that can be obtained from CO_2, we will only consider here the C1 products, *i.e.* without any carbon-carbon coupling. Four different products can thus be generated depending on the number of electrons transferred (and concomitantly, of protons) to CO_2: 2, 4, 6 or 8 electrons processes will give, respectively, carbon monoxide (CO) or formic acid (HCOOH), formaldehyde (HCHO), methanol (CH_3OH) or methane (CH_4).

Reaction	E° (V *vs.* NHE) at pH 7
$CO_2 + e^- \rightarrow CO_2^{\bullet -}$	-1.90
$CO_2 + 2H^+ + 2e^- \rightarrow HCOOH$	-0.61
$CO_2 + 2H^+ + 2e^- \rightarrow CO + H_2O$	-0.53
$CO_2 + 4H^+ + 4e^- \rightarrow HCHO + H_2O$	-0.48
$CO_2 + 6H^+ + 6e^- \rightarrow CH_3OH + H_2O$	-0.38
$CO_2 + 8H^+ + 8e^- \rightarrow CH_4 + 2H_2O$	-0.24
$2H^+ + 2e^- \rightarrow H_2$	-0.42

Table 1.2: CO_2 apparent reduction potentials.[19]

The first electron transfer will distort the sp orbitals and then will force the molecule to bend. However, as mentioned above, the linear structure of the molecule is very stable, so the energy barrier for this step is very high and corresponds to a highly negative redox potential of -1.90 V *vs.* NHE (Table 1.2).

On an inert material, the step-by-step reduction of CO_2 thus requires a lot of energy, mainly due to the formations of the $CO_2^{\bullet-}$ radical anion. As a consequence, this first electron injection is considered to be the rate determining step in CO_2 reduction. In the presence of a catalyst (CAT), the formation of this radical anion is avoided by the formation of a CO_2-CAT adduct which presents a lower activation barrier to form. An alternative pathway relies on the formation of a hydride from the active state of the catalyst. In the presence of a proton source, this hydride can react with CO_2 to drive the formation of formate (Figure 1.7).[20] However formate is usually a dead end product and cannot be further reduced.[21-22]

$$[LM]^n + e^- \longrightarrow [LM]^{n-1}$$

$$[LM]^{n-1} + H^+ \longrightarrow [LMH]^n$$

$$[LMH]^n + CO_2 \longrightarrow [LM]^{n+1} + HCOO^-$$

Figure 1.7: Hydride formation and formate generation on an organometallic LM complex.

The formation of the radical anion can be avoided by a proton coupled electron transfer mechanism (PCET) which will directly lead to an intermediate or a product with a reduction potential much lower than the radical anion, such as carbon monoxide, with a potential of -0.52 V *vs.* NHE. Thermodynamically, the formation of methane from CO_2 is much more favorable than any other product (Table 1.2) but its production requires 8 electron and 8 proton transfers, which induce a drastic kinetic limitation. Moreover, in order to achieve multiple electron and proton transfers, the catalyst needs to stay close to both electron and proton donating sites to achieve either sequential or coupled proton electron transfers.[23]

1.4 Basic principles of photochemistry

Even though in both cases mentioned above, the main reaction is a transfer of electron(s), photochemical and electrochemical processes have specific characteristics and limitations that need to be emphasized here.

1.4.1 Dealing with excited states

In electrochemistry, electrons are transferred directly from the electrode surface to an electron acceptor (for example the catalyst) which will then undergo chemical reactions. In photochemistry, the transfer of electrons is an indirect phenomenon induced by light absorption. Under light irradiation, an electron in the ground state of an absorbing compound (molecule or material) will be promoted to an energetic excited state and can then be transferred to an electron acceptor such as the catalyst. However, unlike an electrode, these excited electrons could follow different reaction pathways than the activation process of the catalyst, in a competitive and generally deleterious way.

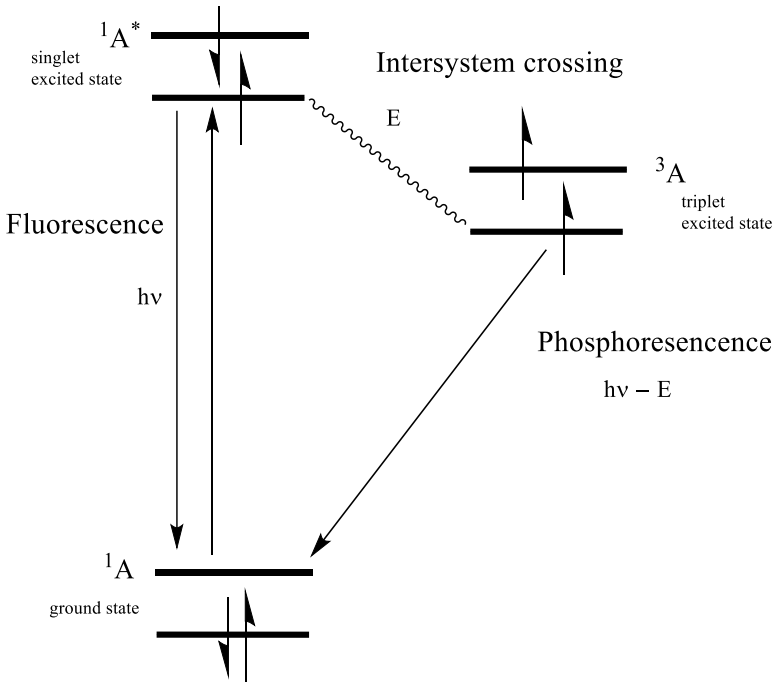

Figure 1.8: Simplified Jablonski-Perrin diagram for a molecule.

First, the electron promoted to a higher level of energy can go back to the ground state by emitting a photon (luminescence) and/or by releasing heat (non-radiative process). To better define this phenomenon, the notion of emission yield is used. It is defined as the ratio of photons emitted to the number of photons absorbed.

$$\phi = \frac{Number\ of\ photon\ emited}{Number\ of\ photon\ absorbed}$$

In addition, the lifetime is another necessary parameter to fully understand the excitation and de-excitation of electrons. It describes the average time the electron spends in an excited state before relaxing to the ground state. For example, de-excitation by fluorescence typically occurs in a

timescale of about 10 ns.[24] Such a short timescale is a strong limitation for processes such as fully homogeneous ones which require a bimolecular reaction and thus the mutual diffusion of two reactants happening in a comparable timescale. The excited electron donor (molecular sensitizer or material) must encounter the electron acceptor (the catalyst) for the electron transfer to proceed. Because of its very short lifetime, a singlet excited state has very little chance to effectively allow this diffusional reaction to occur and it is generally not the state of interest for photocatalysis reaction employing molecules. In some cases, the vibration levels of two states with different spins can overlap, which can result in a change of multiplicity of the electronic state from singlet to triplet, by a phenomenon called intersystem crossing (Figure 1.8). Once the electron donor is in a triplet excited state, it becomes paramagnetic and therefore the transition back to the ground state involves a change in the electronic state of the molecule, which is a forbidden transition. As a consequence, the lifetime of a triplet state is orders of magnitude longer than a singlet one, typically around 1 µs. Therefore, in a diffusional system the probability of molecular encounter between an excited donor in its triplet state and a catalyst acceptor is much higher. For this reason, in the rest of the manuscript, unless otherwise noted, the term excited state will refer to a triplet excited state.

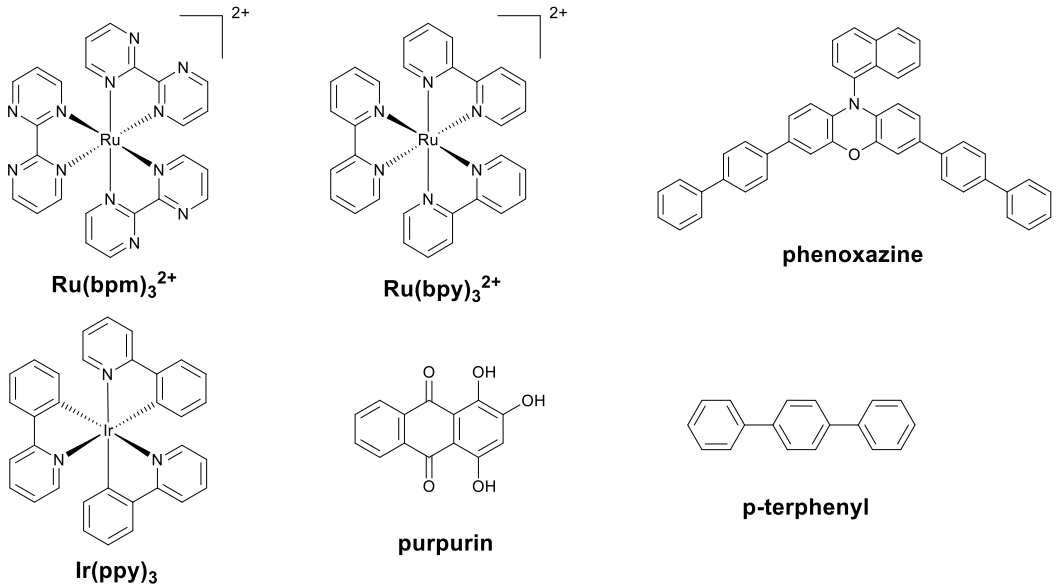

Figure 1.9: Various inorganic complexes and organic molecules used as photosensitizers.

Another parameter needs to be taken in account for the electron transfer between the donor and the acceptor, *i.e.* the redox potential of the donor excited state. In electrochemistry, the potential applied to the electrode can easily be tuned and adapted to the reaction of interest whereas in photochemistry, the potential of the triplet state is a fixed parameter that depends on the structure

of the molecule used. A large variety of molecular photosensitizers exists (Figure 1.9), mostly based on inorganic complexes that contain a rare element such as iridium or ruthenium, but also based on organic molecules such as *p*-terphenyl or phenoxazine (see Chapter 3). This variety of molecules offers a wide range of exited state potentials, from -0.21 to -2.19 V *vs.* SCE for typical complexes $[Ru(bpm)_3]^{2+}$ and $Ir(ppy)_3$ respectively. Tuning their potential more precisely, to screen a range at the few mV scale would require a very tedious synthesis work, in comparison with the application of a set potential to an electrode.[25]

For a given sensitizer, two reduction potentials can, in theory, be accessible to the reaction with the excited state due to the very nature of the reaction. Typically, in a photocatalytic system, three components are needed: a catalyst (CAT), a photosensitizer (PS) and a sacrificial electron donor (SD) as the source of electron (in opposition to an electrode). In a photoreductive process, the catalyst acts as an electron acceptor (EA), because it needs to accumulate electrons in order to be active towards CO_2 reduction. Once a photon promotes an electron of the sensitizer to an excited state PS*, two pathways are then possible depending on the redox potential of the sacrificial donor (Figure 1.10). If the standard redox potential of the couple $SD^{\bullet+}$/SD is negative enough, PS^* can directly accept an electron from the sacrificial donor through a *reductive quenching* step producing a PS^- species. The ground state of the sensitizer is then recovered by transferring one electron to the electron acceptor, in this case the catalyst. The second possible pathway is an *oxidative quenching* pathway, in which the electron from the PS^*excited state is transferred to the catalyst, generated on one side CAT^- and on the other side PS^+. The sacrificial donor will then give one electron to the sensitizer to reduce it back to the PS ground state.

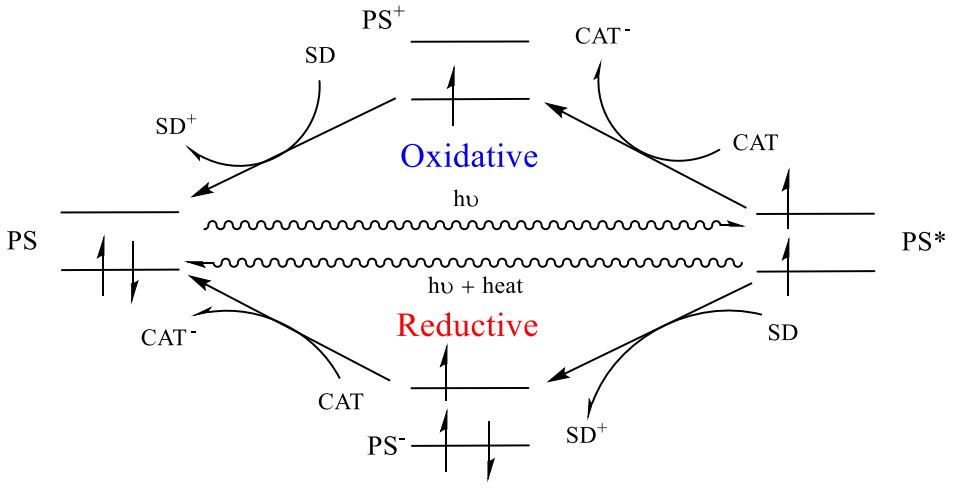

Figure 1.10: Reductive and oxidative quenching pathways for an excited state photosensitizer.

In most cases, the reduction potential of the PS^* excited state is negative enough to directly reduce CAT and, depending on the sacrificial donor employed, the reductive pathway can be in competition with the oxidative one. Because the reaction is limited by diffusion, tuning the concentration ratio between CAT and SD can favor one of the pathways over the other.

The quenching pathway and its efficiency can be evaluated by emission spectroscopy. Upon light excitation, the emission spectrum of the sensitizer is measured in the presence of an increasing concentration of quencher, *i.e.* either catalyst or sacrificial electron donor. If the emission intensity does not change, it indicates that no quenching is possible between the excited sensitizer and the introduced molecule. However, if one is able to quench the excited state of the sensitizer, the resulting emission will then be lowered. The quenching rate can be calculated by using the Stern-Volmer equation that describes the linear relationship between the emission intensity and the concentration of quencher.[26]

$$\frac{I_0}{I} = 1 + k_q \tau_0 [Q]$$

With I_0 the emission intensity in absence of quencher, I the measured intensity, k_q the quenching rate constant, τ_0 the lifetime of the excited state in absence of quencher and [Q] the quencher concentration.

1.4.2 Quantification and efficiency

To evaluate the efficiency of a photocatalytic reaction, two parameters are generally defined: the quantum yield and the turnover number. In an electrochemical process, the efficiency of a catalyst is often described by the number of electrons transferred to the catalyst compared to the theoretical number of electrons needed to generate the expected products, *i.e.* the faradaic efficiency (FE). In a photochemical process, it is extremely difficult to accurately measured and/or calculate the number of electrons that are involved in the reaction. As described before, once a molecule of sensitizer receives a photon, the electron promoted in the excited state can either effectively be involved in the reaction or it can go back to the ground state through a (non)emissive step. Therefore, two quantities are often used to described the activity of a photochemical reaction: the apparent quantum yield (AQY) and the internal quantum yield (IQY). The first one takes into account the number of photons received by the sample, whether or not they will be absorbed and/or

be useful to the reaction. The second one only takes into account the number of photons that will be effectively absorbed by the sample. [27]

$$AQY\ (\%) = \frac{mol\ \ of\ product\ \times thoretical\ number\ of\ electrons\ per\ product}{mol\ \ of\ incident\ photons} \times 100$$

$$IQY\ (\%) = \frac{mol\ \ of\ product\ \times theoretical\ number\ of\ electrons\ per\ product}{mol\ of\ absorbed\ photons} \times 100$$

As in electrochemistry, the turnover number (TON) of a catalytic reaction is defined as the number of catalytic cycles per number of catalysts. The turnover frequency (TOF) is a measure of the catalytic frequency, *i.e.* the number of catalytic cycles per time unit. Both are important figures of merit to evaluate the activity of a catalyst and could be used to compare one over another. However, in a strict definition, TON and TOF should be calculated when the reaction is over, *i.e.* when the catalyst can no longer undergo catalytic cycles, because of deactivation/degradation. In photochemistry, TONs are often reported as number of catalytic cycles during the full time of illumination (so it is highly variable from study to study), whether or not the catalyst is still active. When reported in publications, the definition of these numbers must be clearly emphasized by the authors for fair comparison.

$$TON\ = \frac{mole\ of\ products}{mole\ of\ catalyst} \qquad\qquad TOF(t^{-1})\ = \frac{mole\ of\ products}{mole\ of\ catalyst\ \times t}$$

In any reduction reaction involving a transfer of protons, there could be a competition between the reaction of interest (for example CO_2 reduction - CO2RR) and proton reduction into molecular hydrogen (hydrogen evolution reaction - HER). For CO_2 reduction, up to 8 protons are needed for methane production, and therefore the production of hydrogen from protons can take place over CO_2 reduction products. This is why the catalytic selectivity (CS) is another metric that provides an insight on the efficiency of CO_2 reduction over hydrogen production or any other unwanted products.

$$CS(\%) = \frac{Amount\ of\ one\ specific\ product}{Total\ amount\ of\ all\ \ products} \times 100$$

The selectivity of a catalyst highly depends on the experimental conditions and the production of one particular product over another can be optimized by tuning these conditions. For example, in a heterogeneous system using copper metal electrodes, it has been shown that the local pH at the

electrode plays a major role on the pathway to produce either methane or ethylene.[28] A similar pH dependence can be observed when a molecular cobalt phthalocyanine is immobilized on a carbon paper electrode for the reduction of CO_2 to methanol in which the basicity of the solution enhanced the reaction.[29] Finally, in a homogeneous photochemical reaction, for a given catalyst/sensitizer couple, reaction products ratio depends on the nature of the acid and/or of the sacrificial electron donor used. By immobilizing a cobalt quaterpyridine on a solid graphene acid support, our group has shown that, with the same sacrificial donor, the selectivity can be completely changed from 98% for CO production with a weak acid such as trifluoroethanol (TFE) to 99% for formate using triethanolamine (TEOA) as the proton source. The competition between CO2RR and HER highly depends on the acid used too, but the general trend is that the lower the pKa, the higher the probability of HER over CO2RR. As an example, with an iron porphyrin under CO atmosphere, the selectivity for methane production drops from 87% to 37% when switching from TFE (pKa 12.46) to phenol (pKa 10) under the same conditions.[30]

1.5 CO_2 reduction to methane

1.5.1 Anaerobic digestion

In Nature, some microorganisms called methanogen can digest biodegradable materials in the absence of oxygen to produced methane and carbon dioxide. More generally, the process of biomass digestion includes four steps: hydrolysis, acidogenesis, acetogenesis, and methanogenesis.

Feedstock for anaerobic digestion can be any biodegradable wastes such as paper, food, animal waste, plants, etc., except wood waste that contains a large proportion of lignin which cannot be digested by most microorganisms.

Nowadays, the main feedstock for industrial digester is agricultural waste, both animal or vegetal, but also specially grown crops that gives a better methane yield. This technology for renewable methane production is mature enough to be used at an industrial scale, like in France where this technology was quickly growing in the last three years. However, based on projections, at full capacity, this technology has a limited capacity of *ca.* 140 TWh per year, which is still far below the 970 TWh of the annual French consumption, meaning that the goal of 100% of renewable gas in the 2050's cannot be reached by this only solution. To achieve this goal, other technologies are thus needed.

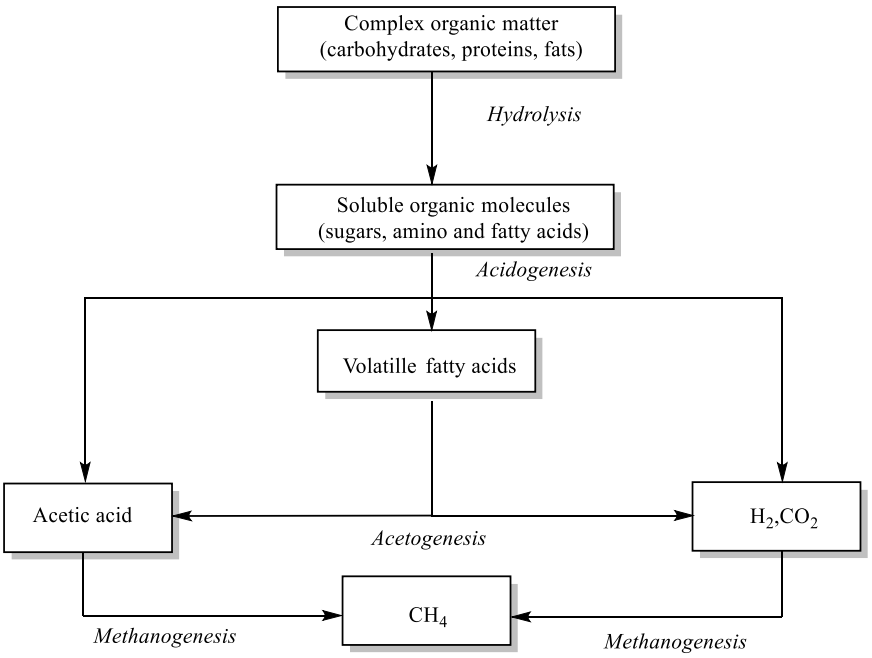

Figure 1.11: The sequential stages of anaerobic digestion.

1.5.2 Methanation

Methanation is the process that converts a mixture of carbon dioxide and molecular hydrogen into methane by either a chemical or biological reaction. Chemically, this reaction generally requires a high temperature (at least 300°C) and typically occurs at a pressure of 5 bars. In order to reduce both temperature and pressure, solid catalysts can be used, on which the gases will adsorbed. Historically, noble metals were used because they present high performances without any prior transformations. Among noble metals, rhodium is one of the most efficient one for this reaction but has the disadvantage to be highly sensitive to oxygen and to be extremely expensive (155 €/g).[31] An alternative to noble metals would be a transition element, such as nickel. Interestingly, the performance of nickel metal catalyst highly depends on the crystallographic facet exposed to the reaction media, unlike noble metal catalyst.[32] Another crucial aspect of catalyst for methanation is the support on which they are dispersed, which can boost or lower drastically the performances towards methane production. Recently, aluminum oxide has been used and has shown a total selectivity for methane production, with a conversion yield for CO_2 of 82%, a rare high conversion rate example at 350°C.[33]

The high temperature needed to activate the reaction requires a high power and therefore a lot of energy. Instead of heating the whole reservoir, one solution could be to only increase the

temperature locally, near the catalytic sites, which could be achieved by a photocatalyst. By absorbing a photon, an electron can be promoted to an excited state that will relax to the ground state by non-radiative process, generating heat. This phenomenon is drastically enhanced when the catalyst exhibits some plasmonic resonance.[34] Furthermore, plasmonic nanoparticles can excite and transfer electrons to an adsorbed reactant or intermediate through "hot electron injection". On rhodium nanoparticles, the plasmonic effect was showed to increase the selectivity for CH_4 production from 60% in dark conditions to more than 90% under light irradiation. In this photocatalytic reaction, hot electrons are selectively injected into the anti-bonding orbitals of CHO intermediate, facilitating the breaking of the C=O bound and enhancing the CH_4 formation.[35]

The process of methanation can also be performed by microorganisms. Biological methanation can be a pathway in anaerobic digestion but this is not necessarily the case and it depends on the type of organisms used. Compare to chemical methanation, using microorganisms has a major advantage: the reaction can be performed at room temperature thanks to the fact that most of the methanogenic bacteria cannot survive under high temperature. Each type of archaea has a specific range of temperature and some can performed methanation at a temperature as low as 0°C.[36] Furthermore, archaeas used for methanation cannot survive at high pressure so the reaction is typically performed at 1 atm. Even though the conditions are milder, the major drawback of using bacteria to produce methane from CO_2 is the stability of the reaction, those microorganisms being very sensitive to any form of contamination. Maintaining the required conditions for bacterial growth generates a non-negligible cost that can disfavored this technology over other sources of renewable methane production.

1.5.3 Electromethanogenesis

Between electrical and biological production of renewable methane from CO_2, we can find a pathway combining both: electromethanogenesis. This technique uses an electrode on which methanogen microorganisms are deposited, thus forming a "bioelectrode". When a current is applied, the deposited organisms can accept electrons to drive the CO_2-to-CH_4 conversion. Even though the exact mechanism for this reaction is still unclear, five pathways have been proposed depending on the type of microorganism employed (Figure 1.12).

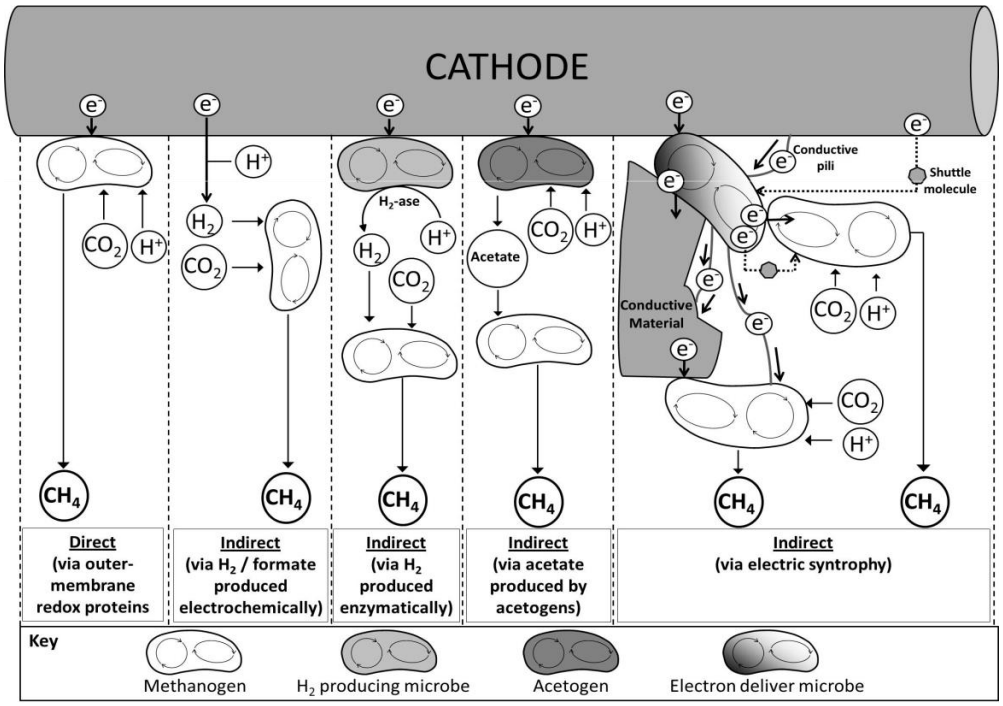

Figure 1.12: Possible pathways for electromethanogenesis. [37]

When the direct pathway is employed, the reaction can have a faradaic efficiency as high as 94%. However, a major limitation for this technique is the high sensibility to both oxygen and high and low pHs which then required a strictly controlled environment. There is also an intrinsic limitation due to bacterial growth. If this happens, it could passivate the electrode and thus preventing CO_2 to reach the active species at the surface of the electrode. As for other types of methane production, the occurrence of side reactions is also an issue here, lowering the faradaic efficiency towards methane, and the stability of such bioelectrode has not reached, to date, more than a few hours.[37]

1.5.4 CO_2 electrochemical reduction

In 1870, M.E. Royer first demonstrated the feasibility of carbon dioxide electroreduction by a zinc electrode.[38] Formic acid was detected in solution and a gas evolution could be observed without identifying it. Already, a first mechanism was proposed because no oxalic acid was detected and therefore it was established that CO_2 was directly reduced to formic acid without apparent intermediates. Historically, rare metals were employed as electrodes and it was first demonstrated that on a ruthenium electrode, CO_2 could be reduced to methane electrochemically, with both CO and CH_3OH as secondary products.[39] Among all metals, transition ones could again be efficient and affordable alternatives to noble metals as electrode material. This is particularly

true for copper that can easily go beyond two electrons transfer to form hydrocarbons such as methane or ethylene as it was first proved in 1985 by Hori.[40] Despite a high efficiency towards CO_2 reduction, the lack of selectivity is a persistent major drawback. Indeed, it has been repeatedly shown many times that copper can produced methane and C2 products, but it is not selective toward one product and therefore the overall activity remains low if we focus on one particular compound.[41]

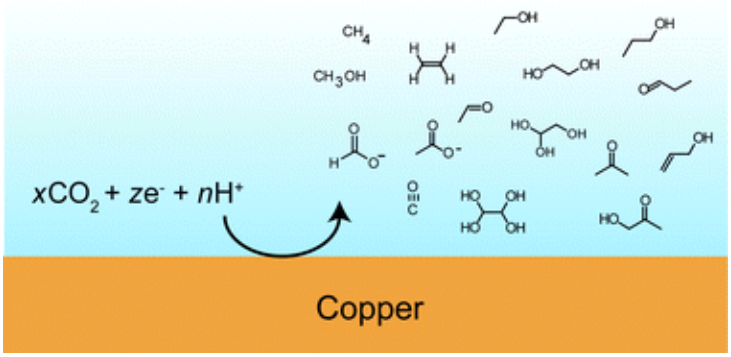

Figure 1.13: Possible products of CO_2 electroreduction on copper foil.[41]

Various solutions to enhance the selectivity toward methane production have been proposed in the literature, such as high dispersed single site catalyst. By pyrolyzing copper precursor on carbon black, an efficient CO_2 reduction catalyst was obtained with a selectivity for methane of 42% however with hydrogen and ethylene as byproducts. The size and the dispersity of the catalyst were proposed to be key factors for methane production over ethylene.[42] Because CO_2 reduction beyond two electrons is a multi-step reaction, stabilizing the key intermediate(s) toward the desired product is thought to be an efficient strategy to increase the selectivity. By adding control thickness of Nafion layer on top of a copper electrode, the faradaic efficiency toward methane production was enhanced from 20 to 88% thanks to, as proposed by the authors, a stabilization of the CO intermediate by the polymer. In the absence of Nafion, CO is released more easily, producing numerous products as shown before, with an overall very low selectivity.[43]

Another strategy for converting CO_2 into methane relies on the use of molecular catalysts instead of bulk metallic electrode, either immobilized on a material (heterogeneous approach) or in solution (homogeneous approach). Such strategy was demonstrated with the use of copper porphyrin modified with -OH groups in the ortho positions on the phenyl rings as molecular catalyst for the reduction of CO_2.[44] The complex was dissolved and deposited on a carbon paper to create the

"catalytic" electrode. A total faradaic efficiency for CO_2 reduction of 50% was achieved at -1.0 V *vs.* RHE, with methane as the main reduction product and ethylene and carbon monoxide as secondary products. Using comparable conditions, an immobilized cobalt protoporphyrin was reported to reduce CO_2 in aqueous media. The overall faradaic efficiency of this system was very low and a maximum of 2.3% could be achieved for the formation of methane. ^{13}C labelled studies confirmed that CH_4 actually comes from the reduction of CO_2.[45] Copper phthalocyanine was also reported to be an active catalyst for methane production from CO_2 with 66% of faradaic efficiency. However, upon XANES and EXAFS analysis, evidence of copper nanoclusters formation during the electrolysis was highlighted and was proposed as active site instead of the original molecular catalyst.[46] In a similar way, our group reported an iron quaterpyridine complex acting as a precursor for the CO_2 to CH_4 reduction in homogeneous acetonitrile solution. Upon constant potential electrolysis, molecular hydrogen is produced as the main product with CO and CH_4 as secondary products, with faradaic efficiency of 4.1 and 2.3%, respectively. By EXAFS studies, it was shown that the starting complex is degraded during the experiment to form nanoparticles that would indeed act as catalyst for methane production. Among other molecular catalysts, binuclear complexes are promising candidates in processes requiring more than two electrons. A Ni^{II}-Fe^{II} diphenylethnaethiolate compound was reported to be able, once immobilized onto a graphite electrode, to efficiently reduce CO_2 to CH_4 with 12% faradaic efficiency. More interestingly, this study was performed in water, with an optimized pH of 4 with however only 3h of stability and 66% of faradaic efficiency for hydrogen production.[47] It should be emphasized that methane production is a small portion of CO_2 reduction studies and among those studies, very few reports the use of molecular catalysts, the four examples above being among the only ones in the literature to date.

1.6 CO_2 photochemical reduction

As mentioned previously, the amount of solar energy received by the Earth every hour is tremendous compare to the global world energy consumption. In Nature, this energy is used by plants to metabolized carbon dioxide and water to create molecular oxygen and energy, mostly in the form of sugars, though the photosynthetic process. A whole branch of research, including chemistry, is developed for years to understand, reproduce and enhance this process in so-called artificial photosynthetic processes. Among the different reactions that can be performed using solar

light, two products attract most of today's research: molecular hydrogen production through water splitting and, what will be the focus on the next section, CO_2 reduction.

1.7 Reduction on a semiconductor

Firstly described by Edmond Becquerel in 1839, the photovoltaic effect has been used not only for producing electricity but also, since 1961 and the pioneer work of Eisenberg *et al.* to trigger electron transfer processes in solution through photoelectrochemical electrodes.[48] Mainly used for hydrogen production, the use of a *p*-type gallium phosphide (*p*-GaP) photoelectrode to reduce CO_2 in solution was first reported in 1978.[49] In order to avoid issues related to the diffusion of CO_2 from the solution bulk to the electrode surface, suspensions of semiconductors can be used in which no outside electrical power is applied. In 1979, Inoue *et al.* proved the feasibility of such system, with the advantage to not need the application of an external electrical bias.[50] In this study, an aqueous suspension of semiconductors such as WO_3, TiO_2, ZnO , CdS, GaP and SiC were used as both catalyst and photosensitizer. Interestingly, the formation of CO was not observed, but a mixture of all the other C1 products from CO_2 reduction, *e.g.* formic acid, formaldehyde, methanol and methane.

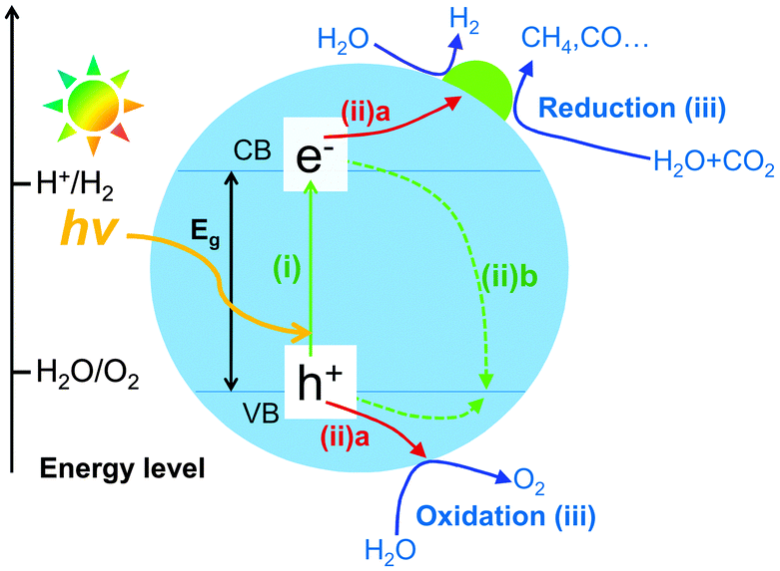

Figure 1.14: Photocatalytic reduction of CO_2 over a semiconductor particle.[51]

It is generally admitted that the CO_2 photochemical reduction occurs by successive steps, starting by the generation of an electron-hole pair, when the semiconductor is illuminated with the appropriate light source. To trigger this first step, the incident photon must have an energy equal or higher than the bandgap (E_g) of the semiconductor (Figure 1.14).

Then, electrons and holes migrate to the conduction band (CB) and the valence band (VB) of the material, respectively (step (i), Figure 1.14). Some of the electrons can then reach the surface of the material and can activate a co-catalyst (step (ii)a, top) whereas the holes can participate in oxidation processes (step (ii)a, bottom). However, most of the generated electron-hole pairs will recombined and release energy in the form of heat or photons, which is the main physical limiting factor for having a semiconductor catalyst with a high quantum yield for catalysis. Because the electron hole recombination is two to three orders of magnitude faster than the CO_2 reduction, a lot of efforts has been put in enhancing charge separation. The size of TiO_2 particles has for example being reported to have a significant role in this process.[52] In a final step, the semiconductor can reduce CO_2 directly or through the assistance of an absorbed co-catalyst (step (iii)) on the surface of the semiconductor whereas the holes will oxidized water, or some other organic molecule. If we consider nanoparticles of semiconductor, their structure plays a key role in the performances of the system because they can affect the different steps of the reaction such as photon absorption, charge separation, surface reaction, either directly with CO_2 or through an adsorbed cocatalyst.

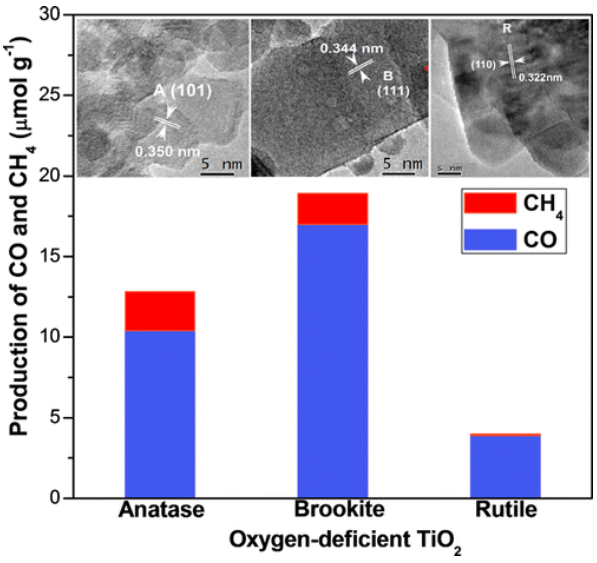

Figure 1.15: Production of CO and CH_4 on different TiO_2 phases.[53]

A nanoparticle can have various crystal phases upon preparation, each one having slightly different properties, for example its surface energy. This is particularly true for TiO_2 which presents three possible crystal phases (Figure 1.15): anatase (tetragonal), rutile (tetragonal) and brookite (orthorhombic). It has been observed that in order to be photochemically active towards CO_2 reduction, TiO_2 needs to present oxygen vacancies at the surface.

By changing the phase of TiO_2 from either rutile or brookite to anatase, the production of CO from CO_2 under light irradiation is enhanced.[53] When oxygen vacancies is favored on the same catalysts, during the synthesis, an increase in CO and CH_4 production for all three phases is observed. However, the enhancement is much higher for the brookite phase and was attributed to the facilitated formation of oxygen vacancies on this particular phase and a faster reaction rate of CO_2^- to either CO or CH_4.

The crystal phase can also play a role on the energy bands and/or the bandgap between them. By switching from orthorhombic to cubic phase of a $NaNbO_3$ nanoparticle, Ye *et al.* have showed that the bandgap decreased, from 3.45 eV to 3.29 eV.[54] The production of methane from CO_2 is two times higher on the cubic phase, not only because of the smaller bandgap, but also by the electronic structure of the cubic phase which favored the electron transfer. As a consequence, controlling the exposed crystallographic facet of a nanoparticle catalyst is as important as the other properties mentioned above and can have an important impact on the performances regarding CO_2 reduction. For example, on the same crystallographic structure (here TiO_2 anatase) when the exposed facet change from {010} to either {101} or {001}, the production of CO and CH_4 decreased.[55] However, by photoluminescence spectroscopy, the electron-hole separation was found to be more efficient in the order {001}> {101}> {010}. Even though the charge separation is more efficient on the {001} facet, it is less active toward CO_2 reduction. By analyzing the conduction band position, it has been shown that the CB was more negative in the order {010}> {101}> {001} which means that the photogenerated electrons in the {010} facet have a more negative potential. Furthermore, this facet exhibited a better CO_2 chemisorption than the other two facets. Overall, this suggests that the electron-hole separation is a less limiting parameter than the reduction potential or the CO_2 chemisorption to have an efficient photocatalyst. Moreover, the exposed facet can not only change the activity but can also completely change the selectivity of the reaction. By exposing the {111} facet of a Cu_2O nanoparticle, in the presence of CO_2 and H_2O, the main product of the reaction is H_2, with traces of CO.[56] However, when the {100} facet is exposed, the selectivity towards CO_2 reduction was enhanced and the production of CO increased, what was mainly explained by the improved CO_2 chemisorption on the {100} facet.

Another limiting factor of a photochemical reaction is light harvesting. A way to increase the efficiency is to use an absorbed or covalently linked sensitizer. For example, by anchoring a copper

tetra(4-carboxylphenyl) porphyrin (CuTCPP) to a TiO_2 catalyst (Figure 1.16), Wang *et al.* have shown that light absorption by this composite system was much higher than the CuTCPP or the TiO_2 alone.[57] As a result, CO_2 reduction to CO or CH_4 was enhanced compare to either TiO_2 or CuTCPP in similar conditions. When illuminated, CuTCPP can injected one electron directly into the TiO_2 CB and then can be used for CO_2 reduction. In parallel, because TiO_2 is photoactive, it can also harvest light and promote an electron to the CB and therefore the amount of accessible electrons for CO_2 reduction was enhanced. At the same time, holes can be injected from the VB to the HOMO of the CuTCPP, improving the electron-hole separation.

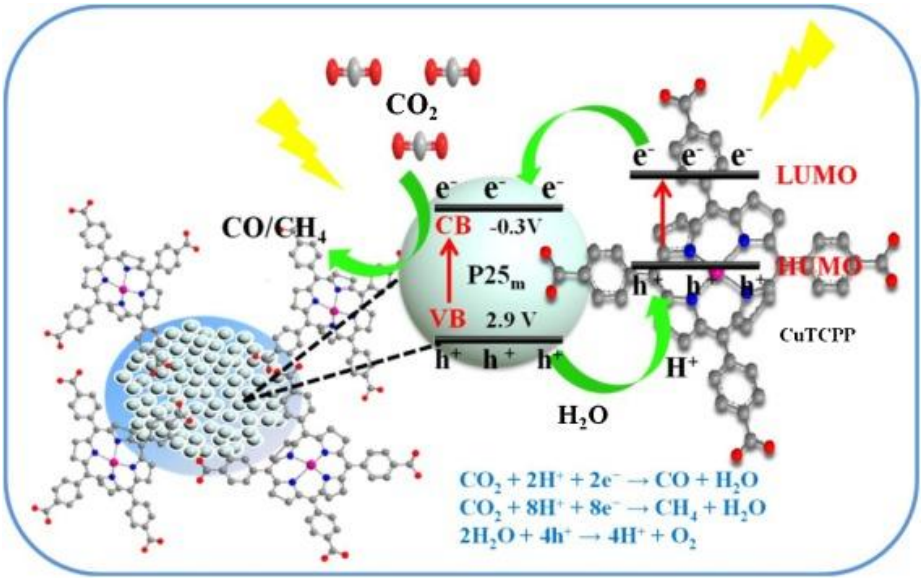

Figure 1.16: The possible mechanism of reduction of CO_2 into CH_4/CO photocatalyzed by CuTCPP/P25m.[57]

Interestingly, in a reciprocal approach, a semiconductor material, non-active towards CO_2 reduction, can be used as sensitizer in association with a molecular catalyst. One recent example is the combination of mesoporous carbon nitride (mpg-C_3N_4) as sensitizer and a polymeric cobalt phthalocyanine (CoPPC) as catalyst.[58] CoPPC was immobilized by non-covalent π-π interactions and upon irradiation the electron promoted into the conduction band of the mpg-C_3N_4 was injected into the catalyst to drive CO_2 reduction to CO. The holes generated in the VB will oxidize triethanolamine (TEOA), the sacrificial electron donor. When the two partners were together in solution, the production of CO remained quite low and an enhancement was only observed when an effective immobilization of the catalyst on the material was achieved, proving the importance of the non-covalent interaction for an efficient electron transfer. A similar approach was employed in our group by immobilizing a cobalt quaterpyridine complex (Coqpy) onto a mesoporous

graphitic carbon nitride (mpg-C_3N_4) through a covalent amide linkage (Figure 1.17).[59] Without immobilization, the production of CO was negligible but was multiplied by 7 thanks to the covalent linkage. Interestingly, the activity for hydrogen production was also lowered and therefore the overall selectivity for CO production was increased.

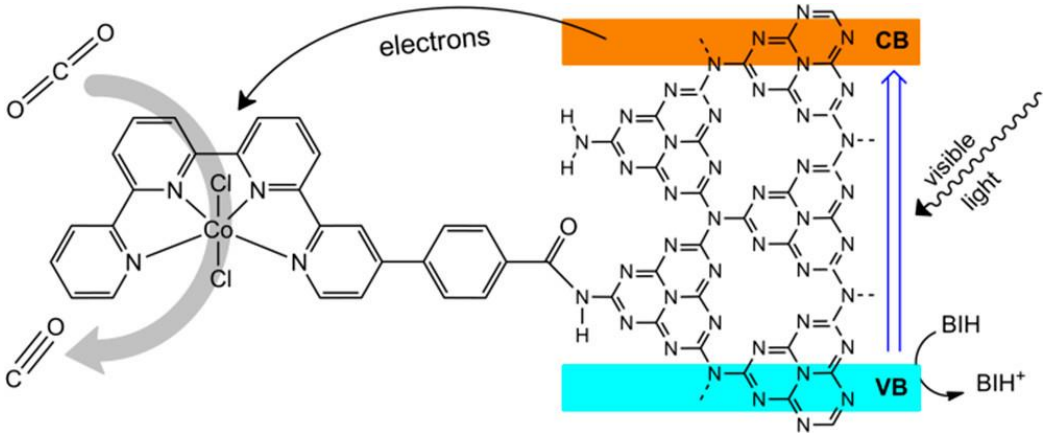

Figure 1.17: Immobilized cobalt quaterpyridine on graphitic mesoporous carbon nitride for CO_2 reduction.[59]

1.8 Reduction by molecular catalysts

In the race to find suitable catalysts for CO_2 photochemical reduction, molecules are in the front line with a particular focus on organometallic complexes. Compare to semiconductors, their structure, *i.e.* their active site and its immediate surrounding environment, is well defined and the mechanism of the reaction can therefore be studied in details through various spectroscopic techniques. In such complexes, the metal center redox potentials can be tuned through ligand modification (thanks to electronic and/or inductive effects), allowing a precise control on the potential offered for CO_2 reduction. These properties pushed the development of a large variety of molecular catalysts for the so-called "solar fuels" production from CO_2 conversion.

The first reported homogeneous photochemical reduction of carbon dioxide was reported by Lehn and co-workers in 1983 with a Re^I complex.[60] In the presence of triethanolamine in a DMF saturated CO_2 solution, the complex can act both as sensitizer and as catalyst to produce CO upon visible light irradiation ($\lambda > 400$ nm) with 100% selectivity and 27 TON. In this study like in many subsequent ones, some typical drawbacks of such homogenous photochemical processes were observed. For example, most metallocomplexes absorb UV light which usually causes photodegradation in the course of long-time irradiation (typically, several hours of continuous illumination). As a consequence, the UV part of the incident light must be blocked to prevent the

photodamage of the complex. To overcome this issue, molecular photosensitizers with an absorbance (much) higher than the catalyst in the specified wavelength are used, reducing the fraction of photons received by the catalyst and therefore enhancing its stability. In 1984, Tinnemans *et al.* employed cobalt cyclams as catalysts, with $Ru(bpy)_3^{2+}$ as sensitizer and ascorbic acid as sacrificial electron donor. Under CO_2 atmosphere, the reaction products obtained were carbon monoxide and molecular hydrogen, with a maximum selectivity of 71% for CO.[61]

These two-pioneer works, among many others, showed the great potential of molecular catalysts for CO_2 reduction. Because of the economic cost of noble/rare metals and of possible toxicity and environmental issues, a lot of efforts has been put on macrocyclic catalysts since then to switch to earth abundant metal centers. Several well documented reviews exist on the topic.[62-65]

1.8.1 Cobalt complexes

After the work of Tinnemans, investigation on the mechanism of CO_2 reduction using cobalt cyclams was investigated in more details. By using ^1H NMR, Fourier-transform infrared spectroscopy (FTIR) and X-ray absorption near edge structure (XANES) analysis, four different isomers of the complex were identified: two five coordinated and two six coordinated isomers.[66]

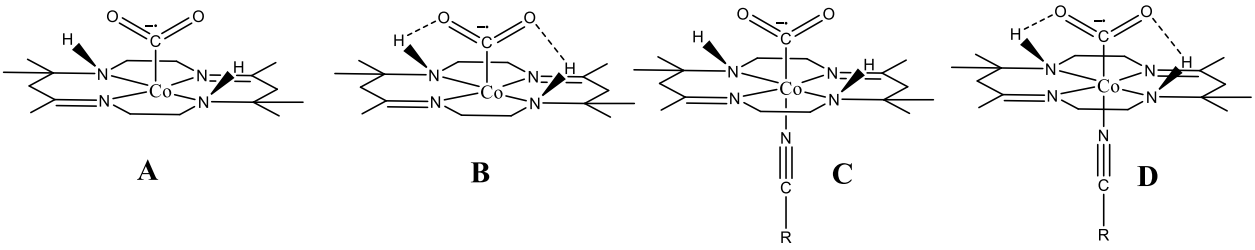

Figure 1.18: Structure of cobalt cyclam isomers either five (A,B) or six coordinated (C,D).

Two isomers exhibit hydrogen bonding between the hydrogen on the amine group and the CO_2 coordinated to the metal center. In acetonitrile medium, a solvent molecule can coordinate to the metal center thus creating the six-coordinate isomer and improving the stability of such intermediate. For either five or six coordinate isomer, charge transfer from Co(I) to CO_2 have been highlighted and proved that two electrons can be promoted to the attached CO_2 to facilitate its reduction. [67] The complex can then be described as a (d^6) Co(III) carboxylate (CO_2^{2-}) complex. By using *p*-terphenyl as sensitizer and TEA as sacrificial electron donor, the main product of CO_2 reduction with the Co(III)cyclam catalyst is CO, with HCOOH as secondary product and almost no H_2 production. When TEA was replaced by TEOA, catalytic performances towards both

products was enhanced, thanks to the better stability of the sensitizer in the presence of hydroxylated tertiary amines. [68]

Apart from cyclams, more conjugated complexes such as porphyrins and phthalocyanines were interesting for CO_2 reduction both in term of performances and stability. In 1998, Neta and co-workers reported that under near UV light irradiation (> 320 nm), a cobalt tetraphenylporphyrin complex was able to reduced CO_2 to CO and HCOOH in the presence of TEA as sacrificial donor. Because UV light can damage the macrocycle of the catalyst, the reaction was limited and eventually stops.[69] To overcome this issue, *p*-terphenyl was introduced as sensitizer and the reaction yield was greatly enhanced due, among other, to the *p*-terphenyl strong absorption of UV light, preventing the catalyst from being degraded.[70] By combining electrochemical and photochemical studies, Co^0 was found to be the reactive state at which CO_2 binds the catalyst. In the absence of sensitizer, TEA successively reduced the Co^{II} to Co^I and Co^0 but the first two steps were reported to have a lower efficiency. In presence of *p*-terphenyl, upon visible light irradiation, TEA can transfer one electron to the excited state of the sensitizer, generating a p-terphenyl radical anion that possesses a redox potential strong enough to reduce Co^I to Co^0 therefore improving the yield of active catalyst generated.

More recently, a modified cobalt porphyrin bearing four N-methylpyridinium (CoTMPyP) groups was reported to be active toward CO_2 reduction in aqueous media (Figure 1.19).[71] A copper complex was used as sensitizer and ascorbate as sacrificial donor in a $NaHCO_3$ buffer (pH 6.7) solution, saturated with CO_2. Even though copper complexes are known to be active in CO_2 reduction, no product were reported in blank experiments in absence of cobalt catalyst. A selectivity of 77% for CO was achieved and a TON of 2680 was reported after 4 h of visible light irradiation. Compare to the previously reported sulfonated cobalt porphyrin (CoTPPS, Figure 1.19A), the CoTMPyP exhibits TONs twice as high, which was explained by the capacity of the ligand to store electrons. Once CO is released, Co^{II} is reduced to Co^I through an internal electron transfer (Figure 1.19B), increasing then the number of catalytic cycles for CO_2 reduction, compare to CoTPPS that requires external electron transfer to be reduced back to Co^I.

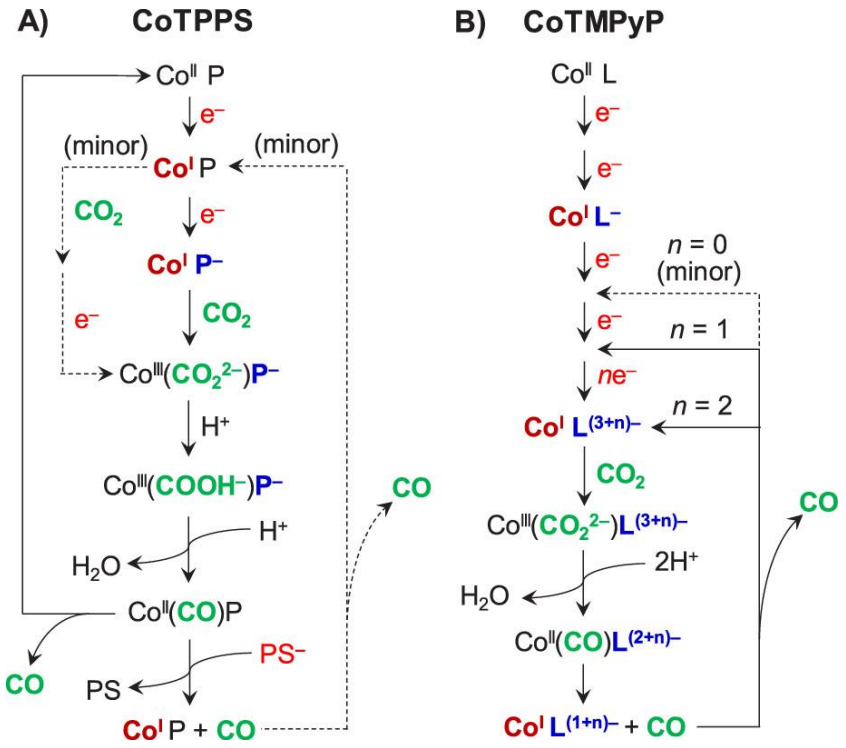

Figure 1.19: Scheme of CO_2 to CO reduction with either CoTPPS or COTMPyP.[71]

1.8.2 Manganese complexes

Among transition metals, manganese is the third most abundant in the Earth crust after iron and titanium, which makes it an interesting candidate for sustainable catalytic metallocomplexes. However, its use as photocatalyst for CO_2 reduction is quite recent and was firstly described in 2014 by Ishitani *et al.*[72] The *fac*-Mn(bpy)$(CO)_3$Br complex was used as catalyst with tris(4,4'-Dimethyl-2,2'-bipyridine)ruthenium ($[Ru(dmb)_3]^{2+}$) as sensitizer and BNAH as sacrificial electron donor in a mix DMF-TEOA solution (Figure 1.20). Under full solar spectrum irradiation, using a 480 nm band pass filter, formic acid was produced as main product with a TON 149, whereas CO was detected using the same complex under electrocatalytic conditions albeit with a TON of only 13.[73] However, the initial Mn complex dimerizes to form what was described as the actual catalyst which then degrade rapidly.

Upon ligand modification, the stability and performances were improved and two pathways for CO_2 reduction were proposed. By adding $–OCH_3$ substituents on the pyridine rings, the stability of the dimer complex was improved and the selectivity for CO_2 reduction was switched: CO was produced as the main product with a TON of 1004, with formic acid as secondary product (TON

of 310).[74] By replacing -OMe by 6,6′-(mesityl)2-2,2′-bipyridne (6mes) substituents, the selectivity for CO production over HCOOH increased, to reach 94%.

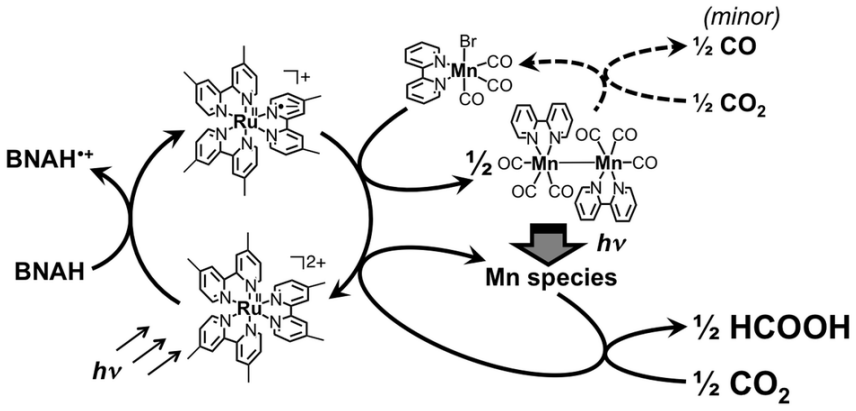

Figure 1.20: Proposed mechanism for the photochemical CO_2 reduction with fac-Mn(bpy)(CO)$_3$Br catalyst.[72]

The stability of such complexes could be improved through their incorporation into a metallic organic framework (MOF) as reported by Fei *et al.*[75] By modifying the pyridine ligand of the catalyst with Zr moiety, an active MOF toward CO_2 reduction could be synthesized with isolated Mn(bpy)(CO)$_3$Br complexes covalently link on the edges, forming a hybrid "cat@MOF" catalyst. With $[Ru(dmb)_3]^{2+}$ as sensitizer and BNAH as sacrificial donor, upon 470 nm monochromatic LED irradiation, TONs of 110 was obtained for formic acid and 4.5 for CO, reaching 96% selectivity for HCOOH production. Because of the anchoring on the MOF, no dimerization of the complex was observed and the hybrid catalyst can therefore be reused under the same conditions for at least three catalytic cycles.

1.8.3 Iron complexes

Among all non-noble metals, iron is the second most abundant in the Earth crust (5.6% in mass), after aluminum. It presents several decisive advantages in terms of potential large-scale applications: it is cheap, widely available and in large quantities; it is found directly as pure metal (and not in an oxide form); it is non-toxic and environmentally non-deleterious. Iron is thus a very good if not the best candidate for the replacement of rare/costly/toxic metals in inorganic complexes used for catalysis.

Polypyridines complexes are very often used in photocatalytic reaction both as sensitizer and catalyst for CO_2 reduction. Ishitani *et al.* reported the CO_2 photochemical reduction by an iron diamine complex ($Fe(dmp)_2(NCS)_2$) in the presence of a copper sensitizer ($Cu(dmp)(P)_2^+$) and BIH

as sacrificial donor, in a 5:1 CH_3CN/TEOA solution.[76-77] Under monochromatic irradiation (436 nm) the reaction was stable for up to 12 h and CO was obtained as main product with a TON of 273 and 78% of selectivity. In similar conditions, an iron quaterpyridine (Feqpy) complex was reported to be highly active for CO production under blue light irradiation (460 nm, Figure 1.21).[78]

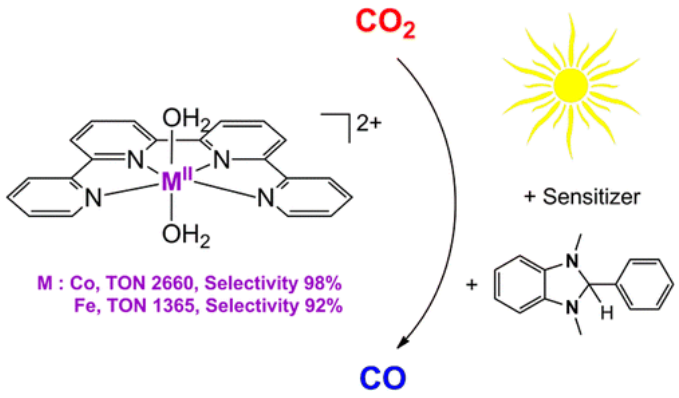

Figure 1.21: CO_2 photochemical reduction by Fe and Co quaterpyridine complexes.[78]

By employing $Ru(bpy)_3^{2+}$ as sensitizer, BIH as sacrificial donor and an ACN/TEOA mixture as solvent, both CO and HCOOH were detected in solution after only 3 h of irradiation, with TON of 3844 and 534, respectively, and a selectivity of 85% for CO production. More interestingly, when the Ru sensitizer was replaced by a fully organic one, *e.g.* purpurin, a TON of 1365 and 115 for CO and HCOOH was detected, respectively, without any H_2 production, leading to a 92% selectivity for CO.

Not all the complexes for CO_2 reduction are necessarily based on pyridines rings and cyclopentadieone-based iron catalysts can also be active in photochemical conditions. By combining a (cyclopentadione)iron-tricarbonyl complex with an iridium sensitizer $[(Ir(dF(CF_3)ppy)_2^-(dtbbpy)](PF_6)$ and TEOA as both electron and proton donor, 596 TON for CO could be obtained under visible light irradiation (400-700 nm).[79] However, it must be noted that after only 1 h of irradiation, the production of CO stopped and could not be reactivated even with re-addition of either catalyst or sensitizer. Because of the presence of three carbonyl ligands on the complex, some of the CO detected (but not all, TON being over 3) could come from the degradation of the catalyst, this hypothesis not being ruled out in the absence of ^{13}C labelled experiments. By switching from the expensive and rare metal iridium sensitizer to a copper one, the overall activity was not strongly affected, with 487 TON for CO after 7 h of irradiation. [80]

As mentioned previously, iron complexes, and especially porphyrins, have attracted a lot of attention over the years for CO_2 reduction, both in electrochemical and photochemical conditions. As for the cobalt equivalent, Neta *et al.* studied the photochemical reduction of CO_2 by an iron porphyrin.[81] Upon near-UV light irradiation, in the presence of triethylamine as electron donor, the iron center is reduced from Fe^{III} to Fe^0 by three successive electron transfers, as also demonstrated in electrochemical conditions. Fe^0 is the redox active state being able to bind CO_2 and thus to enter in the reduction process. CO was found to be the main product and the $Fe^{II}CO$ adduct was identified in solution. As previously mentioned for cobalt, the addition of a sensitizer such as *p*-terphenyl enhanced the overall reaction in the presence of triethylamine. [70]

A main advantage of multi-ring complexes is the possibility to tune their properties through ligand modifications and thus to have a lever to play on the efficiency and selectivity of CO_2 reduction. Under non-sensitized conditions, the reactivity of an iron porphyrin bearing two –OH groups in ortho position of the phenyl rings (Fe-o-OH) showed a different reactivity that the unsubstituted porphyrin (FeTPP).[82] Whereas under light irradiation (> 280 nm) in the presence of TEA as electron donor, Fe-o-OH exhibited a 74% selectivity for CO, FeTPP gave a selectivity of only 31%. This was interpreted by the presence of the –OH groups which stabilized the CO_2 molecule once bound to the Fe^0 center through internal hydrogen bonding. The main limitation of the system was identified to be the formation, during the process, of protonated triethylamine, a strong acid which induced the formation of a metal hydride and thus favored the competing H_2 formation pathway. Moreover, it was shown that the cleavage of the C-O bond requires an extra electron transfer from another Fe^0 molecule, thus limiting its availability for catalysis. The addition of a sensitizer such as $Ir(ppy)_3$ drastically enhanced the performances of the system.[83] Thanks to its strong absorbance in the near-UV-Visible (> 420 nm) region, the UV deleterious photons can be suppressed, limiting catalyst degradation. A linear production of CO could be observed up to 55 h with this sensitizer, indicating that the system was very stable in time, and a TON of 140 with a 93% selectivity for CO was detected. By replacing the iridium sensitizer by the fully organic 9-cyanoanthracene (9CNA), a remarkable 100% selectivity for CO was achieved however with a lower TON of 40 after 45 h of irradiation. By emission spectroscopy, the excited state of 9CNA was proved to be quenched by the electron donor and therefore a mechanism was proposed (Figure 1.22).

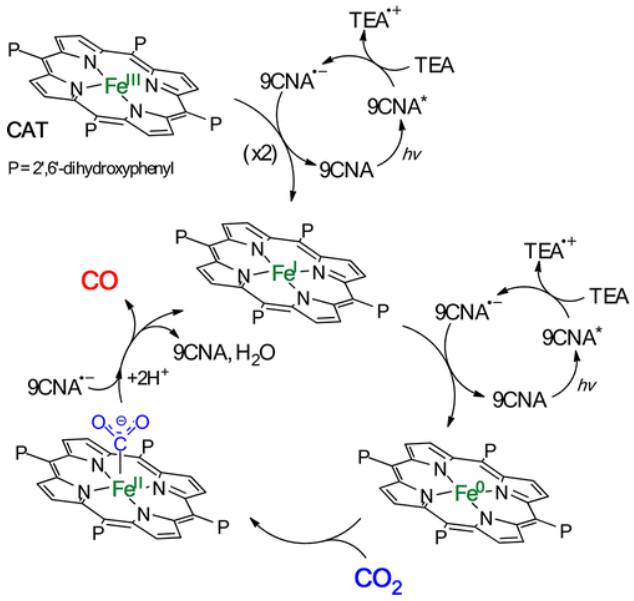

Figure 1.22: Proposed mechanism for CO_2 reduction by substituted iron porphyrins.[83]

In electrochemical conditions, the insertion of four trimethylanilinium groups on the para positions of the phenyl rings was shown to enhance the CO_2-to-CO conversion by both lowering the needed overpotential and by increasing the TOF through columbic interactions between the positive charge of the ligand and the negative charge of the Fe^0-CO_2 adduct.[84] In photochemical conditions, in the absence of a sensitizer, this complex can catalyze the reduction of CO_2 into CO. However, unlike FeTPP, this reduction can be achieved using visible light only, which therefore decreases the degradation of the catalyst. By using BIH as sacrificial donor, a TON of 101 was obtained after 102 h of irradiation, proving the stability of the complex under prolonged light irradiation. Because of the electron withdrawing effect of the anilinium groups, the standard potential for Fe^I/Fe^0 is more positive (-1.26 V *vs.* NHE) than for the non-substituted porphyrin (-1.428 V *vs.* SHE).[84] Thereby, the competition between CO_2 and proton reduction is more in favor of the first one which explain that no H_2 production was observed during the reaction.

As previously observed in the case of Fe-*o*-OH, the addition of a sensitizer greatly improved the performances of the Fe-*p*-TMA catalyst, from 33 to 198 TON for CO production after 47h in acetonitrile solution, with TEA as electron donor. Even more interestingly, with the $Ir(ppy)_3$ sensitizer, CH_4 was detected in the gas phase of the reaction whereas only CO could be obtained with the Fe-*o*-OH catalyst.[85] Under long term experiment, both CO and CH_4 are produced with a linear correlation, proving once again the stability of the catalyst under visible light irradiation. The

addition of an external weak acid such as trifluoroethanol (TFE) improved again the performances of the system both for methane and carbon monoxide production. To achieve the reduction of CO_2 to CH_4, eight electrons and eight protons are necessary, leaving room for all kind of intermediates. In particular, under CO_2 atmosphere, methane could only be detected once a sufficient amount of CO was produced. Indeed, when CO_2 was replaced by CO as starting reactant, the TON for methane was greatly enhanced from 31 to 89 after 47 h irradiation, showing that CO was an intermediate in the reduction of CO_2 to CH_4 and a mechanism was thus proposed (Figure 1.23).

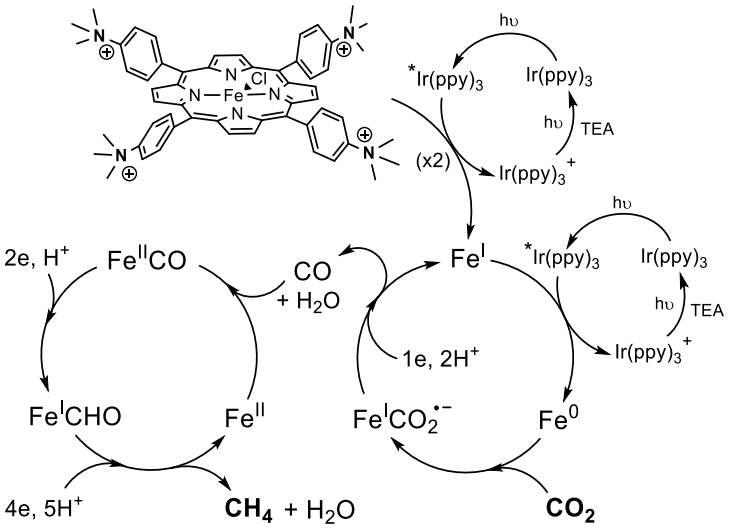

Figure 1.23: Proposed mechanism for the reduction of CO_2 to CH_4 under visible light irradiation.[85]

However, the already demonstrated improved performances of Fe-*p*-TMA compared to FeTPP are not sufficient to explain the methane production because, under electrochemical conditions, only carbon monoxide could be detected.[84] Furthermore, when $Ru(bpy)_3^{2+}$ is employed instead of $Ir(ppy)_3$, only CO and H_2 are detected as reaction products. This could be explained by the more positive reduction potential of the excited state of $Ru(bpy)_3^{2+}$ (-0.81V *vs.* SCE) compare to the one of $Ir(ppy)_3$ (-1.73V *vs.* SCE). When the iridium complex was replaced by fully organic phenoxazine sensitizer, the same trend in the catalyst performances was obtained: CH_4 was obtained after an induction time and the TON was enhanced when switching from CO_2 to CO atmosphere.[30] The phenoxazine sensitizer possesses an excited state redox potential similar as the one of the $Ir(ppy)_3$ (-1.70V *vs.* SCE), reinforcing the hypothesis that a strong driving force through the sensitizer is necessary to trigger methane formation.

1.9 Motivation and outline of this thesis

Developing efficient catalytic systems for CO_2 reduction is a major topic in the renewable energy field. Using visible light as the main source of energy combined with an earth abundant catalyst is a key factor to insure accessibility both in terms of production site and cost for renewable methane production. Unlike hydrogen production, CO_2 reduction still lacks of precisely described mechanisms especially when multi electrons-protons transfer are involved. Moreover, selectivity and efficiency are still far from been optimum.

This thesis aimed at better understanding the process, at the molecular scale, previously reported from our group on the photochemical reduction of CO_2 to methane using a modified iron porphyrin molecular catalyst. In particular, we wanted to identify the key factors and intermediates governing the reactivity with the view to optimize the catalytic process.

Chapter 2 is discussing the possible intermediates in the complete CO_2 reduction to methane and their possible role in the catalytic process. The direct detection in solution of such intermediates was investigated as well as the capacity of the system to reduce each of them.

Chapter 3 is focused on the replacement of the iridium photosensitizer by developing all-organic, and possibly water compatible/soluble, sustainable alternatives.

Chapter 4 is describing the unsuspected role of molecular oxygen in the CO_2 photochemical reduction and its place in the reaction pathway to methane. The possible interactions with the different reactions partners (notably the electron donor) of the system are highlighted.

Chapter 5 is presenting a new electro-assisted photochemical system which can be viewed as the coupling of a pre-reaction unit prior to the photochemical side, and which can also have some applications for further photoelectrochemical studies.

Annexes are finally describing the experimental methods, chemicals and characterization techniques.

Chapter 2 - Investigation of the possible intermediates in the CO_2 reduction process to methane

To achieve highly efficient CO_2 reduction, a complete understanding of the mechanism is necessary in order to optimize the reaction, in particular in terms of operating conditions (co-substrate(s)) and of catalyst structure. For this, the identification of reaction intermediates, either for the catalyst itself (in terms of redox states or adducts) and for possible transient species, is of crucial importance. Reaching highly reduced products, *i.e.* above the commonly faced 2 electrons limit, is a challenge for many research groups.[86]

2.1 CO as the only identified intermediate

Among the various C1 reduction products possibly formed from CO_2 reduction, the most commonly observed is CO, resulting from a 2 electrons and 2 protons process. The mechanism associated with the use of an iron porphyrin as catalyst has been studied electrochemically since the late 1970's. In order to produce CO, the iron center undergoes a series of successive reductions to reach the iron "0" active state at which CO_2 binds the iron center to generate an Fe-$CO_2^{\bullet-}$ adduct.[87] By cyclic voltammetry, it has been showed that a stable $Fe^{II}CO$ adduct is formed during the reaction before being reduced once again in the catalytic cycle to release CO into the solution. Interestingly, among the various modified iron porphyrins synthetized along the years, only one has been showed to be able to reduce CO_2 beyond two electrons in photochemical conditions. Bearing four trimethylanilinium groups on the phenyl ring of the ligand, iron(III) 5,10,15,20 tetra(4'-N,N,N-trimethylanilinium)porphyrin (Fe-*p*-TMA) demonstrated the surprising ability to generate highly reduced products. Robert *et al.* has indeed shown that in photochemical homogeneous conditions, with this catalyst dispersed in an organic solvent, together with an iridium complex as photosensitizer, a sacrificial electron donor and a weak acid, CO_2 reduction upon visible light irradiation produced CO as major product, with H_2 et CH_4 as secondary products.[85] The origin of methane was confirmed by conducting ^{13}C labelled experiments under $^{13}CO_2$, with the corresponding $^{13}CH_4$ indeed formed and identified by mass spectrometry. The 8 electrons and 8 protons process that allows the formation of methane from CO_2 involve multiple steps and the mechanism proposed is shown below (Figure 2.1). For the first part of the reaction, which corresponds to the formation of CO, the mechanism proposed is the same than for FeTPP: an iron "0" state is needed to bind CO_2 and is reduced to an $Fe^{II}CO$ adduct. In electrochemical

conditions, this adduct is simply reduced once and release CO in solution which prevents the formation of CO_2 reduction products above 2 electrons. However, in photocatalytic conditions, methane is produced, which indicates the feasibility of additional electron transfer. The proposed, albeit with no experimental proof, mechanism included the formation of a $Fe^{I}CHOH$ adduct that would undergo a 6 electrons and 6 protons reduction to methane. The exact mechanism, including the possible pathway and the identification of electron/protons transfer steps, was unresolved and my doctoral work was thus primarily focused on the identification of possible intermediates between CO and CH_4.

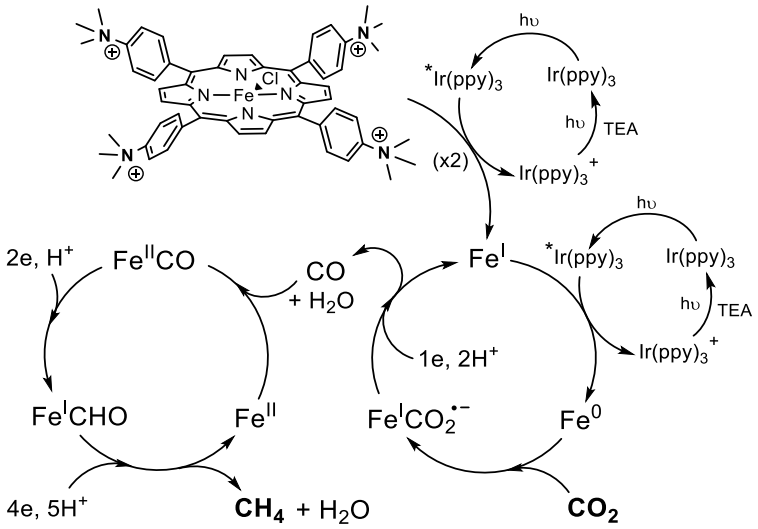

Figure 2.1: Proposed mechanism of CO_2 to CH_4 photochemical reduction.[85]

Even if the exact mechanism for methane formation was still unknown, in particular due to the lack of observable, at least 4 intermediates could be speculated: carbon monoxide as mentioned above, but also formic acid as the second 2 electrons reduction product, formaldehyde (4 electrons) and methanol (6 electrons).

Unless otherwise mentioned, our *standard system* for the photochemical reduction of CO_2 is composed of the following elements (Figure 2.2):

- a substituted iron porphyrin bearing four trimethylanilinium groups in para position as *molecular catalyst* (Fe-*p*-TMA, 2 µM),
- an iridium trisphenylpyridine complex as *molecular photosensitizer* ($Ir(ppy)_3$, 200 µM),
- triethylamine as *sacrificial electron donor* (TEA, 50 mM),
- trifluoroethanol, a weak acid, as an *external proton source* (TFE, 50 or 100 mM).

All these elements are homogeneously dispersed in acetonitrile and saturated with either CO_2 or argon (for control experiments) in a quartz square cuvette of 3 mL liquid volume, surmounted by an empty glassware as headspace. The light illumination at right angle is ensured by a standard AM 1.5G solar simulator, equipped with a glass color filter to block UV (< 400 nm) photons.

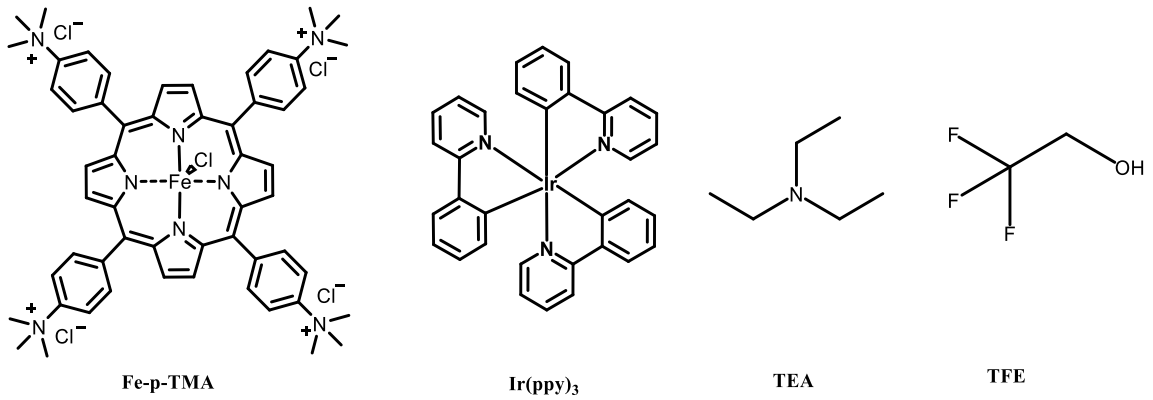

Figure 2.2: Structure of the compounds used in the standard system of this work. Iron catalyst (Fe-p-TMA), photosensitizer ($Ir(ppy)_3$), electron donor (TEA) and proton source (TFE).

Under these standard photochemical conditions, the reduction of CO_2 produced methane, with CO as the major product, H_2 as a minor product, and no formic acid (or other liquid product) detected in the liquid phase. CH_4 could only be detected in the reaction headspace after a few hours of irradiation whereas CO is produced from the beginning of the reaction, suggesting that CO needs to accumulate in a sufficient amount to then trigger methane production. To prove the key implication of carbon monoxide in the mechanism, the reaction was performed under CO atmosphere as starting reactant instead of CO_2, and as a result, the performance toward CH_4 (in terms of turnover number or TON) increased from 31, under CO_2 atmosphere, to 89 for 47 h of irradiation.[85] Moreover, previous spectroscopic evidences, in the absence of photosensitizer whose absorption blinds the porphyrin optical signature, showed the formation of the $Fe^{II}CO$ species along the photochemical process.[82] Given this net increase of TON, CO was confirmed as an intermediate in the mechanism for CO_2 to CH_4 as shown in Figure 2.1.

2.2 Using formate as starting reactant

Regarding the two electron reduction products from CO_2, the formation of formic acid is less thermodynamically favorable, with a standard redox potential of -0.61V *vs.* NHE, compare to -0.53 V *vs.* NHE at pH 7 for CO (Table 1.2).[19] The protonation of the carbon atom is often a dead end

for CO_2 reduction, in the sense that it will lead to formic acid and this product will not be further reduced, thus preventing the reaction to proceed with subsequent electron and proton transfers.[21-22] As mentioned above, formic acid -in fact, its associated base, formate, due to operating conditions- could not be detected in solution by ionic chromatography when methane is produced. Even though it was not expected as an intermediate in the mechanism, the absence of observation of formate in solution is not sufficient to prove that it does not play a role in the process. In the case that formate would be produced but in a highly reactive form or environment, it could be consumed fast enough not to accumulate and/or be detected in solution. To clear this point, we conducted a series of experiments under argon atmosphere, introducing formate in the form of 50 mM sodium formate as starting reactant in the photocatalytic system prior to visible-light irradiation, the solution been saturated with argon. The other parameters (catalyst, sensitizer, electron donor, external acid) were kept constant.

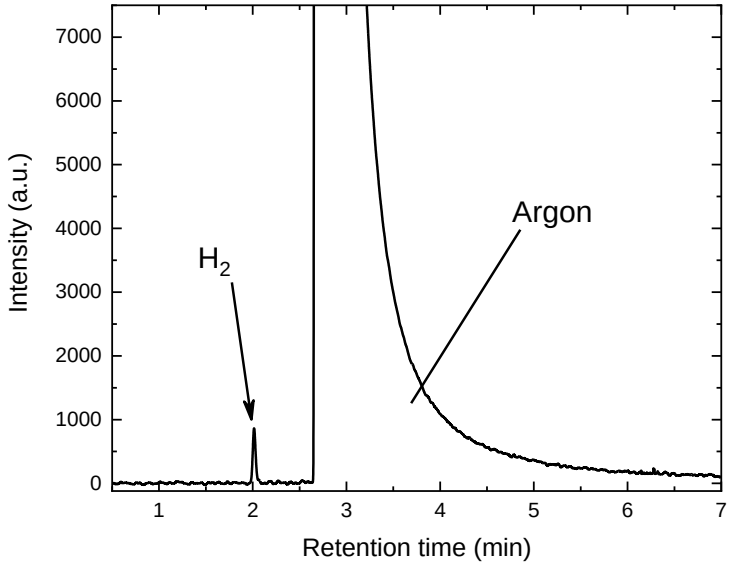

Figure 2.3: Chromatogram of the gaseous headspace after 21 h of irradiation of a catalytic solution containing 50 mM of sodium formate.

As shown in Figure 2.3 after 21 h of irradiation, only molecular hydrogen could be detected as a gaseous product, and analyses of the liquid solution showed the absence of product, *e.g.* either methanol or formaldehyde. Formic acid has therefore been ruled out as an intermediate in the photochemical reduction of CO_2 to methane in our standard conditions.

2.3 Using methanol as starting reactant

2.3.1 Photochemical approach

CO_2 reduction to methanol involves a total transfer of 6 electrons and 6 protons, which makes this conversion particularly difficult to achieve for kinetic reasons. The few examples reported so far were performed on metallic electrodes as electrocatalyst, such has copper.[41] Metallic copper was indeed reported to undergo multiple electron transfers to CO_2 to generate methane as well as various C_2 products such as ethylene.[41] Various mechanisms have been proposed for methane electroproduction, as sketched below.

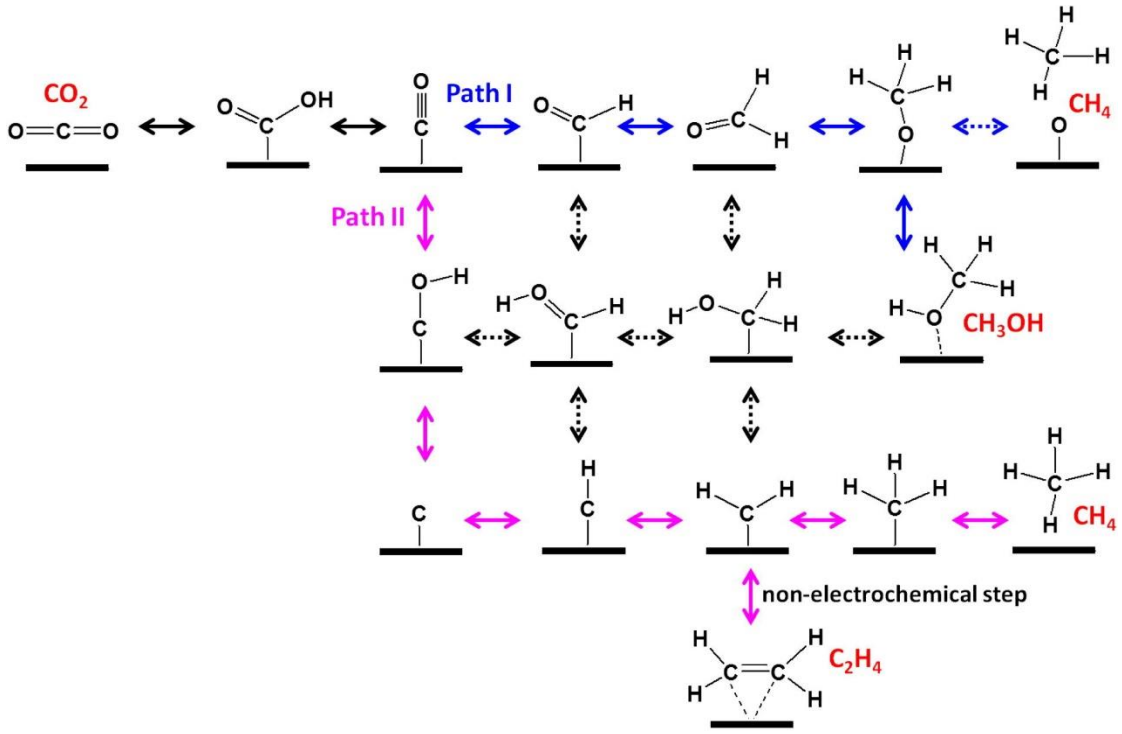

Figure 2.4: Proposed CH_4 production pathways from CO_2 on a Cu (111) surface.[88]

As previously mentioned, if the first protonation occurs on the carbon atom of CO_2, it will lead to formate production that will stop the reaction and is therefore not detailed here. Whatever the pathway followed (Path I or II in Figure 2.4), the first intermediate implying CO is common to both. The pathway is then determined by the protonation site of CO: if it occurs at the carbon atom of CO, it will lead, by keeping the C=O bound intact, to the formation of formaldehyde; if the protonation of CO takes place at the oxygen atom, the C=O bound will be reduced to a single C-O bound, which will further lead to the formation of methanol. Note that in each pathway, the intermediate generated will detach from the electrode by breaking the carbon-copper bound. Even

if the mechanistic pathway on a metal surface cannot be transferred to the molecular case, it gives us clues about the possible transient species that could be expected along the process.

Some molecular catalysts were also reported to reduce CO_2 to methanol electrochemically, for example with a manganese corrole modified with ethylene polyethylene glycol moieties. The catalyst was immobilized on a carbon paper electrode and it could reduce CO_2 to acetic acid with hydrogen and methanol as secondary products. The stability of the system was not evaluated further than 5 h with a reported faradaic efficiency for methanol production as high as 23%.[89] However, no ^{13}C labelled measurement was conducted so the origin of methanol cannot be asserted. In a further study, the same corrole complex was used, replacing the manganese metal center by cobalt, achieving here 59% faradaic efficiency for methanol production from CO_2, but once again with no labelled studies proving that methanol originates from CO_2.[90] In 1984, the Hackerman group showed that cobalt phthalocyanine, when immobilized on a carbon electrode was also able to reduce methanol from CO_2 however with low yield.[91] Recently, our group reinvestigated this catalyst and unambiguously demonstrated, by carefully measurements under $^{13}CO_2$, that methanol indeed comes from CO_2 reduction. We further improved this system with a carbon based conductive ink containing cobalt phthalocyanine catalyst, deposited on a porous carbon paper electrode and showed its capacity of producing methanol from CO_2 or CO.[29] The same catalyst was also able to drive the same process in a photovoltaic assisted electrochemical process (PV-EC).[92] Two pathways were identified for methanol production: the direct reduction of CO to CH_3OH and the indirect CO reduction to methanol through formaldehyde. This necessitated the development of an analytical methodology based on ^1H NMR to readily detect the unstable formaldehyde.[93] Photochemically, a single unit bismuth vanadate layers acting as both catalyst and sensitizer was reported to reduce CO_2 to methanol, again without a required ^{13}C proof, with a selectivity > 80% for methanol production under full solar spectrum irradiation.[94] As for CO_2 electroreduction, CO seems to be the key determining intermediate on graphene TiO_2 surface under visible light irradiation for CO_2 to methanol production.[95]

Here, we must point out a major difference between an electrochemical and a photochemical process. In the case of an electrochemical process, once an intermediate is generated, it diffuses away from the electrode vicinity to the solution bulk and therefore, after several catalytic cycles, the quantity in solution reaches the necessary level to be detectable by standard analytical

techniques such NMR or mass spectroscopy. In a homogeneous system, such as our photocatalytic standard one, because all electron transfers are bimolecular, the reaction is often limited by the diffusion of the reacting species. However, the reaction itself can take place in the whole volume of the cell (the whole solution is illuminated) and is not restricted to a close to surface region as it is in a heterogeneous system. This implies that not all the catalytic sites are in the same oxidation state at a given time, and thus the probability that the intermediate encounters and binds the activated catalyst, *i.e.* at the adequate oxidation state, is much higher than in the case of a heterogeneous system in which all the catalyst molecules are in the same oxidation state near the electrode. In the case of CO_2-to-CO reduction, the required oxidation state of the catalyst is Fe^0 and therefore in a complete homogeneous system, the probability for CO_2 to encounter this state is lower than in a heterogeneous system where all the catalyst will be in this state in the diffusion layer.

In order to detect the two possible intermediates in the reduction of CO_2 to methane, namely formaldehyde and methanol, two main analyses can be performed: NMR and mass spectroscopy coupled to gas chromatography. In the case of NMR, two limitations appear for our system. First, with the available NMR setup, it is difficult to detect a molecule with a near micromolar concentration which thus constitutes the lower limit of detection. For a typically experiment conducted in our standard photochemical conditions, if we suppose that the system undergoes 100 catalytic cycles, because the concentration of the catalyst is 2 µM, the maximum amount of either methanol or formaldehyde that can be produced will be 200 µM, so well below the detection limit, assuming that this theoretical 200 µM amount would not further react with the catalyst. The second limitation relies on the superposition of ^1H peaks coming from the different molecules present in the reaction solution. In particular, the presence of the $Ir(ppy)_3$ sensitizer (200 µM typically) will generate numerous peaks in ^1H NMR around 9 ppm, the region of detection of formaldehyde. This makes difficult the separation of the signals and could confuse or simply prevent the clear and unequivocal compound identification.

Concerning mass spectroscopy, the limit of detection is lower than the NMR and, because it is associated with a gas chromatography, each compound of the reaction solution will be well separated. Moreover, the mass fragmentation pattern associated with a specific peak on the chromatogram will provide evidence about the nature of the molecule detected. However, as

mentioned before, this detection is only possible if the intermediate detached from the catalyst to go in the solution bulk and if it is stable enough, *i.e.* it does not react with the catalyst or evolves too fast to accumulate in sufficient quantity in solution.

So, to investigate the possible role of methanol on the road to methane, we performed experiments in our standard conditions (catalyst, electron donor, sensitizer, external acid) but introducing 5 mM of methanol as the starting reactant, the solution been saturated with argon prior to visible light irradiation. After 21 to 69 h of irradiation, a gas sample from the headspace of the cell was taken and analyzed by GC-MS. The gas chromatogram presented in Figure 2.5 clearly shows an important peak corresponding to the CH_4 retention time.

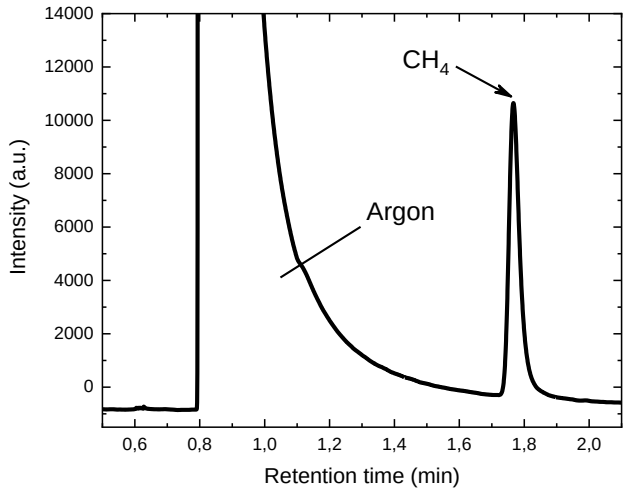

Figure 2.5: Chromatogram of the gaseous headspace after 21 h of irradiation of a solution containing 5 mM of methanol.

Entry	CH_3OH	SD	Acid	Time(h)	TON CH_4
1	5 mM	TEA 50 mM	/	21	5
2	5 mM	TEA 50 mM	TFE 0.1 M	21	12
3	5 mM	TEA 50 mM	TFE 0.2 M	21	11
4	5 mM	TEA 50 mM	TFE 50 mM	21	12
5	5 mM	BIH 5 mM	TFE 0.1M	21	4
6	5 mM	TEOA 50 mM	TFE 0.1 M	69	13
7[a]	5 mM	TEA 50 mM	TFE 0.1 M	21	10
8[b]	5 mM	TEA 50 mM	TFE 0.1 M	21	11

Table 2.1: Methane formation obtained from the photochemical reduction of methanol in acetonitrile solution with 5µM Fe-p-TMA catalyst, 200µM Ir(ppy)3 sensitizer in acetonitrile under argon atmosphere. a with 10mM of CH3OH. b with 50mM of CH_3OH

This experiment has been repeated by changing the nature of the sacrificial electron donor (TEA, TEOA or BIH, Table 2.1). After irradiation, methane has been detected in the gas phase in each case, moreover in a similar amount. As shown in Table 2.1, with no proton source (entries 1 and 5), the TON obtained after 21 h of irradiation is around 5, and does not change significantly when BIH or TEA is used as the electron donor.

As detailed later in this manuscript (Figure 4.11), the sensitizer excited state, once formed, can follow two reaction pathways, either oxidative or reductive. TEA as electron donor does not quench the iridium sensitizer excited state and therefore, in this case, the process is following an oxidative pathway, leading to the generation of the sensitizer excited state which potential is -1.73 V *vs.* SCE.[96] In the case of BIH as electron donor, the iridium excited state is quenched, leading to a reductive pathway and the generation of the reduced iridium complex which potential is -2.19 V *vs.* SCE.[96] This indicates that the reduction of methanol to methane does not depend on the initial sensitizer quenching pathway, *i.e.* on the redox potential available through the iridium complex. Moreover, the fact that the TON for CH_4 does not increase with the initial concentration of methanol (entries 2, 7 and 8 in Table 2.1, from 5 to 50 mM of methanol, respectively) also shows that the limitation of the system is not depending on the initial amount of methanol introduced in the solution.

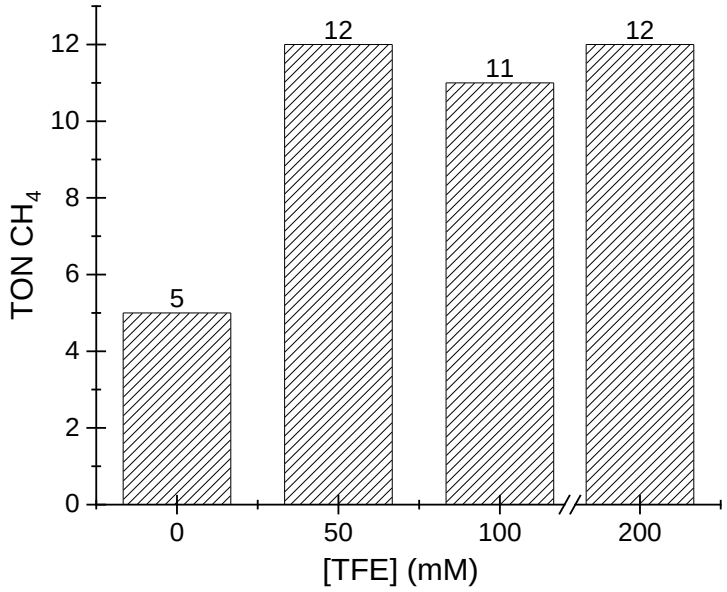

Figure 2.6: TON of CH_4 obtained with various TFE concentrations in an acetonitrile solution containing 5 mM CH_3OH, 5 µM Fe-p-TMA catalyst, 200 µM $Ir(ppy)_3$ sensitizer, under argon atmosphere, after 21 h of irradiation.

TFE was previously shown to be an suitable proton source for the photochemical reduction of CO_2 to methane in our standard conditions: it indeed enhanced the performance of the reaction going from 31 TON of CH_4 to 66 after 47 h of irradiation upon addition of 0.1 M.[85] This effect was also observed for the formation of CO in electrochemical conditions, with an increase of the catalytic wave for CO_2 reduction with addition of TFE (Figure 2.10) in cycle voltammetry measurements. Regarding methanol photochemical reduction, the TON for CH_4 production goes from 5 (Table 2.1, entry 1) to 12 (entry 4) after 21 h of irradiation with addition of 50 mM of TFE. This increase was expected since protons are necessary in the reaction and because without the addition of external acid, the only proton source is residual water present in the solvent. Surprisingly, when higher concentrations of TFE, *e.g.* 110 and 200 mM were introduced (Table 2.1, entries 2, 3, respectively), the TON for CH_4 was not improved as depicted in Figure 2.6. This absence of catalytic enhancement once again suggests that the amount of protons available in the catalytic system is not the limiting factor of the process. We have previously shown that using a phenoxazine type sensitizer and using CO as the starting reactant, the use of a stronger acid (phenol) only slightly increases the formation of CH_4, together with an increase in H_2 formation.[30] Thus, we could hypothesize that the pKa of TFE is too high to efficiently transfer the last proton for reducing methanol to methane.

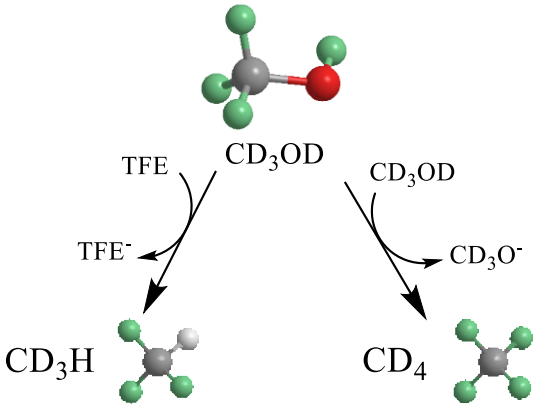

Figure 2.7: Possible pathways for methane formation from methanol taking into account the H/D labelling.

Another point of caution must be taken when the target compound is methane since it can be generated, under certain conditions, from the degradation of various organic molecules and thus its origin should then be investigated carefully. In other words, its "simple" detection by gas chromatography is not a sufficient proof to claim that it is indeed coming from CO_2 or other substrate reduction. One masterpiece of evidence relies on isotope labelled studies, using ^{13}C, to

assert the carbon atom origin. In the present case, two molecules can be used to confirm the formation of methane from methanol. First, as for CO_2 reduction, we could monitor the labelled carbon atom of methanol ($^{13}CH_3OH$) that would give, once reduced, $^{13}CH_4$ with an associated m/z 17 (instead of 16 for regular ^{12}C methane); second, fully deuterated methanol CD_3OD can be employed to monitor deuterium atoms. The advantage of deuterated methanol compared to ^{13}C methanol is that it can give us more information regarding the proton insertion.

Considering CD_3OD reduction, we could expect to detect two different analogues (Figure 2.7), depending on the last protonation step. If fully deuterated methane CD_4 is generated, it is an indication that the last inserted proton comes from another molecule of deuterated methanol that could also plays the role of proton donor. The detection of CD_4 should then be accompanied by the detection in solution of some amount of heavy (D_2O) or semiheavy water (HDO). If, on the contrary, partially deuterated methane CD_3H is detected in the gas phase, it indicates that the last proton does not come from another methanol molecule but from another source, most likely the external weak acid added in solution, *e.g.* TFE. To differentiate the two analogues, GC coupled to mass spectrometry was employed to analyze isotopically labelled experiments, having in mind that the expected m/z are either 20 for CD_4 or 19 for CD_3H.

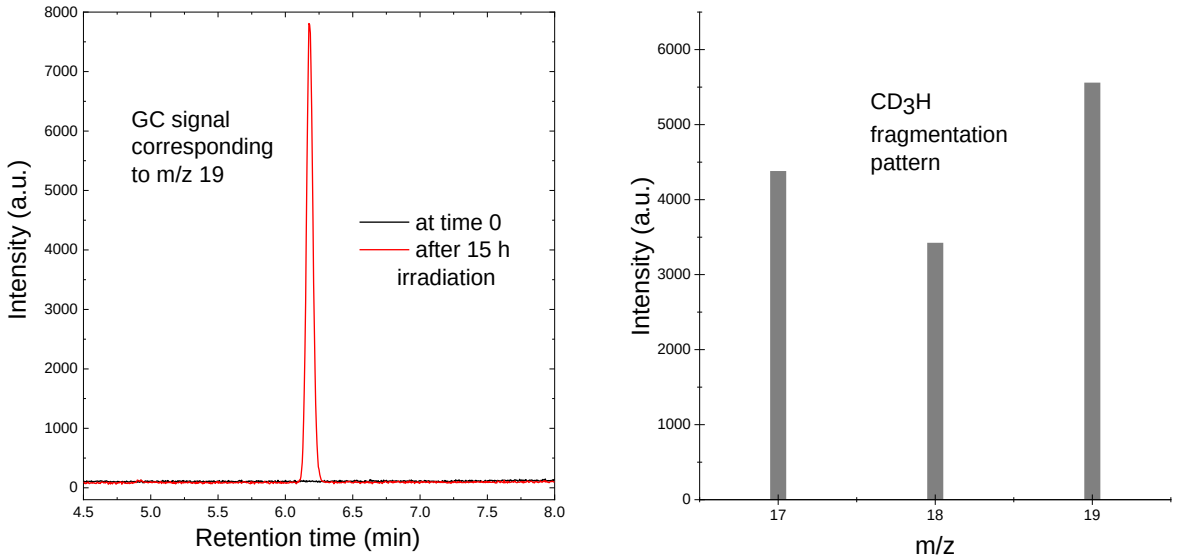

Figure 2.8: Gas chromatogram (left) and corresponding mass spectrum (right) showing the fragmentation pattern of CD_3H (m/z 19).

As shown in the gas chromatogram in Figure 2.8 (left), after 15 h of irradiation, a GC signal is observed at the retention time corresponding to methane. The associated mass spectrum (Figure 2.8, right) to this peak shows three contributions at m/z at 19, 18 and 17, which correspond,

respectively, to CD_3H, CD_3^+ and CD_2H^+. The fact that the m/z 17 peak is higher than the m/z 18 is quite unusual but it can be explained by the fact that a CD_3H molecule (m/z 19) is more likely to lose a (heavy) deuterated atom during the fragmentation in the mass spectrometer than a (light) hydrogen one, making the m/z 17 peak higher than the 18. Indeed, this pattern has already been reported in the literature.[97]

The same standard experiment was repeated using deuterated acetonitrile (acetonitrile-d_3, CD_3CN) solution in the presence of deuterated TFE (2,2,2-trifluoroethanol-d_3, CF_3CD_2OD) as "proton" source. The results obtained was the same, *i.e.* CD_3H was identified in the gas phase.

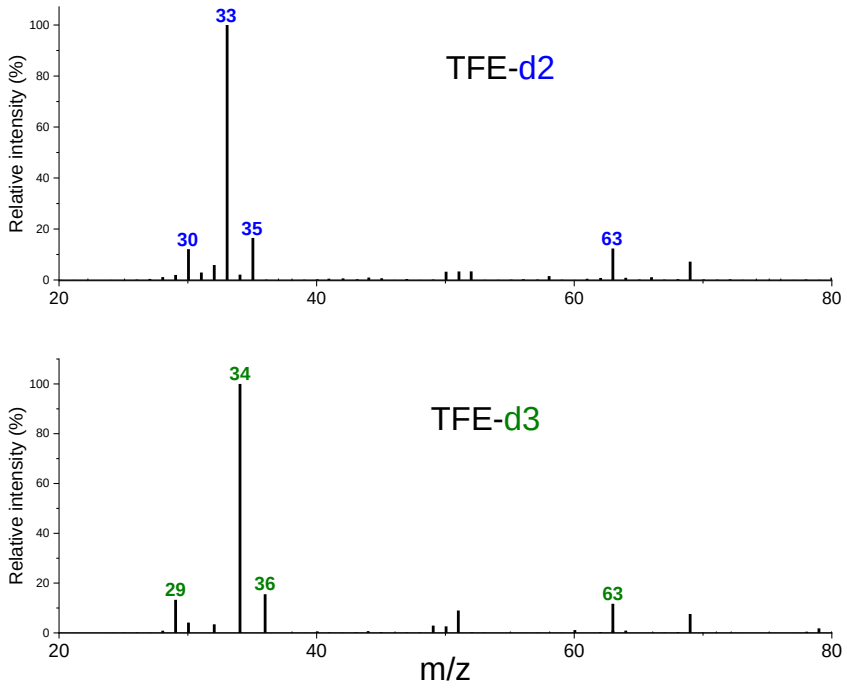

Figure 2.9: Mass spectra showing the fragmentation patterns of doubly (top) or triply (bottom) deuterated trifluoroethanol.

The fact that CD_4 was not identified and that CD_3H seems to be the only reduction product could be explained by the presence of residual water in the system ("dry" acetonitrile always contains few mM of water). As a consequence, some proton exchange may occur, the labile deuterium atom of the alcohol group of methanol being replaced by a hydrogen one. This is also coherent if we consider that the absolute amount of methane theoretically formed in our process is intrinsically low, well below the mM level. This hypothesis is corroborated by the presence of a peak at the retention time corresponding to a TFE-d2 fragment with a m/z 33. This peak corresponds to the CD_2OH^+ fragment whereas in fully deuterated environment, one would expect the CD_2OD^+

fragment at m/z 34. Despite an unresolved last proton insertion step, these results provide quite clear evidences that methanol can be reduced to methane in our photochemical standard conditions, but we cannot assert that methanol is an intermediate in the CO_2-to-CH_4 transformation.

2.3.2 Electrochemical approach

The Fe-p-TMA catalyst studied in our group exhibited particularly high performances, both in terms of turnover frequencies and of overpotential for the electrochemical CO_2 reduction, compare to other iron porphyrins developed so far, with or without substituent on the phenyl rings.[84] This improvement has been attributed to the electron withdrawing effect of the four trimethylanilinium groups that shift the overpotential to a more positive value. Moreover, the positives charges induce a coulombic effect that can stabilize the Fe-CO_2 adduct, therefore improving the rate of the catalysis, this effect being even stronger when the anilinium groups are in ortho positions. In addition, in electrochemical conditions, it has been shown that phenol acts as a good proton source for the CO_2 reduction process.[93] However, for comparison purpose with our standard photochemical system, we here report the use of TFE as external acid in the following electrochemical measurements.

To try to decipher the role of the external acid in the reduction process, we thus have conducted two electrochemical measurements by cyclic voltammetry, with Fe-*p*-TMA as homogeneous catalyst. In the first one, CO_2 is used as the starting reactant, with TFE (1.3 M) as external weak acid (Figure 2.10). Compared to argon atmosphere (black trace), a strong increase in current (red trace) was observed at the Fe^I/Fe^0 wave, showing that TFE is an efficient proton source to assist the catalytic CO_2 reduction by Fe-*p*-TMA.

In the second experiment, methanol was used as starting material instead of CO_2 (Figure 2.11). In the presence of TFE (1.3 M), under argon atmosphere, little to no change in current could be observed at the Fe^I/Fe^0 wave, except a small increase that could be attributed to hydrogen evolution when methanol concentration increased. In other words, with methanol as reactant, there is no catalysis with Fe-*p*-TMA in the presence of TFE in electrochemical conditions, most probably because methanol cannot bind the iron center. So, Fe-*p*-TMA catalyst is not active toward CH_3OH reduction in electrochemical conditions whereas in photochemical conditions, methane can be obtained. This is in line with an observation previously made with CO_2 as starting reagent. In

electrochemical conditions, no further reduced compound than CO can be obtained whereas CH_4 is produced upon visible light irradiation.

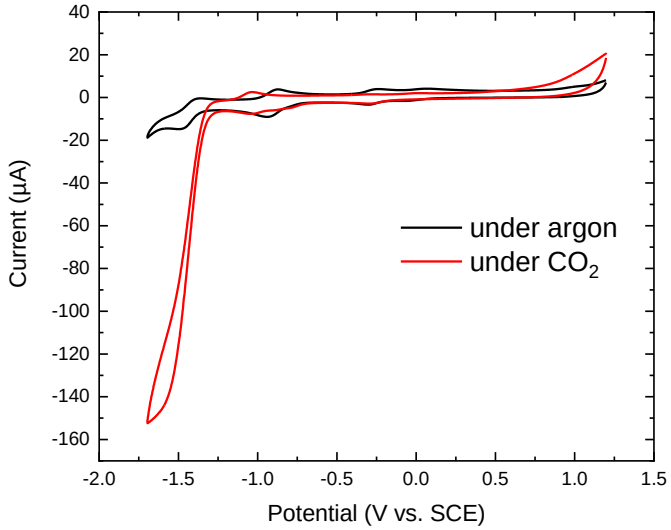

Figure 2.10: CV of Fe-p-TMA catalyst (1 mM) in DMF under argon atmosphere (black) and CO_2 (red) with 1.3 M TFE, on glassy carbon electrode (Ø = 3 mm), scan rate 100mV s^{-1}.

To sum up, the intimate mechanism form CH_3OH to CH_4 is still unresolved. We can however make the hypothesis that there no interaction/binding between the catalyst, whatever its oxidation state, and methanol, since CV measurements in the presence of the latter showed the absence of methane as product. The reduction to CH_4 would not be the result of two successive electron transfers followed/coupled with a proton transfer at a CH_3OH molecule, but would rather results from the reaction with a hydride generated at the iron center in photochemical conditions only.

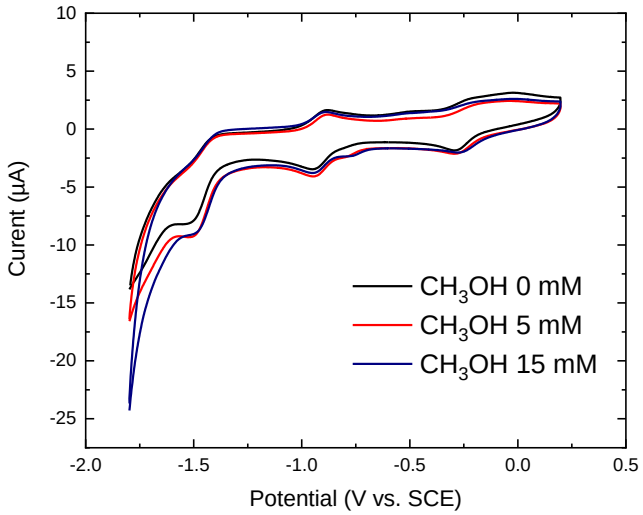

Figure 2.11: CV of Fe-p-TMA catalyst (1 mM) in DMF under argon atmosphere with 1.3 M TFE (black), on a glassy carbon electrode (Ø = 3 mm) with addition of 5 (red) or 15 mM (blue) of CH_3OH , scan rate 100 mV s^{-1}

Actually, the reduction of methanol to methane has been, to date, scarcely reported. An electrochemical example was reported in the late 1980's on ruthenium and copper metal electrodes.[98] Regarding photochemical reduction, under strong UV light (< 300 nm), some metal salts such as Fe^{2+} or Cr^{2+} can reduce formaldehyde to methanol, and even methanol to methane in the case of Cr^{2+} with however very low yield.[99] To our knowledge no other report has been made so far on the molecular photo- or electro-chemical reduction of methanol to methane.

2.4 Using formaldehyde as starting reactant

Interestingly, it has been shown that on a metal copper electrode with no particular facet exposed, methanol was not reduced electrochemically to methane, but, on the contrary, formaldehyde could generate methane under reductive potential.[100]

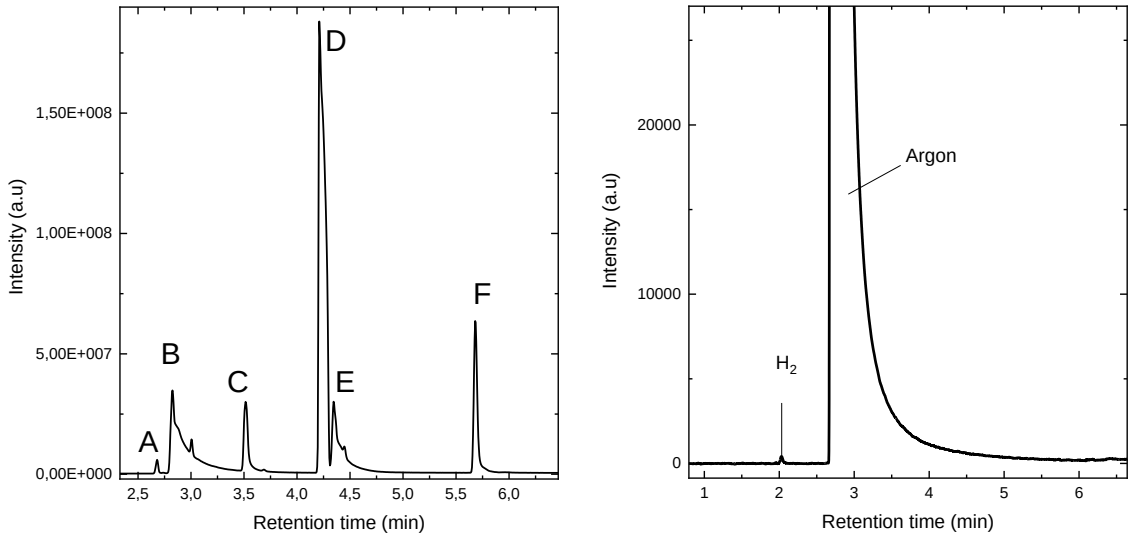

Figure 2.12: Gas chromatograms of an aliquot of catalytic solution containing 20 mM of formaldehyde (left) and of the solution headspace under argon atmosphere (right), after 21 h of irradiation.

The possibility for formaldehyde to be an intermediate in the photochemical reduction of CO_2 to methane by our system was thus also investigated. As for methanol, the standard solution containing the catalyst, the sensitizer, the electron donor and the external acid was placed under argon atmosphere and formaldehyde was added as the starting reactant. After irradiation, the gaseous headspace of the reaction vessel was analyzed by gas chromatography but no gas other than argon could be detected (Figure 2.12, right). The solution was also analyzed by GC-MS and no liquid product could be either detected (Figure 2.12, left). The molecules detected are the ones

introduced in the solution, respectively formaldehyde (B), triethylamine (C), acetonitrile (D) and trifluoroethanol (F). The peak (A) corresponds to the peak of argon and the peak (E) corresponds to residual water in the solvent. Because formaldehyde is a quite unstable molecule which can rapidly polymerize, its monomeric detection is not easy. Thus, a stock solution of formaldehyde was prepared by introducing a known amount of paraformaldehyde in a 0.1 M KOH solution and stirred for 2 h to obtain a complete depolymerization and then was used as starting reactant.

In aqueous solution, formaldehyde can undergo the Cannizzaro reaction (Figure 2.13): two formaldehyde molecules react to form formate on one side and methanol on another side. As shown previously, our photochemical system is able to reduce methanol to methane and therefore, if a Cannizzaro reaction occurs here, methanol and formic acid should be detected in the liquid phase and methane could also be detected in the gas phase due to methanol reduction. However, since none of these molecules were detected in liquid phase, it could suggest that formaldehyde repolymerizes quickly in solution under our standard conditions. To more clearly decipher the implication of formaldehyde in this reaction, further investigations must be made, in conditions which would prevent both Cannizzaro reaction and polymerization of formaldehyde.

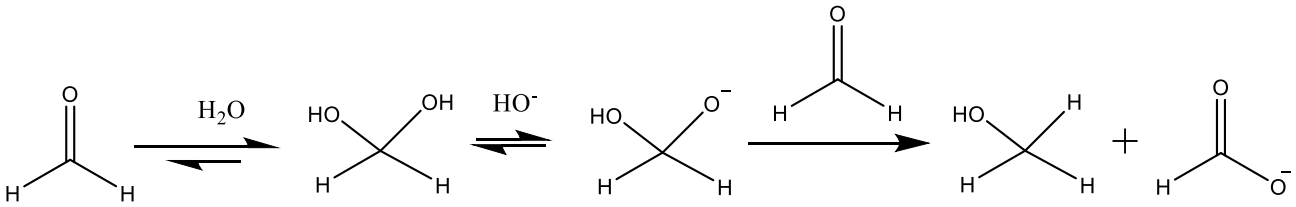

Figure 2.13: Cannizzaro reaction of aqueous formaldehyde.

2.5 Sub-conclusions and perspectives

CO_2 reduction to CH_4 by a molecular catalyst is possible by employing a modified iron porphyrin complex under visible light irradiation in the presence of suitable partners, *e.g.* a strongly reducing Iridium-based photosensitizer, a sacrificial electron donor and an external weak acid. Among the possible intermediates formed during the reaction course, CO was early identified by spectroscopic techniques and by using it at the starting material, and remains the only confirmed one to date. However, part of the mechanism is still unresolved.

Starting molecule	Obtained products
CO_2	H_2, CO, CH_4
CO	H_2, CH_4
HCOOH	H_2
HCHO	H_2
CH_3OH	H_2, CH_4

Table 2.2: Reduction products obtained from various starting reactant with our standard photochemical system

Liquid products corresponding to 4 and 6 electrons reduction, namely formaldehyde and methanol, have not been detected in solution during the CO_2 photochemical reduction in our conditions but it could be due to i) their transient nature in the process and/or ii) their absolute very low amount in solution, especially concerning formaldehyde due to its intrinsic instability. However, it does not necessarily mean that they do not participate in the reaction in some extent. We therefore investigated the capacity of our photochemical standard system to reduce these molecules by employing them as starting materials, in the same way than for CO. We did not succeed in the reduction of formaldehyde to methane, and no other reduction product such as formate or methanol was observed as well, whereas we know that the Cannizarro reaction could generate some. This seems to indicate that formaldehyde is not stable in solution in our conditions, *i.e.* it could be present in the polymeric form which is quite difficult in GC analysis to discriminate from the monomeric form. Therefore, HCHO reduction seems not possible in our standard conditions. Further investigations, with alternative strategies still to build, are needed to rule out this molecule as a possible intermediate. On the other hand, the photochemical reduction of methanol to methane was achieved with an average TON of 10 after 21 h of visible light irradiation. Changing parameters such as the nature of the sacrificial electron donor or the nature of the proton source did not increase the yield of the reaction and the limiting factor to reach higher conversion yield is still unknown. Labelled studies with ^{13}C methanol were conducted and the origin of methane was proved to be the reduction of methanol. However, despite repetitive attempts, when methane is produced from CO_2, no methanol could be detected in solution, rising therefore two hypotheses as depicted in Figure 2.14.

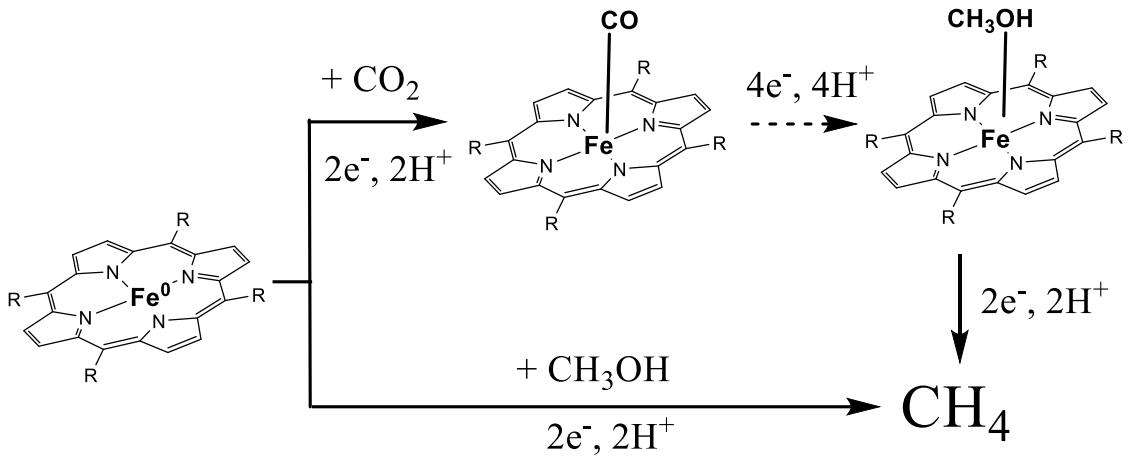

Figure 2.14: Possible pathways on the route to CH_4 from CO_2 reduction.

First, methanol is a reaction intermediate in between CO and CH_4 but its reduction to methane is too fast/efficient thus preventing its accumulation in a sufficient amount to be detected. Second, methanol is not a reaction intermediate, but our strongly reducing photochemical standard system is able to reduce it to methane through a series of electrons and protons to be deciphered.

Our efforts are still ongoing to define alternative strategies to be able to observe transient species and thus to decipher the reaction mechanism.

Chapter 3 - Towards new, all-organic, photosensitizers

3.1 Basics of photosensitization

The term photosensitizer (PS) defines a compound (molecule or material) able to harvest light and to transfer the corresponding energy to another close by compound, most of the time through an electron transfer, H atom abstraction being another alternative. This transfer is possible by the initial promotion of an electron of the PS to a PS* excited state, either singlet or triplet in the case of a molecular species, which will then be transferred to an accepting entity (molecule or material). For commonly used molecular inorganic PSs, the electron transfer generally proceeds from the longer-lived triplet state after an initial, fast $^1A \rightarrow ^3A$ intersystem crossing (Figure 1.8). At the end of the process, the PS returns to its ground state through a compensating electron transfer from an electron source such as a biased electrode or a sacrificial electron donor in homogeneous systems.

In a fully homogeneous system like ours (see description in Chapter 2 section 2.1), three parameters of the photosensitizer are of particular interest: the emission quantum yield, the excited state triplet lifetime and the excited state reduction potential. The first one relies on the number of photons that are spontaneously emitted when an electron initially promoted to an excited state, relaxes to the ground state. The smaller this parameter, the higher $^1A \rightarrow ^3A$ intersystem crossing is likely to happen, and thus favoring the proportion of excited electrons reaching the triplet state. The latter is of high interest in homogeneous systems since it is generally of (much) longer lifetime (up to µs timescale typically) than singlet states. Electron transfers indeed occur thanks to bimolecular diffusional encounters and so the excited state lifetime is a key parameter that drives the probability of electron transfer between the donating and the accepting compounds. Finally, the reduction potential of the excited state, which can be compared to the potential applied to an electrode in an electrochemical process, defines the energy available to the electron to launch the reaction. In other words, it defines the limit between accessible and non-accessible redox states for the process. Taking into account these three key parameters, organometallic complexes, mostly based on rare or noble metals (ruthenium, iridium) have been massively employed in photochemical processes for CO_2 reduction since the pioneer work of Lehn in early 1980's.[60, 96, 101]

3.2 Organometallic sensitizers

Thanks to their extensive π system, macrocycles are interesting candidates for visible light sensitization and have been widely developed for another field of photochemistry, *i.e.* dye-

sensitized solar cells (DSSC).[102-104] For example, by incorporating copper in a phenanthroline macrocyclic, an efficient sensitizer exhibiting a triplet lifetime of 3.19 µS and an excited state redox potential of -1.10 V *vs.* SCE was reported, showing interesting photochemical performances, especially in terms of quantum yield, when associated with an iron based complex for the reduction of CO_2.[76] Bipyridine based sensitizer are widely used, with the best example is $Ru(bpy)_3^{2+}$ which is used in all fields of photochemistry with numerous analogues reported based on modification of the ligand.[25, 105] Earth abundant metal such as copper can also be incorporated into a bipyridine ligand to obtain a sensitizer with properties close to the ruthenium one in terms of absorption and emission wavelengths combined with a more negative reduction potential (-1.44 V compared to -1.33 V *vs.* SCE for $Ru(bpy)_3^{2+}$).[25, 106] Other types of ligand, such as the phenylpyridine one of the $Ir(ppy)_3$ sensitizer we are using in our standard system, are also widely employed and reported in numerous publications. [25, 85, 107]

Among the variety of macrocycles, porphyrins are of particular interest since their properties can be tuned by modifying the ligand, as reported for many examples of Zn-porphyrin sensitizers.[108-110] Non-metallated porphyrins can also be used as visible light sensitizer but they generally suffer from photobleaching, a phenomenon of less importance when a metal center is incorporated in the complex.[111] Undesirable phenomena, such as fast excited state deactivation or reverse electron transfer from the excited state, can be countered by linking an electron storing moiety (forming so-called "dyads"), thus resulting in a more efficient visible light sensitization.[112] Porphyrins are also known as catalysts in numerous reactions such as organic synthesis, polymerization, protons reduction, CO_2 reduction, and they present the capability to play two roles, *i.e.* they can both harvest light and act as catalyst without the presence of an external sensitizer.[113-115] Regarding CO_2 photochemical reduction, a zinc porphyrin has for example been reported to be an efficient photosensitizer associated with a manganese complex thanks to a very long excited state triplet lifetime of 1.5 ms even if the stability of the system was not exceeded 3 h upon irradiation.[116] The capacity of zinc porphyrins to efficiently harvest light was also demonstrated when associated with TiO_2/Re(I) nanoparticles for CO_2 to CO reduction with a quantum yield of 4.8% and a corresponding TON over 2500 after 46 h of irradiation, showing the good stability of such molecule.[117] Once again, a number of dedicated reviews exists in the literature on this topic, especially because sensitizers are also employed in photodynamic therapy.[96, 118-122]

3.3 Towards all organic sensitizers

In recent years, extensive studies have been carried out to find sustainable alternatives to noble metal based sensitizers, for example by using transition metals or by switching to fully organic compounds, as more commonly done in organocatalysis.[123] In that objective, highly delocalized π-systems are targets of choice because they are expecting to exhibit strong visible light absorption and good stability under photo irradiation, as well as easier synthesis than organometallic complexes. In this thesis work, we thus have explored two possible purely organic alternatives to the costly iridium-based sensitizer used in our standard system.

3.4 Coumarins

Discovered in 1820 by both the French chemist N. Guibourt and the German chemist A. Vogel, the coumarin is a small aromatic molecule composed of a benzyl ring bearing an adjacent cyclic ester and is naturally present in many plants (Figure 3.1).[124] Numerous analogues have been reported through years. Their photophysical properties are largely documented since they are often employed in sensors, pharmacology as well as in dye-sensitized solar cells.[125-128]

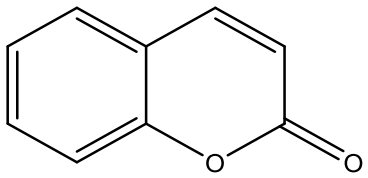

Figure 3.1: Structure of the coumarin core.

This family of molecules combine two characteristics that are essentials for an environmentally friendly and sustainable CO_2 reduction photochemical system: a full organic structure, free of rare/noble/toxic metal and a high solubility in water, bypassing the use of organic solvent. These two properties, shared by a lot of other organic dyes, however must be combined with two other requirements, already mentioned previously: i) an excited lifetime long enough to allow diffusional encounters and bimolecular electron transfers and ii) an excited state reduction potential able to transfer electrons to a catalyst up to its active state. Because iron porphyrin catalysts need to be reduced to the Fe^0 state to reduce CO_2, a reduction potential as negative as -1.47 V *vs.* SCE is necessary to reach the active state of Fe-*p*-TMA catalyst (and even more negative for other analogues).[129] Combining all these properties is far from being trivial and it necessitates synthetic engineering in order to obtain the desired compound. In collaboration with Pr. Pier Cozzi at University of Bologna, Italy, a new coumarin derivative, absorbing in the visible domain (Figure

3.2), was developed and send to us to evaluate its possible ability to play the role of photosensitizer in CO_2 reduction process in aqueous environments.

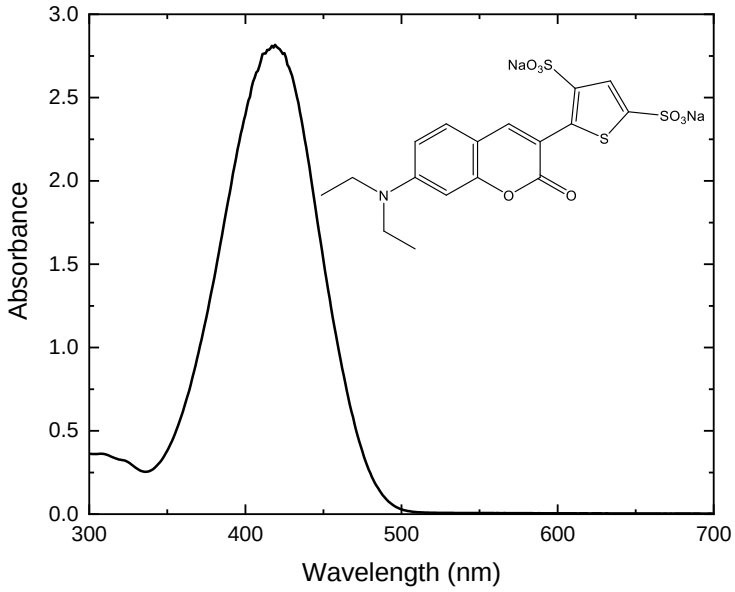

Figure 3.2: UV-visible spectrum of 1 mM coumarin aqueous solution and its molecular structure.

Before integrating this molecule as photosensitizer in our standard catalytic system, spectroscopic characterizations were performed and, in particular, we performed emission quenching measurements to determine the excited state quenching pathway. Upon monochromatic excitation at 420 nm, according to its UV-Visible absorption spectrum (Figure 3.2), the coumarin excited state is formed. In the presence of increasing amount of TEA (the typical sacrificial electron donor we use), no emission quenching was observed, corresponding to an absence of electron transfer between the two compounds. On the contrary, in the presence of increasing concentration of Fe-*p*-TMA catalyst, a clear decay of the emission intensity was observed, and the corresponding Stern-Volmer analysis gave a quenching rate of 1.05×10^{13} M^{-1} s^{-1} corresponding to a diffusion-limited process. As a consequence, we have determined that the coumarin excited state is efficiently quenched by the catalyst following an oxidative pathway (see Chapter 1, Figure 1.10).

The electron transfer thus occurs from the coumarin excited state, with a reported reduction potential of -1.87 V *vs.* SCE, to the iron catalyst allowing the catalyst to be reduced down to the Fe^0 state since it is negative enough.[130] From a thermodynamics point of view, the proper activation of the catalyst is thus possible.

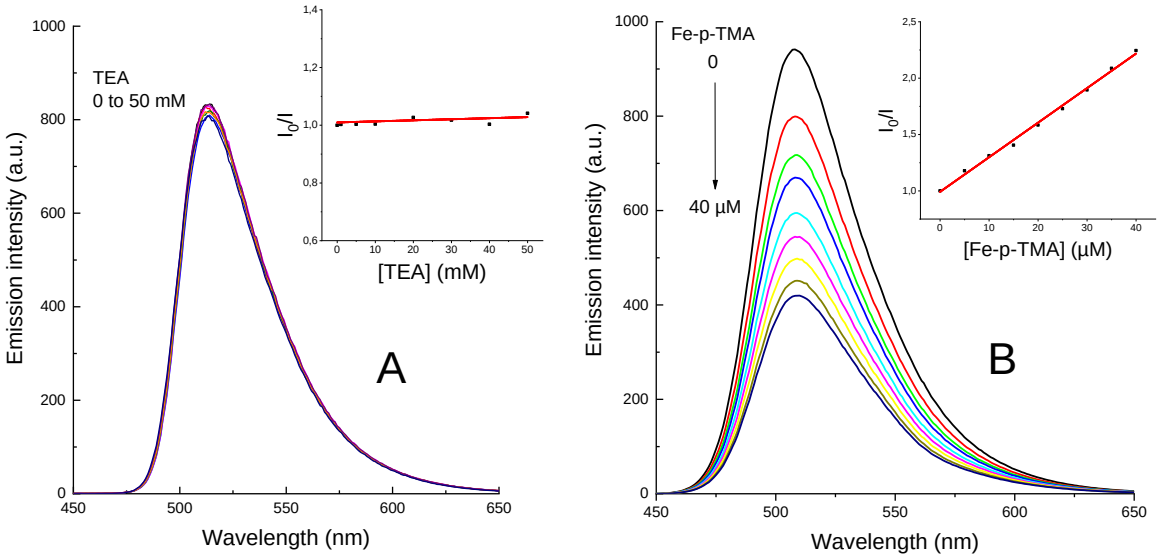

Figure 3.3: Emission quenching measurements of coumarin (1 mM in degassed water), and corresponding Stern-Volmer analysis (inset), upon addition of TEA (A) or Fe-p-TMA (B) , with λ_{exc} = 420 nm.

Using water as solvent induces to take into account additional aspects compared to an organic solvent, including, but not exclusively, pH, ionic strength and solubility issues. Thanks to the presence of four positively charged groups on the ligand, Fe-*p*-TMA catalyst is soluble in water at the condition that chlorine is used as counter anion instead of PF_6 (see Annexes 5.5). Moreover, its high activity is in part due to the presence of these charged groups which can have stabilizing columbic interactions with CO_2.[84] In aqueous solutions, HO^- ions are likely to interact with the -$N(CH_3)_3^+$ groups resulting in a slightly weakened stabilization of the CO_2 adduct and thus of the intrinsic activity of the catalyst. This influence of the solvent can be investigated by cyclic voltammetry (Figure 3.4). The redox waves of the catalyst are less defined, in particular the Fe^{III}/Fe^{II} reduction wave is almost not visible and the Fe^{I}/Fe^{0} wave cannot be observed at all, because of protons reduction occurring at the electrode surface, and also catalyzed by the porphyrin, at this potential.

However, under CO_2 atmosphere, Fe-*p*-TMA catalyst still exhibits high catalytic current and the reduction of protons is strongly limited by the presence of CO_2 for which the catalyst has high affinity, as demonstrated by a previous report from our group showing that the selectivity for CO production under controlled potential electrolysis remains as high as 98% even after 72 h of reaction.[131]

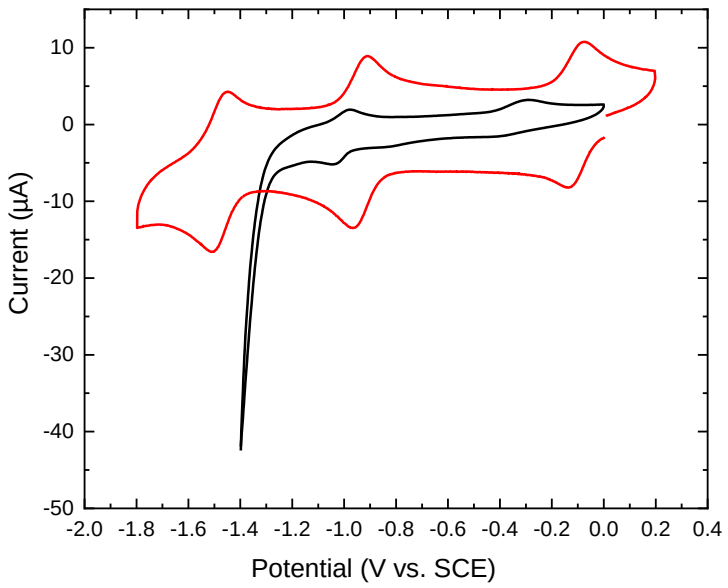

Figure 3.4: Cyclic voltammetry of 0.5 mM Fe-p-TMA under argon in DMF solution (red), in water with $KHCO_3$ 0.5 M (black), scan rate 0.1 V s^{-1}

To explore the possible pH effect either on the catalyst, the photosensitizer and/or the sacrificial electron donor, various experimental parameters were tuned in homogeneous photochemical conditions (Table 3.1).

Entry	Medium	Coumarin	SD	External acid or base	Time (h)	TON CO	TON H_2
1	ACN	0.2 mM	TEA 50 mM	TFE 0.1 M	68	97	4
2	H_2O	1 mM	TEA 50 mM	/	40	0	0
3	H_2O	0.2 mM	TEA 50 mM	HCl 10 mM	20	0	0
4	H_2O	0.2 mM	TEA 50 mM	NaOH 10 mM	20	0	0
5	$KHCO_3$ 0.1 M	0.2 mM	Ascorbate 50 mM	/	20	0	0
6	$KHCO_3$ 0.1 M	0.2 mM	TEA 50 mM	/	40	0	0
7*	$KHCO_3$ 0.1 M	0.2 mM	Ascorbate50 mM	/	20	35	53

*Table 3.1: Photochemical reduction of CO_2 by Fe-p-TMA catalyst (10 µM in aqueous solution) under visible light irradiation using various conditions. * with $Ru(bpy)_3^{2+}$ as photosensitizer.*

As can be seen from Table 3.1, in aqueous environments, no CO_2 reduction activity could be observed when using the coumarin as sensitizer (entries 2-6) in combination with Fe-*p*-TMA catalyst, in comparison with entry 7 in which the photosensitizer was $Ru(bpy)_3^{2+}$. With the latter, molecular hydrogen was the main reaction product (TON 53), with CO as the secondary one (TON 35), thus showing that Fe-*p*-TMA is indeed an active catalyst for CO_2 reduction in aqueous

solutions, albeit with poor selectivity. In contrast, in ACN (entry 1), a modest TON of 97 for CO was obtained after 68 h of irradiation, indicating that the coumarin sensitizer is able to provide electrons to the porphyrin catalyst, as expected from the emission quenching measurements (Figure 3.3), to yield a high CO selectivity.

The lack of reduction products for entries 2-6 can most probably be explained by a crucial intrinsic property of the coumarin sensitizer, *i.e.* its triplet state lifetime. It has indeed been reported to be as short as 2.9 ns along with a fluorescence quantum yield of 0.57 (measured in DMF).[130] As previously mentioned, this cannot be suitable for an efficient electron transfer in a diffusion controlled process, the coumarin triplet excited state being not long living enough to statistically let the catalyst to diffuse to it. As a consequence, unless more structural modifications (not identified yet) can be made to greatly increase the excited state lifetime, the coumarin family seems to not be the good track to follow to replace organometallic PS for the photochemical CO_2 reduction in aqueous environments.

3.5 Phenoxazines

Phenoxazines are a class of photoactive organic molecules composed of a oxazine core with two benzene rings attached (Figure 3.5).[123, 132]

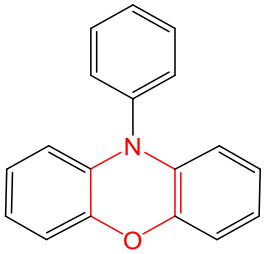

Figure 3.5: Structure of the phenoxazine core, based on the 1,4-oxazine unit (red).

Primarily used for their pharmacologic properties as antitumoral agents, the photophysical properties of phenoxazines were firstly described in 1943, their oxidation being evidenced under light irradiation.[133] Since the early 2000's, their light harvesting and redox properties have known a renewed interest, especially in the field of organic dye-sensitized solar cells.[134-140] The aromaticity of the core can be extended through ligand modification, tuning the HOMO-LUMO bandgap and achieving a solar energy-to-electricity conversion of 7.7%, close to the 8% reported for a ruthenium organometallic complex (RuN719).[134] This class of molecules was later used in homogeneous conditions as photocatalyst for organocatalyzed atom transfer radical

polymerization.[141-142] By modifying the ligand of the phenoxazine core, the group of G. M. Miyake at Colorado State University, USA, has managed to tuned a variety of their physical properties, including the location of the maximum of both the absorption and emission wavelengths, or the oxidation and reduction potential of both ground and excited states. Their work resulted in the synthesis of several derivatives possessing interesting properties as potential strongly reducing photosensitizers replacing metal-based ones. In collaboration with this research group, we have thus studied 6 phenoxazine compounds (Figure 3.6) to check if their properties could match with the one of the $Ir(ppy)_3$ PS in terms of accessible reduction potential, light absorption and excited state triplet lifetime.

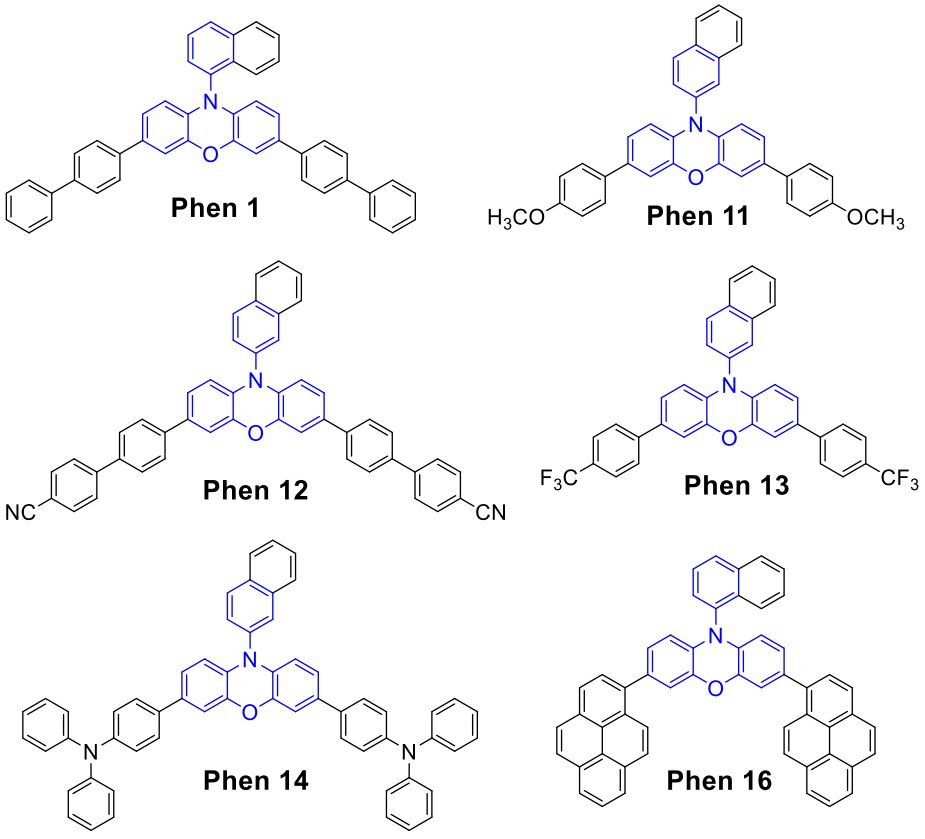

Figure 3.6: Structures of the phenoxazine sensitizers used in this chapter (in blue, the phenoxazine common core).

These properties are presented in Table 3.2. Please note that the phenoxazine names/numbers originate from a report published by the Miyake group, so we have decided to keep them for the sake of simplicity.

In a preliminary work from our group, a first attempt was made by replacing the $Ir(ppy)_3$ PS by Phen 1 using the same standard conditions (catalyst, sacrificial donor and weak acid

concentrations). In that study, CO_2 was successfully reduced to CO and then to methane under visible light irradiation, reaching a TON(CO) of 140 and TON(CH_4) of 29 after 102 h of light irradiation with CO_2 as the reactant. Under initial CO atmosphere, CH_4 was produced with a TON of 80, a selectivity of 85% and a quantum yield of 0.47%. Interestingly, the phenoxazine PS was significantly more efficient than $Ir(ppy)_3$, both in terms pf amount of CH_4 produced (2 times more) and quantum yield (3 times higher).[30] This work provide evidence that the photophysical properties of the phenoxazine family were well adapted to the requirements of the photochemical reduction of CO_2 with our model iron catalyst.

Phen	**λ_{max} abs (nm)**	**λ_{max} em[a] (nm)**	**E^0_{red} ($Phen^{\bullet+}$/Phen*)**	**E^0_{ox} ($Phen^{\bullet+}$/Phen)**
Phen 1	388	506	-1.70	+0.42
Phen 11	363	528	-1.91	+0.37
Phen 12	411	506	-1.42	+0.62
Phen 13	388	469	-1.58	+0.58
Phen 14	382	527	-1.88	+0.30
Phen 16	379	548	-1.85	+0.45
$Ir(ppy)_3$	375	518	-1.73	+0.77

Table 3.2: Photophysical and redox properties of several phenoxazine derivatives together with the $Ir(ppy)_3$ reference compound for comparison.[96, 141] [a] under 400 nm excitation. Potentials are given in V vs. SCE.

One important fact must be pointed out here. In all the studies done in our group before this PhD thesis, the photochemical cell used was suffering from some (known) leaks, which are quite unavoidable with a homemade cell. Gas chromatography analysis always showed the presence of some air (O_2 and N_2) in the headspace, due to an imperfect sealing but also to the multiple gas sampling made through the rubber septum on top. It was known and quantified, and some minimal loss of gaseous products was thought to be the only drawback of this. In Chapter 4 of the present manuscript, we will however discuss in details the unexpected influence of molecular oxygen during the catalytic process, which was clearly identified after the development and the use of a new photochemical, airtight, cell. In the study dedicated to the phenoxazine derivatives, this airtight cell was used and no methane can be observed due to the absence of O_2 (see Chapter 4 for the discussion). So, only CO could be produced from CO_2, including with the previously employed

phenoxazine PS which showed the formation of CH_4. In the following paragraphs, the reasoning is thus only based on the CO_2-to-CO conversion.

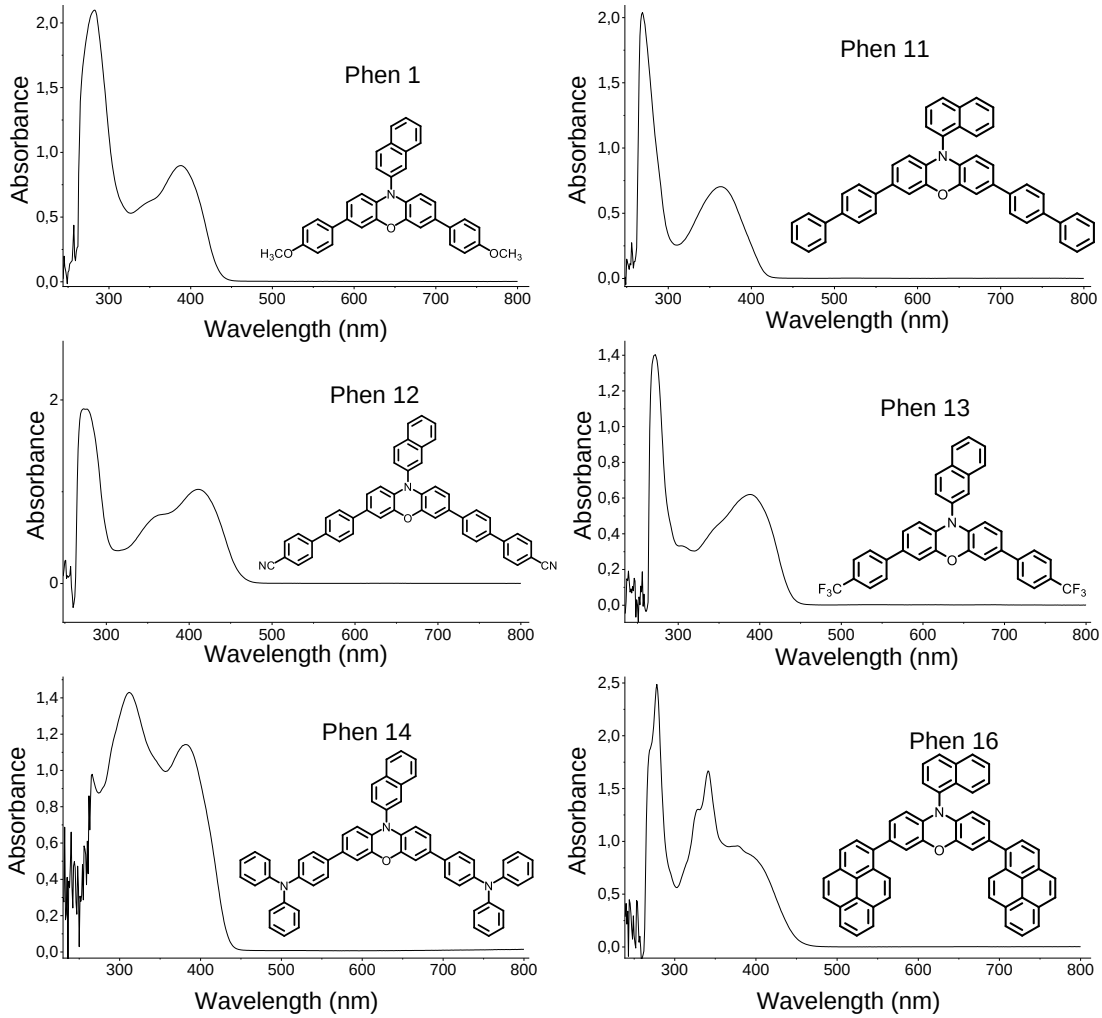

Figure 3.7: UV-Visible spectra of 30 µM ACN solution of the phenoxazine derivatives.

Based on the experiments done with our standard system, we know that to trigger the photochemical reduction of CO_2 using the Fe-*p*-TMA catalyst, a potential of -1.47 V *vs.* SCE is necessary to reach the catalyst active state. The potential accessible with the $Ir(ppy)_3$ PS is -1.73 V *vs.* SCE, so much more negative than theoretically needed. Using the variety of phenoxazine derivatives furnished by the Miyake group, which covers 330 mV of triplet excited state potential (E^0_{red} ($Phen^{\bullet+}$/Phen*)), from -1.58 for Phen 13 to -1.91 V *vs.* SCE for Phen 11 (Table 3.2), we wanted to see if a potential threshold could be observed.[1] We thus have systematically investigated

[1] Note that the potential here is technically an oxidation potential but its reductive power is studied here we will then refer to it as E^0_{red}.

each phenoxazine derivative and correlated the catalytic performance towards CO_2 reduction with their properties.

Even though the absorption maximum of the phenoxazine PSs are all (except Phen 12) below the irradiation wavelength of 400 nm typically used as lower limit for irradiation to stick to the visible domain, they still absorb significantly in the visible range to act as efficient PSs. Fe-*p*-TMA catalyst also absorbs at 400 nm, with an extinction coefficient of 45500 M^{-1} cm^{-1} but the molar ratio of Phen to catalyst was 100 (200 *vs.* 2 µM, respectively). Taking into account the extinction coefficient of the Phen (Table 3.4), the catalyst absorption only accounts for a very minor part of the total absorption, from *ca.* 1% (with the higher absorbing Phen 14) to *ca.* 5% (with the lower absorbing Phen 11).

The conditions used for these experiments were as follow: Fe-*p*-TMA catalyst 2 µM, of Phen PS 200 µM, BIH sacrificial electron donor 5 mM and TFE external weak acid 0.1 M, in ACN, under visible light (> 400 nm) irradiation for 21 h.

	Cat (µM)	**SD (mM)**	**Phen (µM)**	**Time (h)**	**E^0_{red} ($Phen^{\bullet+}$/Phen*) (V *vs.* SCE)**	**TON (CO)**	**TON (H_2)**
Phen 11	2	5	200	21	-1.91	88	12
Phen 14	2	5	200	21	-1.88	32	56
Phen 16	2	5	200	21	-1.85	88	0
Phen 1	2	5	200	21	-1.70	103	26
Phen 13	2	5	200	21	-1.58	112	12
Phen 12	2	5	200	21	-1.42	115	0

Table 3.3: CO_2 photochemical reduction results after 21 h of visible light irradiation using 6 phenoxazine derivatives as photosensitizers.

Under visible light illumination, CO and H_2 formation was observed through gas chromatography analysis. For all the systems containing Phen photosensitizers, except for Phen 14, CO was formed as the main gaseous product and H_2 as the minor product No liquid product was detected by ionic chromatography or NMR, and no CO or H_2 was formed when the same reaction mixture was saturated with argon instead of CO_2. All derivatives are in the same range of catalytic performances, except for Phen 14 which produced a lower TON and selectivity for CO. TON(CO) ranges in between 88 for Phen 16 to 115 for Phen 12, and CO selectivity ranges from 80% with Phen 1 to

100% with Phen 12 and 16 (Table 3.3). Thus, TON(CO) and CO selectivity seem to be quite insensitive to photosensitizer absorption coefficient and absorptivity.

The results obtained with Phen 12 could be surprising since it presents an excited state reduction potential of -1.42 V *vs.* SCE, *i.e.* in theory slightly too positive to generate Fe^0, whereas it induces the production of CO. However, this phenomenon is also observed electrochemically: in the presence of an important concentration of acid, the catalysis for CO_2 reduction starts with an onset potential (that can reach 200 mV depending on the acid concentration) more positive than the potential of the Fe^I/Fe^0 wave (Figure 3.8). This is also corroborated in photochemical conditions using $Ru(bpy)_3^{2+}$ as PS with the same Fe-p-TMA catalyst. Indeed, the accessible potential for the catalyst with this PS is only -1.33 V *vs.* SCE, which is, like in the case of Phen 12, supposed to be not negative enough to reduce Fe^I to Fe^0 but CO can still be detected in the gaseous headspace after visible light irradiation under CO_2 atmosphere.

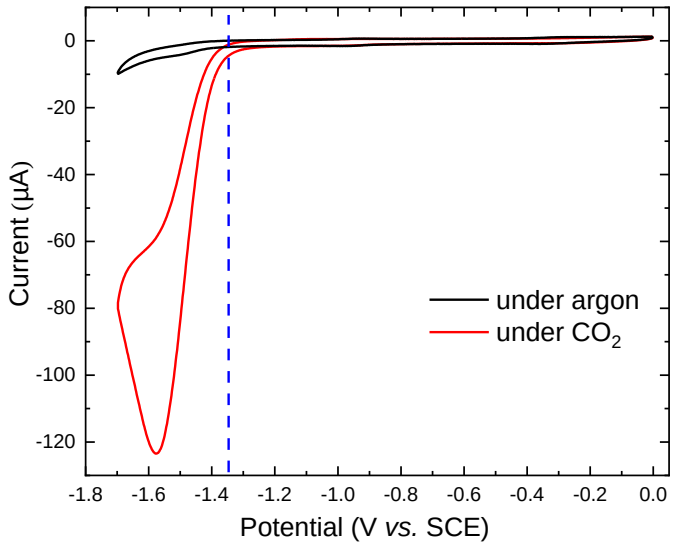

*Figure 3.8: CV of Fe-p-TMA (1 mM in 0.1 M $TBAPF_6$ ACN solution under argon (**black**) or CO_2 (**red**) in the presence of 1 M of TFE.*

The functionalization of the Phen core changes the energy levels of the photosensitizers and their intermediates formed during photocatalysis. To investigate the effects of this, TON(CO) was plotted as a function of the $E°_{ox}(Phen^{\bullet+}/Phen)$ and $E°*_{red}(Phen^{\bullet+}/Phen^*)$ (Figure 3.9 and Figure 3.10 respectively). In both cases, the data point corresponding to Phen 14 has been put in red and into brackets because it is apart from the general trend, due to its larger H_2 production as compared to CO in contrast with other derivatives. This observation is quite surprising since our group showed

that Fe-*p*-TMA catalyst, without sensitizer and with BIH electron donor, was remarkably selective towards CO formation, with no H_2 formed even in the presence of a relatively strong proton donor such as phenol.[113] The generation of H_2 with iron porphyrins was indeed proposed to be related to the formation of a hydride from the active Fe(0) state,[82] but Fe-*p*-TMA catalyst, thanks to the strong electron withdrawing effect of the trimethylammonio groups, is less likely to follow such pathway. Phen 14 is indeed the only one of the six derivatives bearing groups with acid-base properties. Triphenylamine is however known to be a poor base due to the delocalization of the nitrogen lone pair so its protonation is unfavored.[143] The exact reasons why Phen 14 leads to H_2 formation are still unresolved but the triphenylamino groups play for sure a non-innocent role.

The plot of TON(CO) as a function of $E°_{ox}(Phen^{\bullet+}/Phen)$ (Figure 3.9) shows a clear trend (red dotted line) since TON(CO) increases as $E°_{ox}(Phen^{\bullet+}/Phen)$ shifts to more positive values. The driving force of the ET_{regen} step (Figure 3.13) and the rate of Phen regeneration is determined by the difference in potential between the oxidized Phen and the sacrificial electron donor (BIH). The more positive $E°_{ox}(Phen^{\bullet+}/Phen)$ (*i.e.* larger driving force) the faster the regeneration of the photosensitizer. Since BIH has an oxidation potential of +0.33 V *vs.* SCE,[144] the ET_{regen} step thus proceeds at 40 mV (with Phen 11) to 290 mV driving force (with Phen 12), corresponding to the lower and the higher TON(CO) obtained, respectively. This evolution strongly suggests that the photosensitizer regeneration is the rate-limiting step in our process.

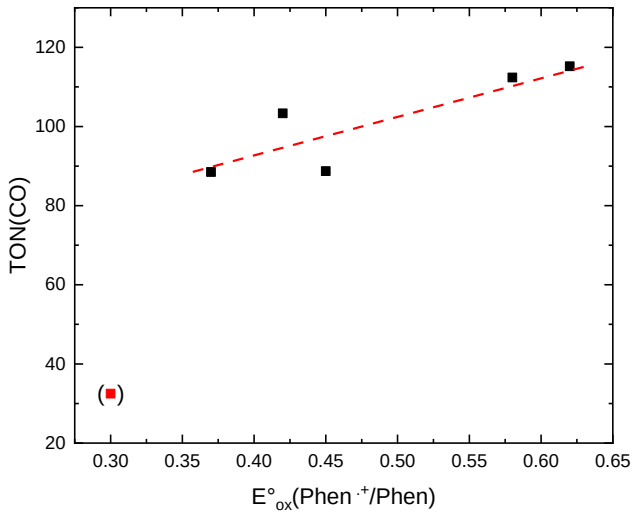

Figure 3.9: TON of CO after 21 h of irradiation vs. $E^0_{ox}(Phen^{\bullet+}/Phen)$ of the phenoxazine derivatives used as sensitizers in combination with Fe-p-TMA catalyst.

The driving force and rate of the electron transfer activating the catalyst (ET_{act}, Figure 3.13) is determined by the difference in potential between the iron porphyrin $Fe^{(x-1)}/Fe^{(x)}$ redox couple and the $E°*_{red}$ ($Phen^{\bullet+}/Phen^{*}$). It is generally thought that the performances of a photocatalytic system are very sensitive to the catalyst activation step, and thus directly related to the driving force for the ET_{act} step. As shown in Figure 3.11, a linear correlation (blue dotted line) can be drawn between the triplet excited state potential $E°*_{red}(Phen^{\bullet+}/Phen^{*})$ and the TON(CO), with a higher TON (115, Table 3.3) obtained with Phen 12, *i.e.* the derivative having the less reducing excited state potential. On the contrary, the lowest TON(CO) (88-89) is obtained with the two most reducing excited state potentials, with Phen 11 and Phen 16. The results of Figure 3.11 are actually mirrored those of Figure 3.10 since the derivative having the most negative excited state potential (Phen 11) is also the one that with the less positive oxidation potential, and inversely. This observation comes in support of our hypothesis that the rate-determining step is indeed the photosensitizer regeneration and not the catalyst activation state.

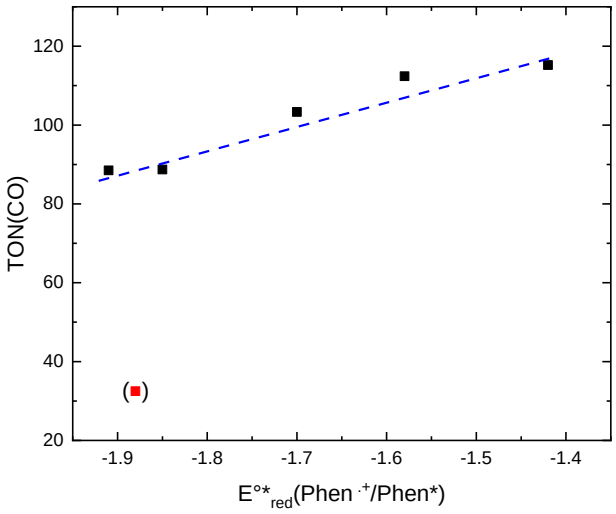

Figure 3.10: TON of CO obtained after 21 h of visible light irradiation vs. E^{0}_{red} ($Phen^{\bullet+}/Phen^{*}$) of the phenoxazine derivatives used as sensitizers in combination with Fe-p-TMA catalyst.

As detailed previously in the general case and in the particular one of the coumarin, the excited state triplet lifetime and the emission quantum yield play important roles in the overall photochemical reaction and can be strongly limiting factors. These phenoxazines were indeed designed to be efficient sensitizer, *i.e.* with an important intersystem crossing and a long lived triplet excited state. For example, Phen 1 has been extensively investigated and a 10% only quantum yield of fluorescence was reported together with a 480 µs triplet lifetime.[141, 145-146]

Since all the phenoxazines sensitizers studied here possess the same core structure, their associated emission quantum yield and triplet lifetime are considered to be of the same order of magnitude as those measured and reported for Phen 1. We thus assumed that upon light excitation, phenoxazines PSs are mainly in their triplet excited state and since they are a 100 times higher amount than the catalyst, the electron transfer between the triplet state and the catalyst should be of the same order of magnitude for all derivatives. To evaluate this electron transfer, we conducted emission quenching measurements with all the phenoxazine derivatives in the presence of increasing concentration of Fe-*p*-TMA catalyst (Figure 3.11).

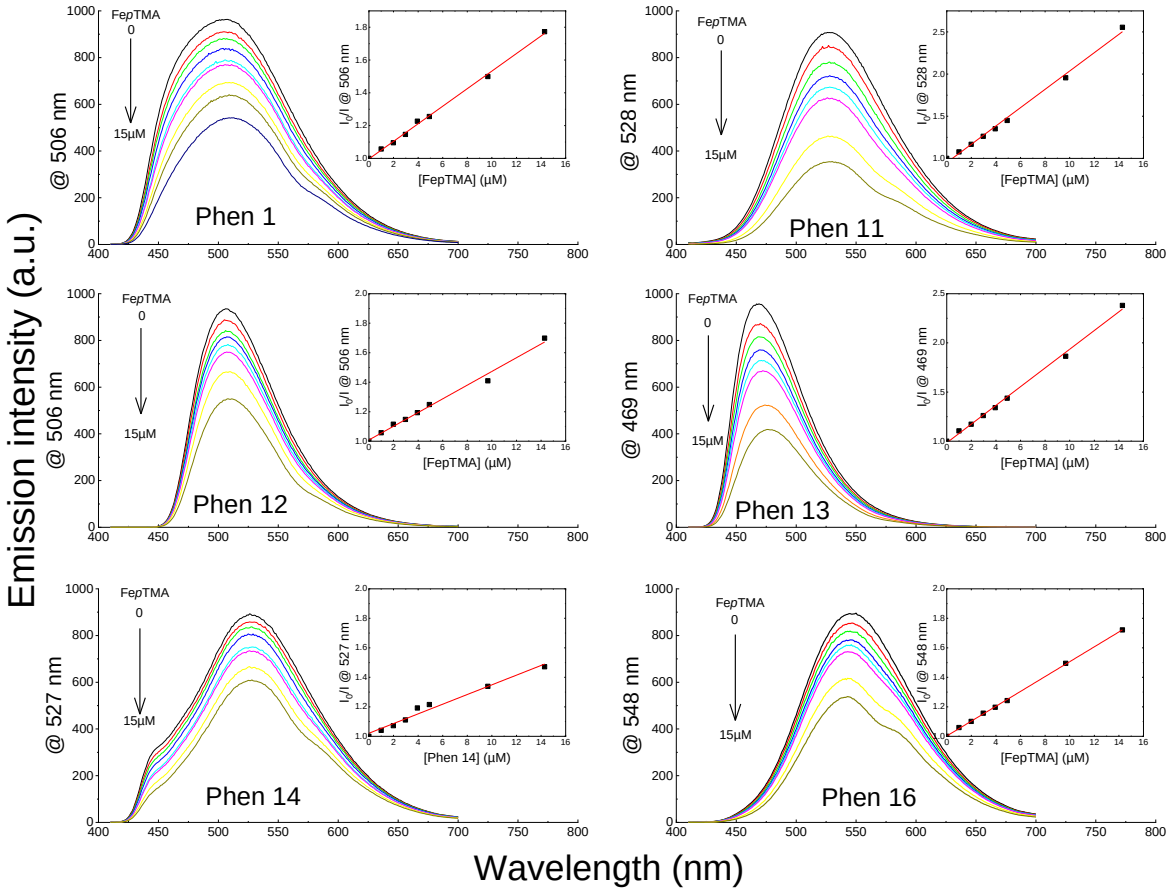

Figure 3.11: Emission spectrum of the phenoxazine derivatives (0.2 mM in ACN) under argon atmosphere with increasing concentration of Fe-p-TMA catalyst. λ_{exc} =400 nm. Insets: Stern-Volmer analysis.

Using the Stern-Volmer analysis (see section 1.4.1 of the manuscript), we have determined the Stern-Volmer constant K_{sv}, representing the overall quenching efficiency, ranging from 3.2×10^4 to 1.1×10^5 M^{-1}, which corresponds to a quenching rate constant k_q of *ca.* 10^8 M^{-1} s^{-1}, assuming an excited state lifetime of *ca.* 400 µm for the phenoxazine. The electron transfer between the

phenoxazine excited state and the catalyst is thus efficient and fast, not far from a diffusion limited process (Table 3.4).

	ε(M^{-1} CM^{-1}) at 400 nm	**λ_{em} max (nm)**	**K_{SV} (M^{-1})**	**τ (μs)**	**k_q (M^{-1} s^{-1})**
Phen16	28259	550	50371	~400	~10^8
Phen12	29151	507	46471	~400	~10^8
Phen14	30702	526	32814	~400	~10^8
Phen1	25625	509	53596	480	~10^8
Phen11	8437	530	105358	~400	~10^8
Phen13	18740	469	95157	~400	~10^8

Table 3.4: Photophysical properties of the phenoxazine derivatives and Stern-Volmer parameters obtained from the quenching measurements with Fe-p-TMA catalyst

A series of control experiments was conducted in the very same conditions but adding increasing amount of the sacrificial electron donor (BIH) instead of Fe-*p*-TMA catalyst, and no emission quenching occurred (Figure 3.10).

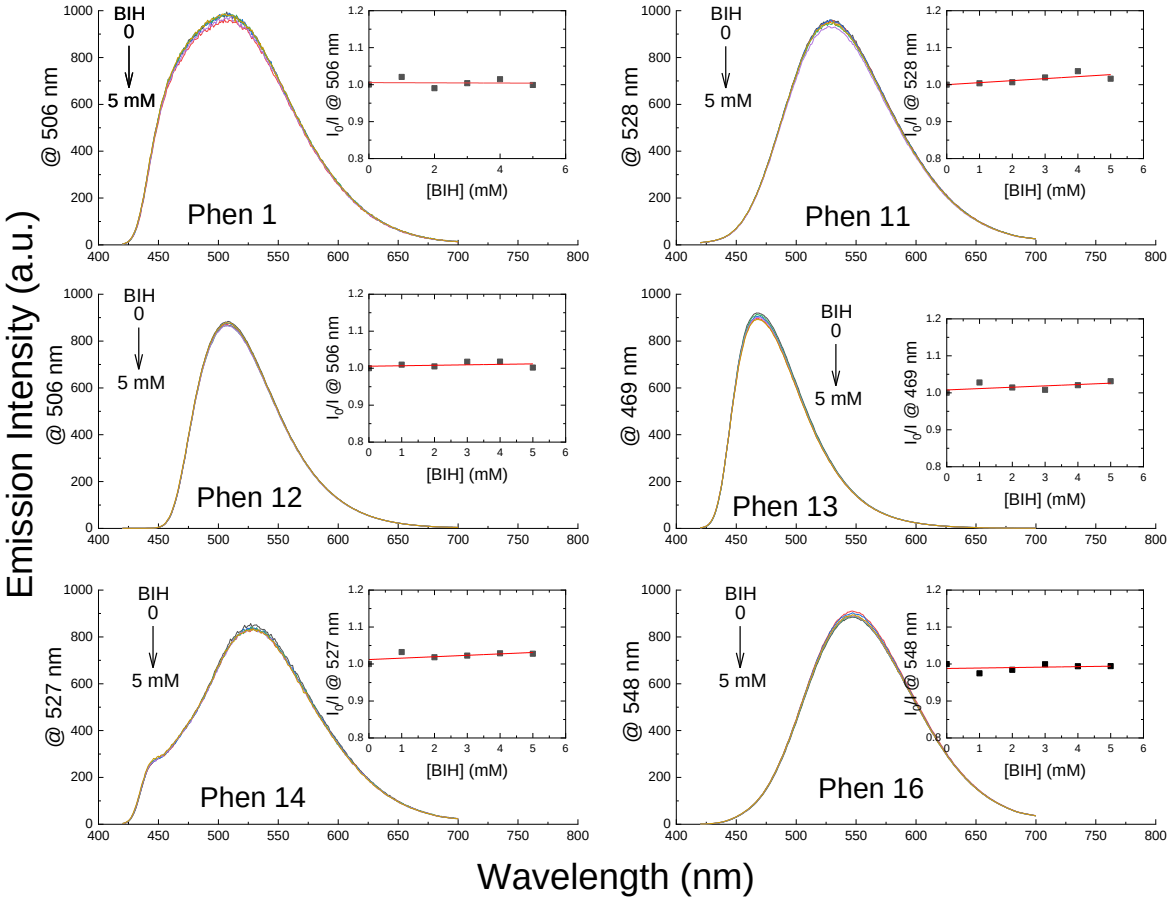

Figure 3.12: Emission spectrum of the phenoxazine derivatives (0.2 mM in ACN) under argon atmosphere with increasing concentration of BIH electron donor. λ_{exc} = 400 nm. Insets: Stern-Volmer analysis.

After transferring an electron from its excited state to the catalyst (ET_{act} step, Figure 3.13), the phenoxazine PS is in its oxidized $Phen^{\bullet+}$ form and it thus requires an electron transfer (ET_{regen}, Figure 3.13) to go back to its initial, neutral ground state. This electron is provided by the sacrificial electron donor, in this case BIH. The regeneration of the PS is thus governed by two main parameters: the rate of the electron transfer between $Phen^{\bullet+}$ and BIH, which depends on the driving force of the reaction, and on the probability of encounter, *i.e.* the diffusion of both species towards each other. Because the amount of BIH is 25 times higher than the amount of phenoxazine in solution, the diffusion does not limit the species encounter. Considering that the diffusion of species is not a limiting factor, we can propose to analyze our results using the Marcus theory. The two reactants (oxidized phenoxazine and BIH) are described as harmonic oscillators and their energy potential is depending on their nuclear configuration (degree of freedom). The two species (one acceptor A, one donor D) must collide and undergo reorganization prior to any potential electron

transfer, what is characterized by an equilibrium constant of formation of the transition state pair AD, k_a (1):

$$A + D \overset{k_a}{\rightleftharpoons} AD \quad (1)$$

$$AD \overset{k_{et}}{\rightleftharpoons} D^+A^- \quad (2)$$

$$D^+A^- \xrightarrow{k_d} D^+ + A^- \quad (3)$$

Once the transition state is formed, the possibility of an electron transfer between the two reactants depends on the electronic coupling matrix element H_{AB}. If the coupling is negligible, the electron is formally localized on the donor and no transfer take place to the acceptor. Because CO, as CO_2 reduction product, can be detected in our process, we can consider that the coupling matrix is not equal to zero and therefore that the coupling between the acceptor and the donor is sufficient to trigger the electron transfer. The other parameter that governs the electron transfer is the overall Gibbs free energy of the reaction. At equilibrium, combined with the Nernst equation, the Gibbs free energy can be expressed as follows:

$$\Delta G^0 = -nF[E^0(D^{x+1}/D^x) - E^0(A^x/A^{x-1})$$

With F the Faraday constant, and E^0 the standard potential of either the donor D or the acceptor A. The driving force of the reaction is controlled by the difference in standard potentials between the oxidation of the donor and the reduction of the acceptor. The larger the difference, the higher the Gibbs free energy and therefore the driving force of the reaction. In the conditions described above, when using a phenoxazine PS and BIH as electron donor, the observed results are in agreement with the proposed analysis. The CO production is increasing with the oxidation potential of the phenoxazine used (Figure 3.11), *i.e.* with the driving force of the electron transfer reaction. This analysis shows that the electron transfer between the oxidized state of the sensitizer $PS^{\bullet+}$ and the electron donor (here BIH) is indeed the limiting factor in the overall photochemical reaction in our conditions.

As a consequence, our initial hypothesis stating that the main limiting factor of the reaction would be the accessible excited state potential of the photosensitizer seems clearly discarded. The

accessible potential only needs to be negative enough to reduce the iron center of the porphyrin to the Fe^0 active state to allow CO_2 reduction. The formation of the sensitizer excited triplet state is also not limited by light absorption or by intersystem crossing. For Phen 1, the measured molar extinction coefficient is indeed high (ε = 25625 M^{-1} s^{-1} at 400 nm) and the quantum yield of charge transfer triplet excited state is large too (90%). Therefore, phenoxazines sensitizers easily and quantitatively form a long-lived triplet state upon.[145] The excited state quenching is not limiting either, since our measurements indicate a close to diffusion limited process between the PS excited state and the catalyst.

All in all, this suggests that the direct ET_{act} step is not sensitive to the driving force of the reaction. On the contrary, the production of CO is strongly related to the oxidation potential of the phenoxazine sensitizer, thus implying that the redox properties of the latter are important parameters for its regeneration through the ET_{regen} step with the sacrificial electron donor. This indirect effect emphasizes the importance ET steps not directly involved in the catalytic step of a photocatalytic cycle. More qualitatively, this means that the availability of PS and consequently of of excited PS* are crucial to enhance the proportion of activated catalyst and so to make the catalytic cycle more efficient.

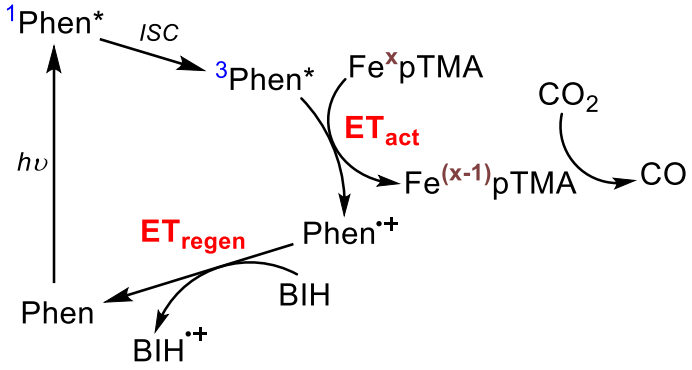

Figure 3.13: Scheme of the phenoxazine excited state by Fe-p-TMA catalyst and its regeneration with BIH as electron donor.

Regeneration of the sensitizer to its ground state is possible by employing various efficient sacrificial electron donors, as it is the case for BIH, TEA or TTF. However, we show here that the difference in redox potential between the sacrificial donor and the oxidized state of the sensitizer could constitute the main driving force of the reaction. A particular attention must be paid on this factor to check, for a particular PS and catalyst, depending on the quenching process, that the appropriate electron donor with the optimum redox potential is employed.

3.6 Sub-conclusions and perspectives

In this chapter, we have shown that replacing metal-based inorganic sensitizers by all-organic ones is not an easy task. A number of requirements, from the excited state lifetime, the absorption in the visible domain and the adequate redox properties, render the identification of a good candidate quite tricky. We however have explored two possibilities. Coumarin, which possess an excited state lifetime that is too short to allow bimolecular electron transfer. As a consequence, unless structural modification can be made to change this parameter, this is not a promising track. On the contrary, phenoxazines are very interesting since they fulfill several criteria. The study of several derivatives allowed us to highlight the prominent role of the sensitizer regeneration step.

Among the other possible all-organic photosensitizers, carbon nitride (C_3N_4) is an emerging class of materials having interesting redox and photophysical properties.[147-151] In our group, we for example have reported the non-covalent association of an iron quaterpyridine catalyst with mesoporous carbon nitride (mpg-C_3N_4). This mixed system quite efficiently drives CO_2 reduction upon visible light irradiation, reaching 155 TON for CO, with a selectivity of 97% and an apparent quantum yield of 4.2%.[152] We also employed the same material building up a covalent hybrid system thanks to an amide linkage with a cobalt quaterpyridine complex. The catalytic activity towards CO of the catalyst showed a total TON of 500 after 4 days of visible-light illumination, keeping an excellent selectivity (98%).[59] These two examples show that molecular-material hybrid systems are promising tracks to both improve photochemical catalytic performances and robustness, and to access recyclability. So, the suitable sensitization could come from either molecules or materials, depending on the process at play.

Chapter 4 - The unexpected role of dioxygen

4.1 Context

Usually, CO_2 reduction studies are performed under oxygen-free conditions in which the airtight reaction vessel is initially saturated with the reacting gas. Molecular oxygen is known to be an excited quencher for inorganic complexes and thus is thought to be deleterious for molecular catalysts by lowering either the selectivity and/or the efficiency towards CO_2 reduction. However, in some cases the presence of O_2 has proved to promote the CO_2 reduction activity, especially in the case of copper catalyst.[153] On copper nanowires, the presence of subsurface oxygen seems to be necessary to reduce CO_2 towards C_2 products such as ethylene.[154] Under electrochemical conditions, metallic copper nanowires would mostly make C_1 products with very little amount of ethylene, whereas oxygen bearing nanowires could exhibit a faradaic efficiency up to 45% for ethylene production with also an enhanced production of methane.[154] Giving those results, molecular oxygen seems to be the key for controlling the stability and the dimerization of CO towards C_2 products.[154] Molecular catalysts active for CO_2 reduction are often potentially active towards other reduction reactions such as proton reduction or oxygen reduction, lowering then the overall selectivity for CO_2 reduction products. In Nature, the iron porphyrin contained in the hemoglobin protein is able to bind both O_2 and CO_2 to transport them either from/to the muscles and the lungs. Evidences of reversible oxygen adduct formation in an iron porphyrin was first demonstrated by UV-Vis spectroscopy, with a clear shift in the absorption of the complex under oxygenated conditions.[155] Under electrochemical conditions, iron porphyrin is able to catalyze oxygen reduction reaction by a preferential 4 electrons process to form water. During the process, a ferric-superoxide $Fe^{III}(TPP)(O_2^{\bullet-})$ adduct is formed and its protonation is the rate determining step.[156] During the reduction of oxygen by an iron porphyrin, it is also possible to access even higher valence species and the formation of a Fe^{IV} was highlighted by spectroelectrochemistry.[157]

Before exploring the possible effects of O_2 on CO_2 photochemical reduction, a reminder of the standard system studied in this thesis is necessary. Unless otherwise mentioned, the catalyst, the photosensitizer, the sacrificial electron donor and the proton donor are the same than our standard system *i.e.*: a substituted iron porphyrin (Fe-*p*-TMA, 2 µM), an iridium complex ($Ir(ppy)_3$, 200 µM), triethylamine (TEA, 50 mM) and trifluoroethanol (TFE, 100 mM), respectively. All these molecules are dissolved in acetonitrile (3 mL) to give a homogeneous solution. This solution is

then saturated with CO_2 before irradiation with a solar simulator. To prevent the absorbance of the incident photons by the reactor material, a high-quality quartz cell (see Annexes) is employed, with four transparent windows. In order to increase the available gaseous headspace of the cell, a homemade glassware system was designed (Figure 4.1) and originally consisted in a screwable glass piece, connected to the cell by a short PTFE tubing, to reach a total headspace volume of 23 mL.

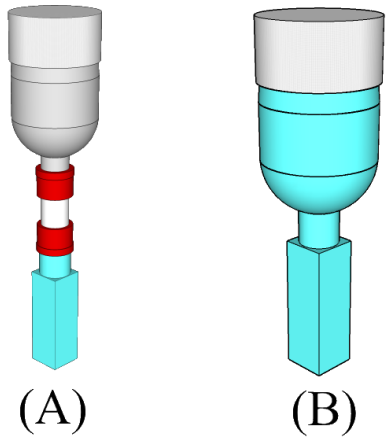

Figure 4.1: Scheme of two different cells used in this chapter

However, this original cell (A) exhibited some flaws, in particular related to the intermediate screws and tubing subject to ageing, which resulted in small but non negligible gas leaks, especially upon multiple sampling. The photochemical cell was thus upgraded by replacing the mobile top glassware by a sealed one (B), the bottom part still being a 1x1 cm quartz cell. This new cell version has the advantage of being completely airtight, keeping the reaction mixture under close to constant atmosphere, with no detectable gas leak.

When an identical reaction solution was studied in the two versions of the photochemical cell, the results obtained were quite different: in cell (A), molecular hydrogen, carbon monoxide and methane could be detected as CO_2 reaction products, whereas in cell (B) only CO was detected, moreover in a lower amount. This result was unexpected and appeared to be in complete opposition with what was expected regarding the presence of O_2, *i.e.* a system with less air leaks would give better results as O_2 is supposed to be deleterious to the reaction of interest.

To better understand the apparent effect of air (from leaks) on the chemical process, two experiments were performed: in the first one, after CO_2 saturation of the system, a defined amount

of molecular nitrogen was injected in the gas phase, whereas in the second one a defined amount of molecular oxygen was added, in parallel with a control experiment in which only CO_2 was present. In the first case, the amount of gaseous products was approximatively the same than in the CO_2 only cell, and no methane could be detected. In the second case, the amount of CO was much higher than in the control experiment and methane was produced. As a consequence, this is a strong indication that O_2 is playing a non-innocent role in the catalytic reaction.

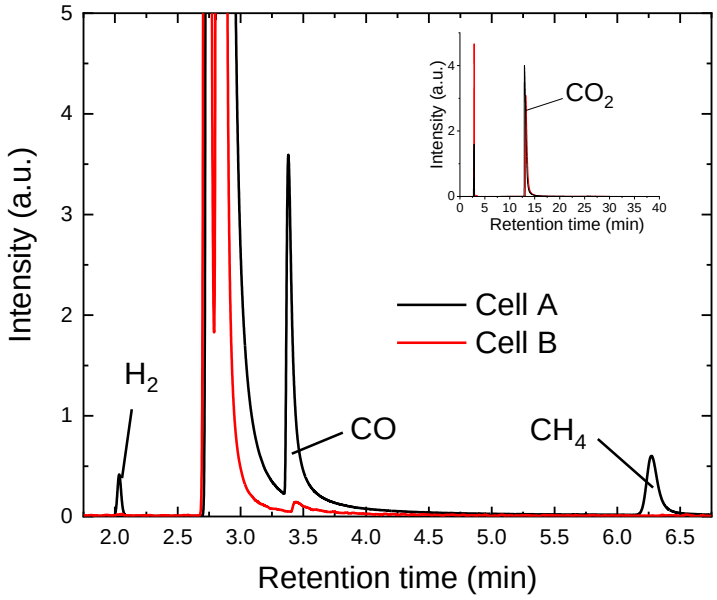

Figure 4.2: Gas chromatograms of the headspace sample for the two cell versions. Inset: full chromatogram.

To investigate this role, a simple test was first conducted: a solution in the standard conditions was purged with CO_2 without the cap on, allowing air to be present in the headspace of the solution. The cell was then closed and placed in front of the solar simulator for irradiation. GC measurements were regularly done to follow the gas composition of the headspace. From 0 to 40 h irradiation (Figure 4.2), there is a clear decrease of O_2 concentration in the headspace whereas the amount of N_2 remains at a constant level. This suggests first that gas leaks are negligible (no increase in N_2) but also that O_2 is consumed in some way during the process. Acetonitrile is an interesting solvent because O_2 solubility is not negligible, and thus one can think that the observed decrease could be due to its simple, progressive dissolution. However, the maximum solubility of O_2 in ACN being 8.1 mM, its amount in the headspace could not diminish in such a way that would explain the measured chromatograms of Figure 4.3.[158] The fact that the final amount of O_2 is much lower than the one that could be explained by a dissolution effect thus suggests that O_2 is being consumed

during the reaction by interacting with at least one of the component of the system, either the photosensitizer, the sacrificial donor, the proton donor or the catalyst.

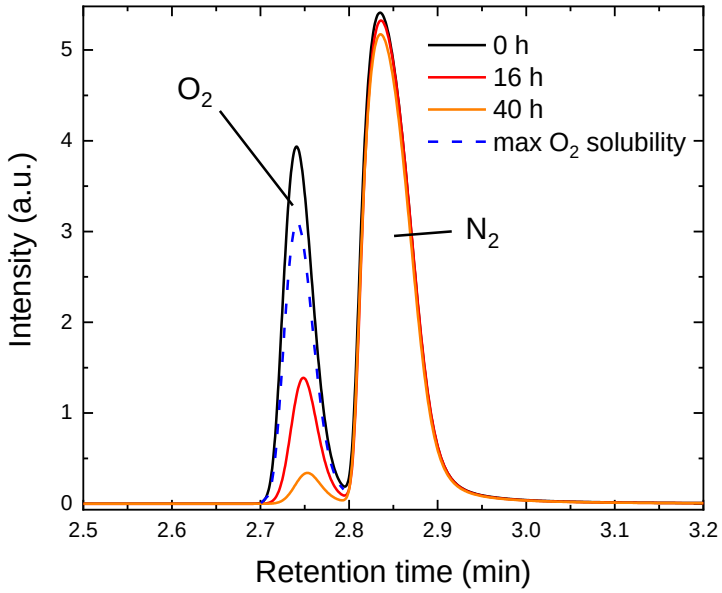

Figure 4.3: Evolution of the gas composition in the photochemical cell headspace over irradiation time.

As a consequence, a series of experiments was performed in which a known volume of molecular oxygen was manually injected in the gas phase of the cell with a gas syringe before irradiation. The results showed a quasi-linear correlation between the amount of oxygen injected and the TON for CO or H_2 (Figure 4.4 and Table 4.1).

Entry	O_2 injected (µL)	Time (h)	TON CO	TON CH_4	TON H_2
1	100	17	12	1	21
2	200	17	25	1	25
3	250	17	30	2	36
4	300	17	44	3	35
5	400	17	61	5	53
6	N_2 250µL	17	5	0	35

Table 4.1: TON for CO and H_2 with various injected volumes of O_2 in the photochemical cell headspace, and N_2 as control experiment.

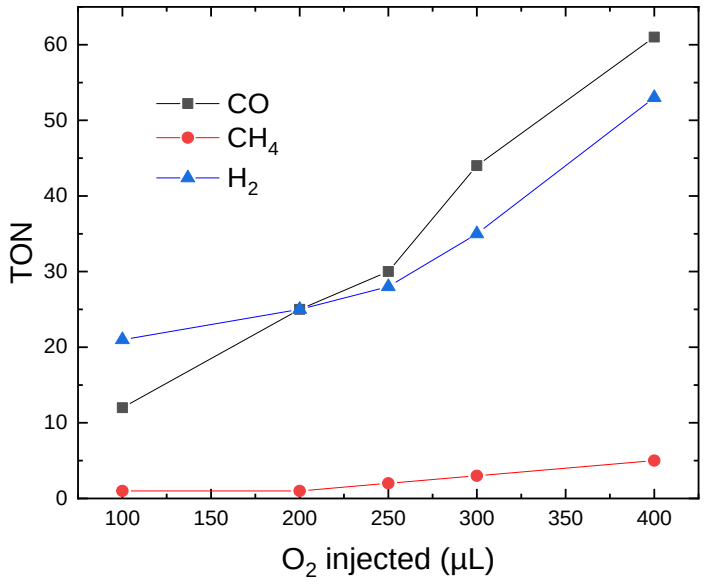

Figure 4.4: Evolution of the TON for CO, H_2 and CH_4 as a function of the amount of O_2 injected in the system.

Regarding methane production, the correlation does not seem to be as linear as for CO and a threshold value of *ca.* 200 µL of O_2 in the headspace seems necessary to trigger CH_4 formation. Among the possible products formed from CO_2 reduction, formic acid can be detected by ionic chromatography, in its formate form. In airtight conditions, no formate could be detected and CO is the preferential 2 electrons reduction product. However, when some air was allowed to enter the system, important quantities of formate could be detected. To confirm this observation, this experiment was repeated under CO_2 and under CO atmosphere, both in the presence of air. In both cases, formate was detected in the liquid phase at the same order of magnitude. To understand the origin of formate production, several experiments were then conducted varying different parameters (Table 4.2).

Entry	CAT Fe-*p*-TMA	PS $Ir(ppy)_3$	SD TEA	Acid TFE	TON formate
1	2 µM	/	50 mM	0.1 M	0
2[a]	/	0.2 mM	50 mM	0.1 M	1297
3	2 µM	0.2 mM	/	0.1 M	88
4	2 µM	0.2 mM	50 mM	/	1440

Table 4.2: TON of formate obtained under various photochemical conditions under visible light irradiation.
[a] theoretical TON calculated as if 2 µM of catalyst was present in the catalytic solution

First, in the absence of electron donor (entry 3), a very low amount of formate was observed, as expected since the absence of electron donor is drastically limiting the process. Surprisingly, entry 2 shows that the iron catalyst plays almost no role in the production of formate, with a similar production than entry 4, which seems to indicate that formate is not coming from CO_2 reduction, since $Ir(ppy)_3$ is known to be inactive towards this reaction. Finally, in the presence of molecular oxygen but without sensitizer (entry 1), no formate was detected. To confirm the origin of the formate detected, a labelled study was performed, using $^{13}CO_2$ instead of the standard $^{12}CO_2$. If the formate detected would bear a ^{13}C atom, confirming it originates from CO_2 reduction, the corresponding NMR signal should split into two equivalent signals, due to the isotope effect of the marked atom.[159] As seen in Figure 4.5, no split could be detected in presence of $^{13}CO_2$, indicating that formate does not comes from CO_2 reduction in the presence of O_2.

To explain these results, we can propose the following mechanism: the excited state of the sensitizer is reductive enough to transfer an electron to O_2 to form the superoxide radical anion $O_2^{\bullet -}$ which would generate formate (among other products) through a still unresolved reaction pathway involving TEA.

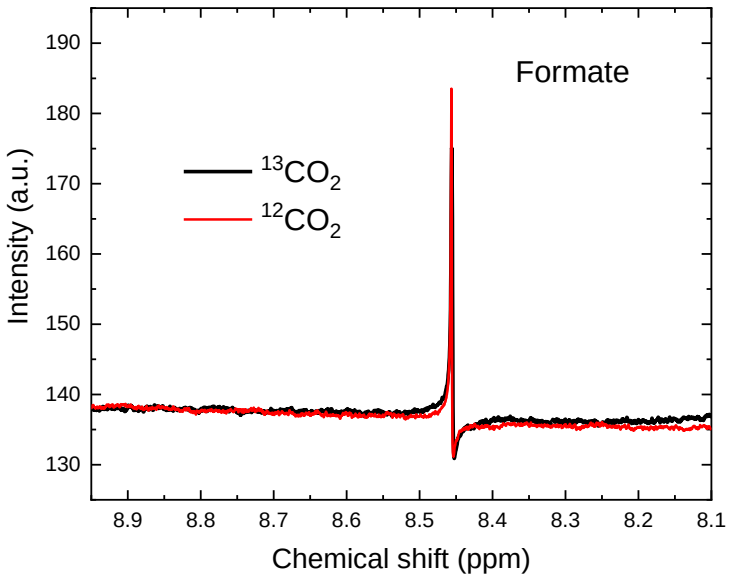

Figure 4.5: NMR of catalytic solution after 18h of irradiation either under $^{12}CO_3$ (red) or $^{13}CO_2$ (black).

4.2 Effect of O_2 on the sacrificial donor

In most of the reactions performed, TEA is used as sacrificial electron donor as it has been successfully employed previously in association with $Ir(ppy)_3$.[85] Tertiary amines are known to be

easily oxidized under oxygen atmosphere and it was indeed shown that in the presence of ruthenium(III) ions TEA can be oxidized to several products. Two main pathways are possible (Figure 4.6): either an oxygen atom is transferred to the nitrogen to create the N-oxide form of the triethylamine or it is transferred to a carbon atom leading to the dismutation of one of the ligand to create diethylamine and acetaldehyde in a 1:1 ratio.[160]

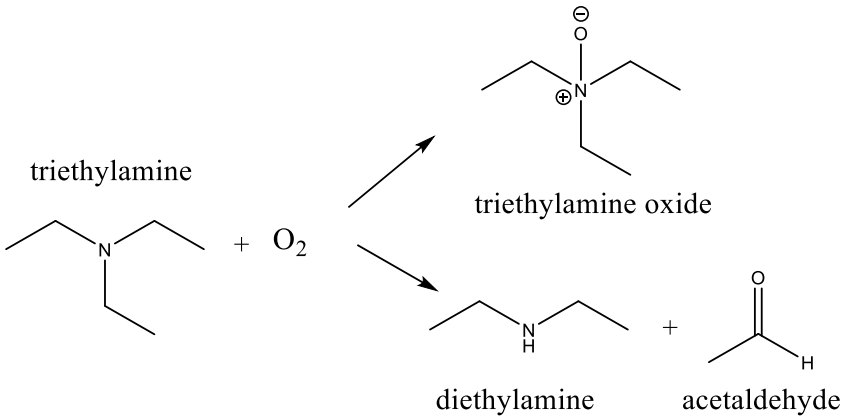

Figure 4.6: Possible TEA oxidation products.

In order to track the possible presence of such products in the liquid phase under irradiation and in the presence of oxygen, two main analytical techniques could be used. NMR is a common tool for analyzing solutions and it can give insights on the reactivity of certain molecules with however some limitations: in the present case, the possible products obtained from TEA oxidation have a similar structure so the corresponding NMR peaks will then have a similar chemical shift and it could be difficult to identify them without a proper separation prior to the analysis. To overcome this issue, GC-MS is used as a second analysis technique. Before reaching the mass analysis part of the setup, the vaporized solution goes through a capillary column that will separate the different molecules of the mixture based both on their boiling point and their affinity for the column internal material. In our case, only molecules having a boiling point below the temperature of the injector (250°C) can be analyzed. This means that other compounds such as organometallic complexes or salts cannot pass the injector and therefore cannot be analyzed by the mass spectrometer. In particular, triethylamine oxide, having a boiling point above 250°C, would not be detected by our GC-MS setup even if it is present in the solution mixture.

An example of such an analysis is shown in Figure 4.7 for an experiment performed in the presence of O_2.

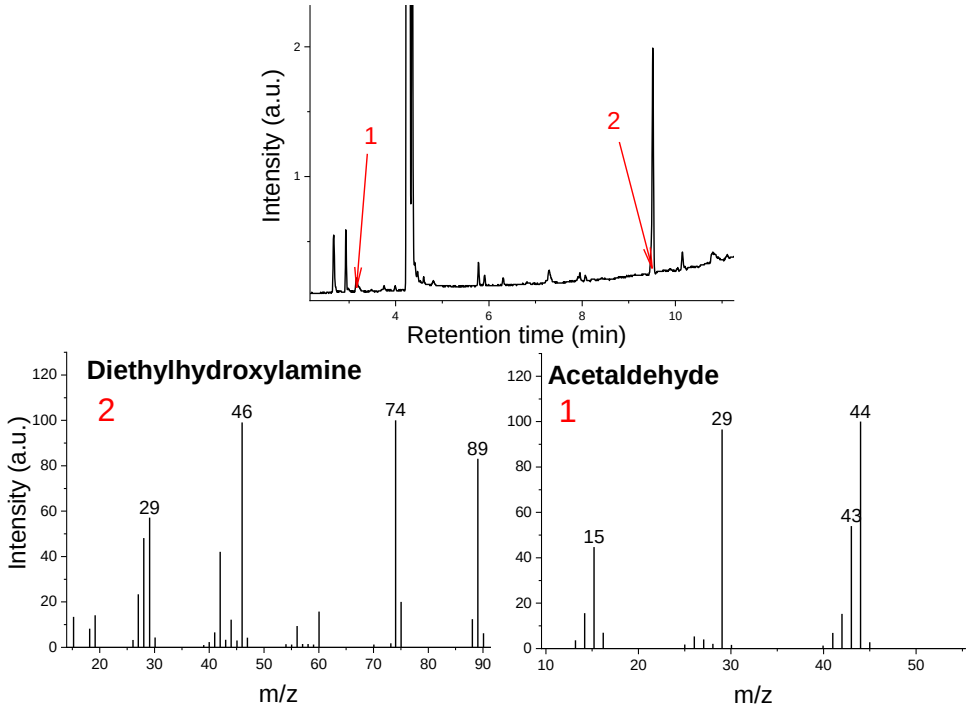

Figure 4.7: GC analysis of the reaction solution after 47 h of irradiation in the presence of CO_2 and O_2 (top) and the associated mass spectra (bottom).

As suspected, acetaldehyde can be identified in solution, but instead of diethylamine, diethylhydroxylamine was also detected. The chemical oxidation of TEA by hydrogen peroxide is indeed reported to gives various products, including the latter, and different from than reported for the electrochemical reduction.[161]

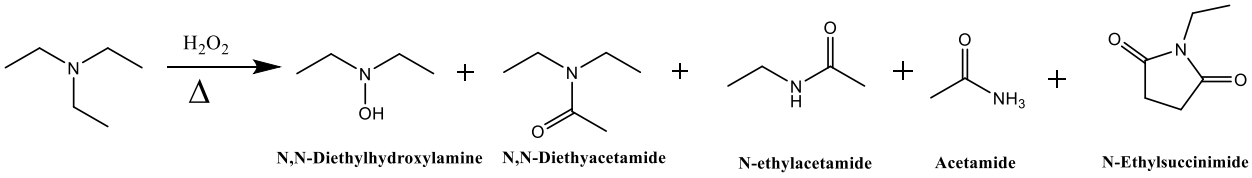

Figure 4.8: Possible products obtained by the chemical oxidation of TEA.

In the presence of nitric acid, TEA can be oxidized to N-nitrosodiethylamine, acetamide and N,N-diethylformamide (DMF).[162] Acetamide and DMF could indeed be detected in solution but N-nitrosodiethylamine was not, whereas it is the main product obtained by chemical oxidation of TEA. Molecular oxygen can also be used as oxidant in the presence of catalysts containing rare metals such as gold or ruthenium and in moderately high temperatures, usually between 100 and 150°C. Very few examples of reactions at room temperature were reported. One of them showed that a platinum catalyst can oxidize trimethylamine to the corresponding amide, but when

triethylamine was used as subtract, no oxidation products could be detected.[163] Finally, TEA can be photochemically oxidized to acetaldehyde and diethylamine when irradiated with UV light under oxygen atmosphere.[164]

Among the oxygen reactive species that could be generated upon electron transfer from the excited state of the catalyst to molecular oxygen, the superoxide radical anion $O_2^{\bullet-}$ is the most likely to be formed in our standard conditions. Some reports proposed that, in the presence of TEA, the superoxide could be protonated to give the hydroperoxyl radical $HO_2^{\bullet}$.[165-166] Unlike $O_2^{\bullet-}$, $HO_2^{\bullet}$ is a strong oxidant which could explain the variety of products we detected in solution under full oxygenated atmosphere. Another report showed that upon photooxidation, in the presence of a sensitizer, TEA could interact with the superoxide radical anion. The products obtained were the same as reported before, *i.e.* acetaldehyde and diethylamine, together with some of N-ethylethanimine.[166] The latter might be present in our system since we detected a signal in mass spectrometry at m/z 71, but the exact fragmentation pattern is unknown and therefore further analysis should be performed in order to confirm the presence of such molecule in our catalytic solution.

Under complete O_2 atmosphere, using our standard system, all five products could be identified in the liquid phase, along with other non-expected products such as N,N-dimethylformamide and N,N-diethylformamide (Figure 4.9).

TEA can undergo chemical reactions in the presence of molecular oxygen but the rate is very slow if not catalyzed and it should not affect the reaction in the typical reaction timescale. As another control experiment, the iridium sensitizer, with triethylamine, under O_2 atmosphere, were stirred in the dark for 21 h and no significant change in the solution could be observed as can be seen in Figure 4.10. However, as shown in Figure 4.9 many products can be observed after irradiation of the catalytic solution in the presence of O_2. This seems to indicate that it does not react in the dark with the reaction partners but, upon light irradiation, superoxide radical anion is most likely generated from the quenching of the excited state of the sensitizer and it can then interact with TEA to lead to the compounds detected.

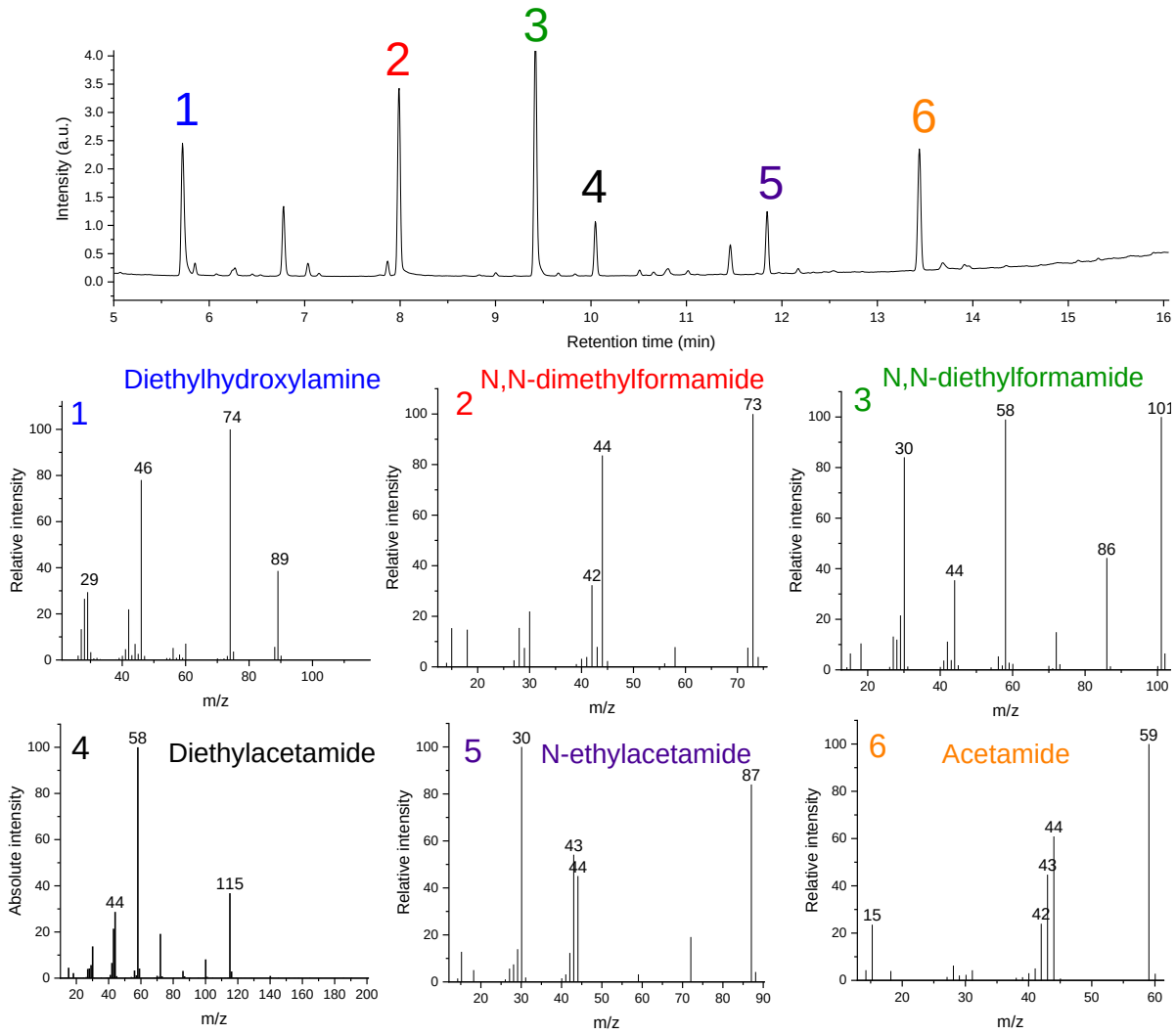

Figure 4.9: TEA Oxidation products obtained after 21h of visible-light irradiation of catalytic solution under complete oxygen atmosphere.

The same experiment under full O_2 atmosphere, in the absence of the catalyst, was performed and the analysis of the liquid phase showed the same composition than the standard catalysis solution. This strongly suggests that the catalyst does not play any role in the oxidation of TEA and that the major reactant is a reactive oxygen species, generated by one or several electrons transfer from the excited state of the sensitizer. Our system is then as oxidant as hydrogen peroxide, and to our knowledge it has never been reported as such. Even though the selectivity toward one product in particular is low, this could be thought a valuable alternative to chemical oxidation of alpha-carbon of amines.

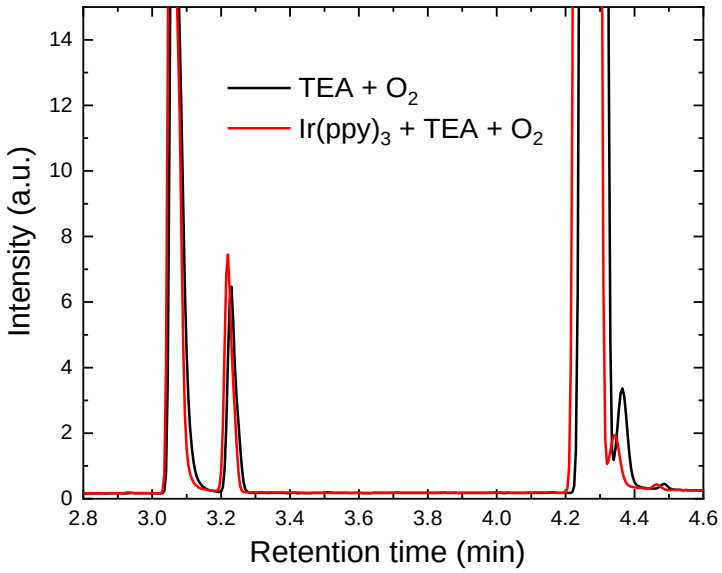

Figure 4.10: GC-MS of solution under oxygen atmosphere, in absence of iron catalyst after 21h of stirring in the dark

Regarding CO_2 reduction, a first hypothesis that can be made at this point is that the presence of molecular oxygen induces an increase in overall reactivity through the formation of a more efficient sacrificial electron donor than TEA through the formation of secondary oxidation products. However, for a molecule to play the sacrificial electron donor role, its oxidation potential should be close to the reduction potential of either the excited state or the oxidized state of the photosensitizer, depending on the quenching pathway (Figure 4.11).

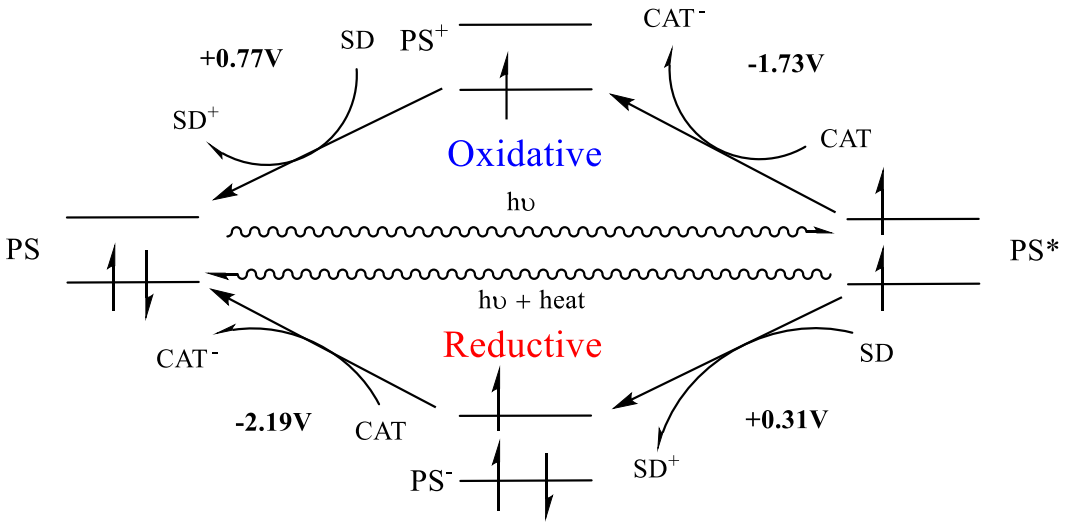

Figure 4.11: Possible quenching pathways of $Ir(ppy)_3$ upon visible light irradiation. Potential are given in V vs. SCE.

In the case of $Ir(ppy)_3$, the oxidation potential of the electron donor should be then close to +0.31 V or +0.77 V *vs.* SCE to achieve an efficient electron transfer, as depicted above.

Entry	Electron donor	E_{ox} (V *vs.* SCE)
1	Triethylamine	+0.96
2	Triethanolamine	+0.82
3	Diethylamine	+1.30
4	BIH	+0.33
5	TTF	+0.32

Table 4.3: Oxidation potential of several typical sacrificial electron donors.

To explore this hypothesis, various compounds that could be generated from the oxidation of TEA were directly used as potential sacrificial electron donors instead of TEA in our standard photochemical conditions. Note that here, in order to investigate their potential as sacrificial donor, the reactions were performed in O_2 free conditions. In the case of diethylamine and diethylhydroxylamine, no reduction products from CO_2 could be detected, either in the liquid or in the gas phase.

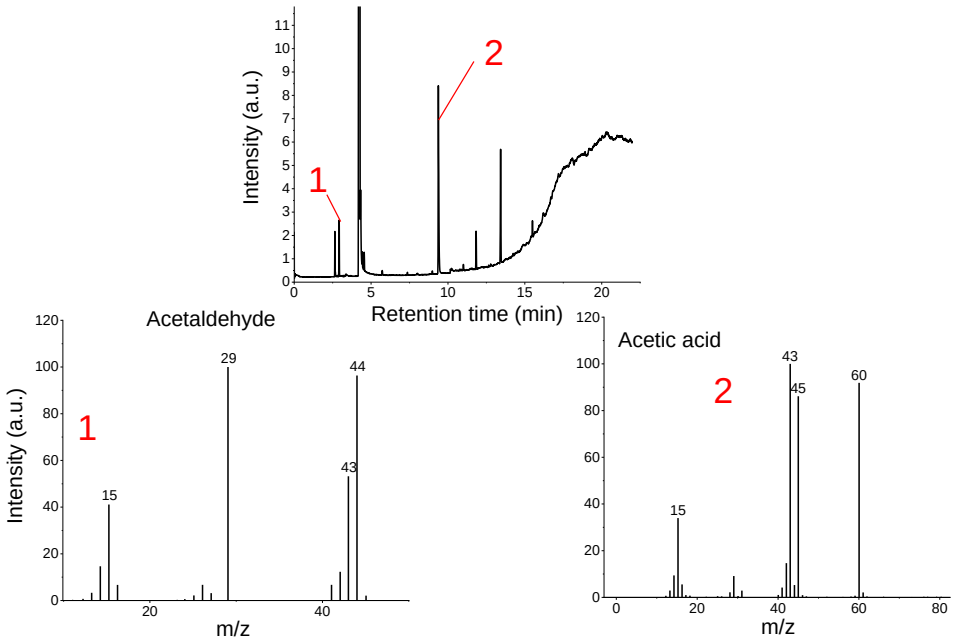

Figure 4.12: Gas chromatography analysis of the reaction solution after 60 h of irradiation with 10 mM of acetaldehyde as sacrificial electron donor (top) and related mass spectra (bottom).

Interestingly, when acetaldehyde is used as sacrificial electron donor, in the presence of O_2, acetic acid can be detected in liquid phase, as shown in Figure 4.12. Acetic acid is industrially produced

by acetaldehyde oxidation under high pressure and high temperature, even if recent research has been able to performed this reaction with a 95% yield under air atmosphere at 0°C.[167] The photooxidation of acetaldehyde is also possible and historically, it has been carried out under UV light.[168] Recent advances in the field shown that doped TiO_2 with transition metals such as copper and cobalt provide efficient photocatalysts for the degradation of acetaldehyde under visible light irradiation, but, to our knowledge, no molecular catalyst for such oxidation has been reported to date under standard temperature and pressure.[169] The presence of acetic acid in the solution highlights once again, the fact that a still non-elucidated oxidation process takes place in the reaction mixture in the presence of O_2 and involving TEA.

As an alternative to the typically used tertiary amines as sacrificial agent, 1,3-dimethyl-2-phenyl-2,3-dihydro-1H-benzo[d]imidazole (BIH) has been shown to be an efficient electron donor for CO_2 photochemical reduction.[170] Compare to TEA, using BIH in association with $Ir(ppy)_3$ presents several advantages. First, the oxidation potential of BIH (+0.33 V *vs.* SCE) is very close to the reduction potential of the $Ir(ppy)_3$ excited state (+0.31 V *vs.* SCE). Photochemically induced electron transfer is thus possible from BIH to the excited state of the iridium complex during a reductive quenching process whereas this pathway is not possible with TEA due to a too positive oxidation potential (+ 0.96V *vs.* SCE).[171] Quenching experiments (Figure 4.13) were performed to check this thermodynamics hypothesis.

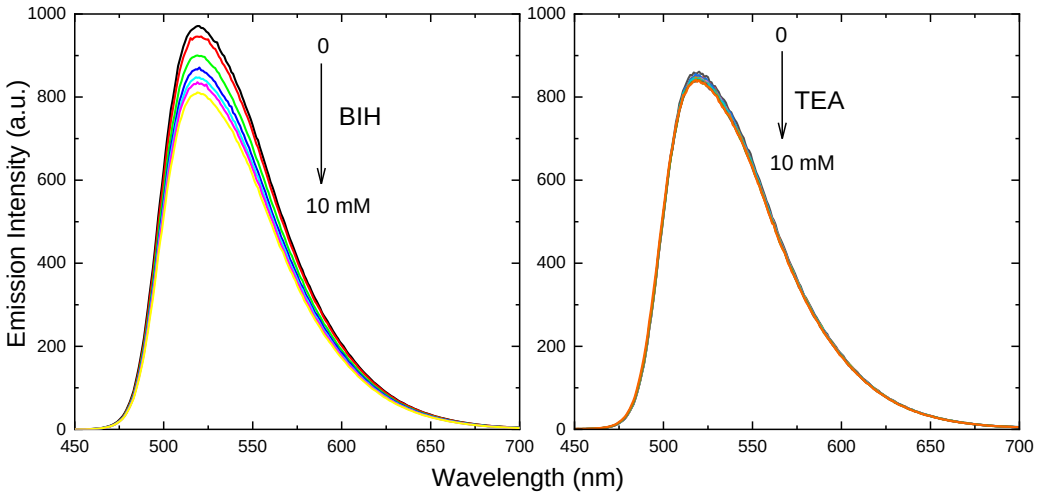

Figure 4.13: Emission spectra $Ir(ppy)_3$ (200 µM in acetonitrile solution) with increasing concentration of either BIH (left) or TEA (right) from 0 to 10 mM (λ_{exc} = 400 nm).

As can be seen in Figure 4.13, the addition of increasing amount of TEA do not induce any attenuation of the emission intensity, thus proving that no electron transfer occurs between *$Ir(ppy)_3$ and TEA. On the contrary, a gradual decrease in emission intensity is observed in the presence of BIH, thus proving that an electron transfers between the two molecules. After the monoelectronic electron transfer to the excited state of the sensitizer, the radical cation $BIH^{\bullet+}$ formed by the oxidation of BIH will rapidly release a proton to generate the neutral radical $BI^{\bullet}$. Because the proton transfer is fast, it prevents the back electron transfer between the reduced sensitizer and $BIH^{\bullet+}$.[170] Moreover, $BI^{\bullet}$ is a strong reductant too and thus it can transfer a second electron either to the sensitizer or even directly to the catalyst. It was previously shown that a non-sensitized CO_2 photoreduction in presence of Fe-*p*-TMA catalyst and BIH was possible and that BIH can reduce the iron porphyrin up to Fe^0 under light irradiation.[113] Giving that the reduction potential of $BI^{\bullet}$ is -1.66 V *vs.* SCE, a direct electron transfer to the porphyrin is possible since the potential for Fe^1/Fe^0 reduction is located at -1.47 V *vs.* SCE.[131] This indicates that after the first electron transfer to the sensitizer excited state, a second electron transfer to the catalyst could be possible , enhancing the formation of the catalyst active state and thus the overall reaction rate, which could explain the better results generally obtained with BIH compare to TEA.

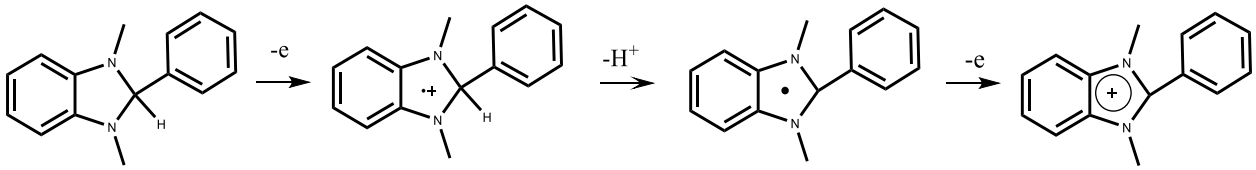

Figure 4.14: BIH successive oxidation scheme.[172]

Under CO_2, O_2-free atmosphere, a solution containing BIH produces *ca.* 5 times more CO with BIH than with TEA, but with no methane can be detected. In a previous work from the team, even though a different sensitizer was used, the Fe-*p*-TMA catalyst associated with BIH could produce some methane, but this experiment was realized in the first version of the photochemical cell, so the role of O_2 is again suspected.[30] To the best of our knowledge, no report was made on the reaction of O_2 with BIH and so complementary experiments must be made on this question too.

4.3 Effect of molecular oxygen on the photosensitizer

In photochemical conditions, the presence of molecular oxygen, independently from the catalyst, will affect the emission of the photosensitizer because it is a good excited state quencher.[173] In the case of $Ir(ppy)_3$, the electron in the excited state can easily be transferred to O_2 to form the superoxide anion ($O_2^{\bullet-}$) because its reduction potential is quite positive compare to the one of the

sensitizer (-0.85 V *vs.* SCE).[174] Therefore, in the presence of O_2, a lower amount of electrons will be available to the catalyst and the overall yield of the CO_2 reduction reaction should decrease. As mentioned previously for the sacrificial electron donor the influence of O_2 on the sensitizer excited state can be monitor by emission spectroscopy. As shown in Figure 4.15, the intensity of the emission spectrum of $Ir(ppy)_3$ is drastically decreased in the presence of O_2 compared to argon atmosphere. Moreover, it is known that organometallic complexes can undergo a structural modification, and particularly ligand exchange, in the presence of O_2. However, in our case, the structure of $Ir(ppy)_3$ is very stable under oxygenated atmosphere and can even be used as optical oxygen sensing material without any structural modifications.[175] As most of the reported organometallic complexes, the quenching of the excited state of $Ir(ppy)_3$ most likely proceeds through an electron transfer, generating the superoxide radical anion or another reactive oxygen species, depending on the number of electrons and/or protons transferred.

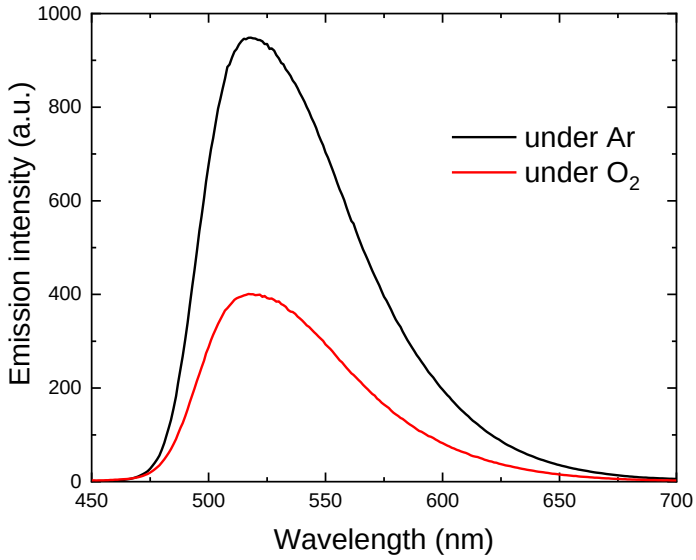

Figure 4.15: Emission spectrum of $Ir(ppy)_3$ (200 µM solution in ACN) under argon (black) or oxygen (red) atmosphere.

To check the robustness of the iridium sensitizer, we conducted cyclic voltammetry measurements (Figure 4.16) under either argon or oxygen atmosphere. Under Argon, two characteristic peaks can be observed, at 0.77V *vs.* SCE, corresponding to the $Ir(ppy)_3^+/Ir(ppy)_3$ couple and at -2.19 V *vs.* SCE corresponding to the $Ir(ppy_3)/Ir(ppy)_3^-$ couple, as previously reported.[25] Because the CV is performed with glassy carbon as working electrode material, an additional peak arises at -0.9 V *vs.* SCE, corresponding to the reduction of oxygen at the electrode.[174] Despise the distortion due to the latter process, the peaks corresponding to the iridium complex can be clearly identified with no

significant changes. A small shift in the potential of both the oxidation and the reduction waves can be observed under O_2 atmosphere, and are attributed to the slight surface modification of the electrode due to the already mentioned oxygen reduction. This tends to prove that the ground state of the iridium sensitizer is neither affected by molecular oxygen or by the superoxide anion $O_2^{\bullet-}$.

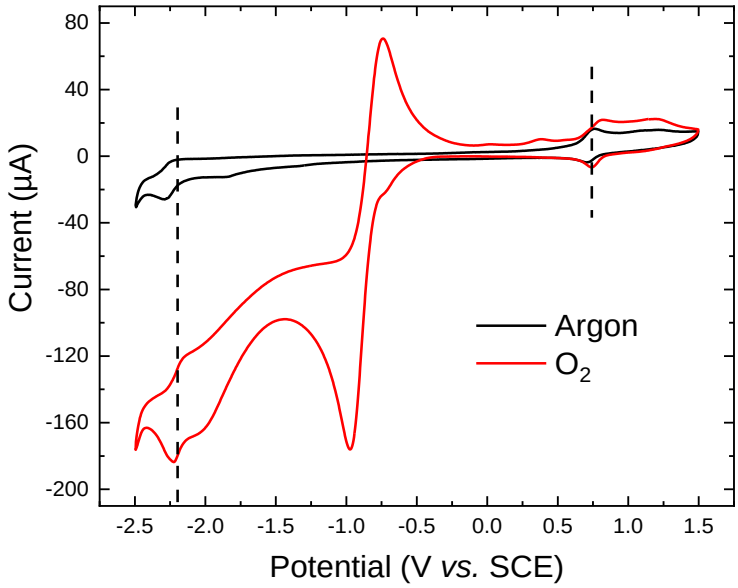

Figure 4.16: CV of 500 µM $Ir(ppy)_3$, 0.1 M $TBAPF_6$ ACN solution on 3 mm Ø glassy carbon electrode under either argon (black) or oxygen (red) atmosphere at 100 mV s^{-1} scan rate.

A converging observation was made in photochemical conditions, when a solution of iridium was purged with O_2 prior to irradiation, in presence or not of TEA. The excited state of the sensitizer was quenched by O_2, generating superoxide radical anion. In the presence of TEA, the sensitizer is regenerated back to its ground state after being quenched by O_2, which in theory generates more superoxide anions than without electron donor. However, in both cases, the UV-Visible signature of the solution (Figure 4.17) does not change significantly, which indicates that the structure of the sensitizer remains unaffected even in presence of $O_2^{\bullet-}$. The slightly higher absorbance observed below 400 nm in the presence of TEA can simply be explained by the higher absorbance of the solution in the near UV region related to TEA absorption.

Based on these observations, an interaction between O_2 and the sensitizer is very unlikely and is most probably not responsible of the change in catalytic reactivity.

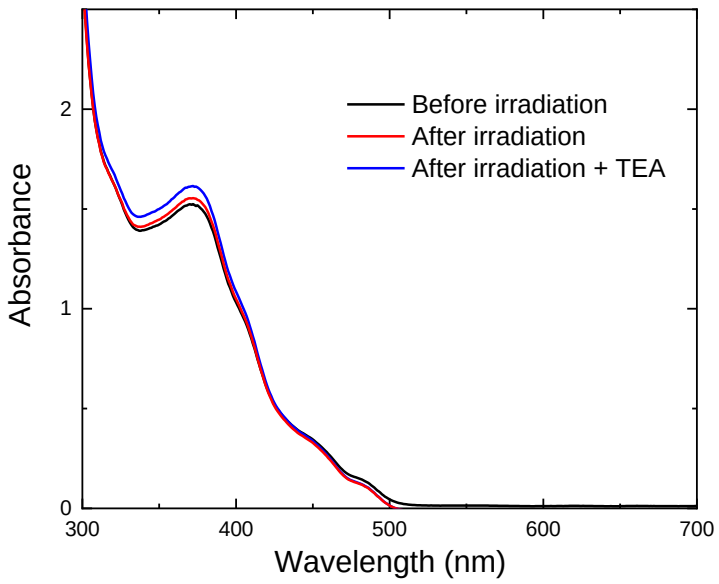

Figure 4.17: UV-Visible spectra of $Ir(ppy)_3$ (200 µM solution in ACN) under O_2 atmosphere before (black) and after (red) 90 h visible light irradiation.

4.4 Effect of molecular oxygen of the iron catalyst

As described previously, by changing the nature of either the sacrificial electron donor or the sensitizer, the CO_2 photochemical reduction is still possible even though in O_2 free conditions only 2 electrons reduction products could be obtained. As a consequence, this could indicate that the action of O_2 is related to the last parameter of the system, *i.e.* the iron porphyrin catalyst.

O_2 as a very high affinity towards the iron center of porphyrin complexes and when it binds, a species known as superoxo is generated and can undergo several electron and proton transfers to generate a hydroperoxo or even a higher valence species such has Fe(IV) (Figure 4.18). The main difference concerning the reactivity of O_2 or CO_2 towards the iron center is the oxidation state at which they bind to it. With CO_2, previous studies have shown that no interaction could be detected at the Fe^{III}, the Fe^{II} nor the Fe^{I} state of the catalyst. However, once the catalyst is reduced beyond Fe^{I}, CO_2 can bind the iron center to undergo the catalytic reduction. [176]

With O_2, the interaction with the iron center occurs at a higher oxidation state than CO_2, because it only needs to be reduced with one electron from Fe^{III} to Fe^{II} to be able to binds oxygen. Studies regarding oxygen activation demonstrated the existence of a doubly bound oxygen to a Fe^{IV} species. Another possible interaction is the creation of a dimeric species, linked by an oxygen atom, called a µ-oxo dimer. The synthesis and characterization of this species has been reported for an

iron tetraphenylporphyrin and some of its derivatives, but not for our tetramethylanilinium modified one.[177] Chemically, $[FeTPP]_2O$ can be prepared by the addition of sodium hydroxide to a FeTPP solution in the presence of O_2. This reduction process could also be performed by an electro- or photochemical electron transfer, to generate the µ-oxo species.

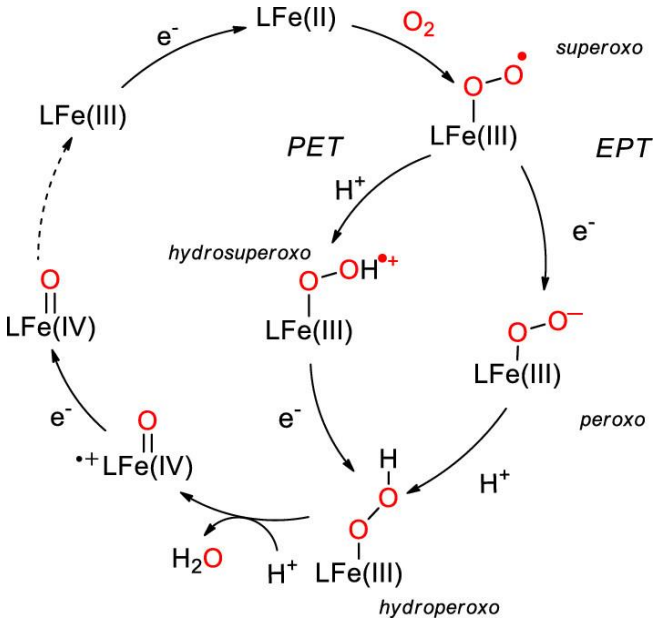

Figure 4.18: Proposed mechanism for O_2 activation by an Fe(F_{20}TPP).[157]

In our standard system, the required conditions for a reduction of the porphyrin to a Fe^{II} state in the presence of O_2 are indeed met and therefore the existence of this µ-oxo species could be postulated. However, even if the presence of such an iron dimer in theory is possible, its stability under photocatalytic conditions is questioned for several reasons. First, it has been previously shown that in reductive conditions, *i.e.* at potentials lower than -1 V *vs.* SCE , the µ-oxo bridge is not stable and the dimer decomposed.[178] Having in mind the strongly reducing character of the iridium sensitizer (from -1.73 V for the excited state to -2.19 V *vs.* SCE for the reduced state), the probability of an accumulation of the µ-oxo species is thus very low. Second, in the presence of protons, the potential for breaking the µ-oxo bridge between two iron tetraphenylporphyrin is even more positive because the dismutation happens at -0.93 V *vs.* SCE.[179] Third, most of our experiments were conducted in the presence of 0.1 M TFE as proton source, which then put the reduction potential for breaking the oxo bridge even more positive. For all these reasons, the role of O_2 in the catalytic process can probably not be explained by the formation of an oxygen-bridged

dimer of the catalyst, and even if a catalyst-O_2 interaction cannot be excluded based on our observations, not experimental proof points towards this possibility.

4.5 Sub-conclusions and perspectives

By improving the design of our photochemical cell, making it leak less or so, we discovered that molecular oxygen plays a key role in the complete reduction of CO_2 to methane in our conditions. In the total absence of O_2, no CO_2 reduction product beyond 2 electrons is formed. The possible interaction of molecular oxygen with the different compounds of our standard system was investigated individually and a strong oxidation pathway was evidenced due to the electron transfer from the excited state of the sensitizer to molecular oxygen to most likely generate superoxide radical anions, even if other transient reactive oxygen species could also be generated in the process. These unexpected results open an alternative way pointing to TEA oxidation, upon irradiation and implying molecular oxygen. Apart from TEA, which reaction with oxygen was highlighted, the other molecules present in the catalytic solution are stable under oxygenic atmosphere and does not exhibit structural changes upon visible light irradiation. The iron porphyrin catalyst can possibly interact with molecular oxygen to either create a dimer or an oxo-species, as it was shown previously in our team.[157] However, the reductive conditions and the quite important acid concentration we typically used, tend to discard the hypothesis of an implication of an oxo species in the overall reaction. As a consequence, the exact role of molecular oxygen is still not eluded and further investigations are ongoing to understand the exact mechanism of the CO_2 to methane photochemical reduction with this unexpected partner.

Chapter 5 - Electro-assisted CO_2 photochemical reduction

A major advantage of photocatalytic systems compare to electrochemical ones is the origin of the energy input, *i.e.* the use of light, possibly coming from the Sun, as the main if not the only energy source. However, in both cases, the goal of the reaction is the same, *i.e.* electron and/or proton transfers to a substrate. In photochemical processes, energetic electrons are generally provided through a sensitizer, either a molecule or a material, that can absorb light and promote an electron from the ground state to an excited state. This electron is then usually transfer to a catalyst that will subsequently transfer it to the substrate in the case of a reduction process. If no other process takes place in the reaction, once excited with the appropriate wavelength, the sensitizer could only undergo single electron transfers and will evolve toward an oxidized form, generally of no interest for the reaction. To cycle the process, the sensitizer can be regenerated into its initial state through a compensating electron transfer from a sacrificial electron donor. The whole point of this reaction partner is to transfer electrons irreversibly, what is generally achieved by the quick formation of secondary, dead ends, products after its oxidation. One could argue that this molecule is consequently a second source of energy, stoichiometrically consumed, and therefore that the reaction is not only fed by light energy. The second problem with the use of a sacrificial donor is that the reaction is intrinsically limited by its introduced amount, unless it is constantly refreshed/replaced. From a practical point of view, this implies a regular intervention on the system that must be avoided as much as possible if industrial applications are considered. One solution to extend the lifetime of the reaction is to increase the starting amount of sacrificial donor but that can be deleterious to the system. An alternative solution would be to *in-situ* regenerate this compound without stopping the reaction of interest by opening the reaction vessel. A tentative approach like this will be developed in this chapter by combining electrochemistry for the electron donor regeneration side to photochemistry for the catalysis side, and applied to our model system.

5.1 System description

The electrochemical system used here is similar to a classical one composed of three electrodes (working, counter and reference electrodes). The photochemical cell is the same than previously described: a standard 1x1cm quartz cuvette equipped with a homemade quartz headspace sealed by a septum. The volume of solution is 3 mL, the headspace being 27 mL. The major difficulty in building this setup was to fit three electrodes in a 3 mL volume. The standard 3 mm diameter glassy

carbon electrode used in the group so far was not appropriate, neither was the saturated calomel electrode for reference. The first design thus used was a 3 mm diameter, 1 cm height, glassy carbon rod as working electrode, for a total surface of 1.08 cm^2. The reference electrode was a platinum wire and the counter electrode was a platinum grid, the reference compartment being separated from the bulk of the solution by a glass frit. The three electrodes were inserted in the cell through a septum and the whole system was purged with the appropriate gas prior to the reaction (Figure 5.2, left).

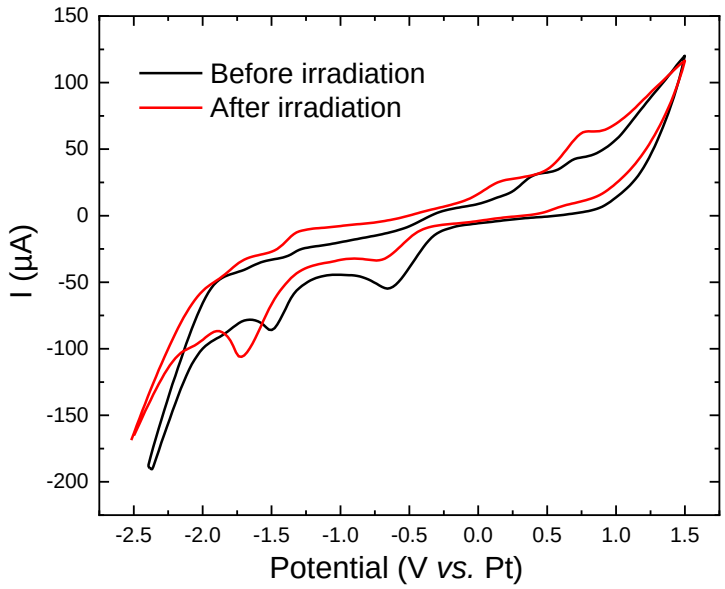

Figure 5.1: CV of the catalytic system before and after irradiation.

Two issues have been faced. First, as can be observed in Figure 5.1, the potential of the different peaks present in the CV is shifted toward more negative potentials after irradiation. This is most likely due to the nature of the platinum wire reference electrode used here, a material known for being active for proton reduction. Since the electrode is not immerged in a specific compartment (as it is the case for SCE electrodes) but directly in the catalytic solution, a change in the local pH can have an important effect on the measured potential and it is most likely the case here because of the high protons concentration (0.1 M TFE). The second issue is the small surface area of the working electrode that limits the volume of the diffusion layers and therefore the number of molecules that can reach the electrode and undergo electron transfers, even under vigorous stirring.

To overcome these issues, the glassy carbon rod was replaced by a carbon paper electrode. The flat geometry of the electrode provides a larger surface area, between 1 and 2 cm^2 which is two orders

of magnitude larger than the carbon rod, therefore opening the possibility of reducing a larger amount of catalyst. Moreover, the carbon paper is located along one wall of the cell, leaving the possibility of conducting UV-Visible spectroscopy at 90° angle without light blocking. Finally, the platinum wire was replaced by a 1 mm diameter Ag/AgCl leak free electrode which provides more stability and a better control of the potential (Figure 5.2 right).

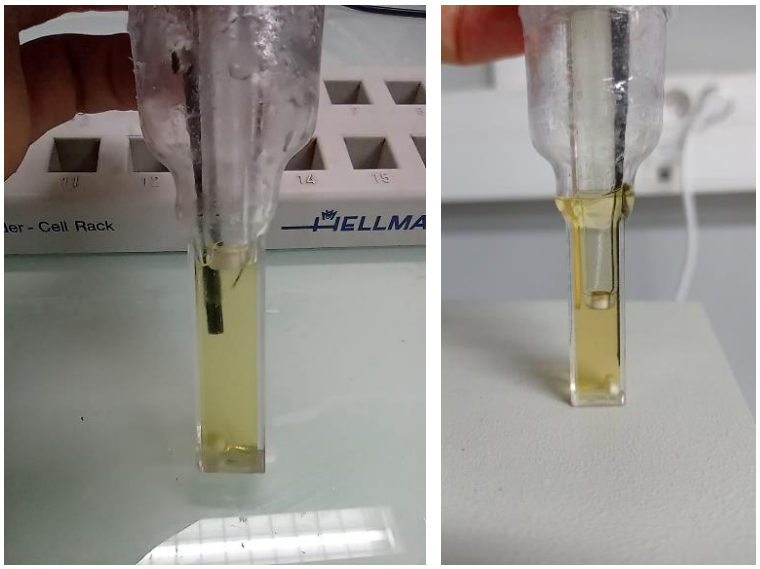

Figure 5.2: Electro-assisted photochemical setups with a carbon rod (left) or a carbon paper (right) working electrode.

5.2 Sacrificial donor regeneration

In order to be used as sacrificial electron donor, a molecule should be easily oxidized to provide a driving force for the electron transfer to happen. Among others, tertiary amines are probably the most commonly employed and triethylamine has proved to be an efficient compound when combined with many sensitizers, including $Ir(ppy)_3$. As described in Chapter 4, TEA oxidation leads to a very reactive N located radical. Subsequent reactions, generally with another TEA molecule, rapidly lead to the formation of diimine secondary compounds. TEA oxidation is thus considered as irreversible, as confirmed by CV (Figure 5.3) and therefore the regeneration of TEA to its initial state is not possible without a cleaver strategy.

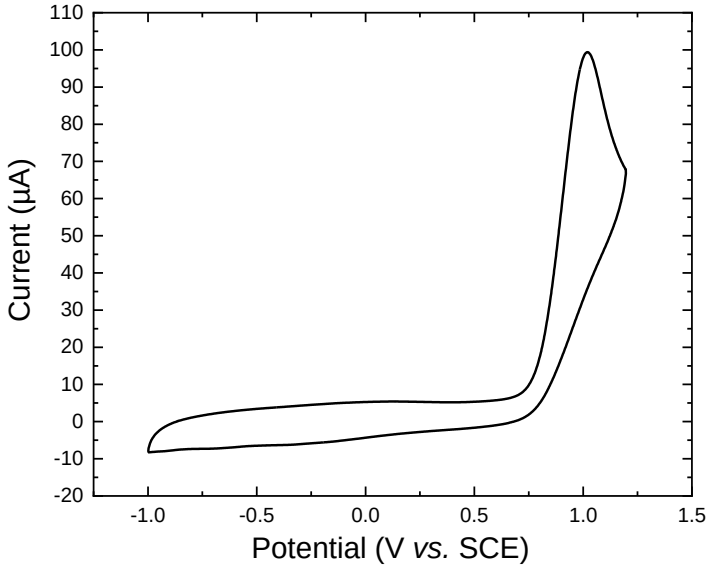

Figure 5.3: CV of a 10 mM TEA, 0.1M $TBAPF_6$, ACN solution, with a 3 mm diameter glassy carbon electrode, scan rate 0.1 V s^{-1}.

Tetrathiafulvalene (TTF, Figure 5.4) is another interesting candidate as electron donor, thanks to its capacity of transferring two electrons, and to the quasi absence of reactivity of the species formed upon those two electron transfers.[180] Interestingly, the first oxidation potential is located at +0.32 V *vs.* SCE, so very similar to the one of BIH (+0.33 V *vs.* SCE) and to the reduction potential of $Ir(ppy)_3$ excited state (+0.31 V *vs.* SCE). TTF can therefore quench the latter in a reductive pathway as confirmed by the emission quenching measurements we conducted (Figure 5.5).

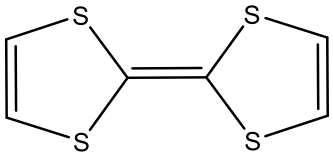

Figure 5.4: Molecular structure of tetrathiafulvalene (TTF).

A key factor in the choice of TTF was that, unlike TEA, the two oxidation steps do not imply any chemical step such as proton transfer or polymerization, and both are very reversible. This reversibility might however involve an easy back electron transfer from the exited or the reduce state of the sensitizer to the oxidized TTF, then lowering its efficiency as sacrificial electron donor. But it was shown that in the presence of TTF, CO_2 reduction products (such as CO) could be obtained with our standard system under visible light irradiation. So based on the above arguments, TTF was chosen as electron donor candidate in our electro-assisted photochemical setup for CO_2 reduction, with the view to be able to *in situ* regenerate it. Unless otherwise mentioned, the

conditions were kept constant, *i.e.* Fe-*p*-TMA 10 µM, $Ir(ppy)_3$ 200 µM, TFE 0.1 M and TTF 2 mM in ACN.

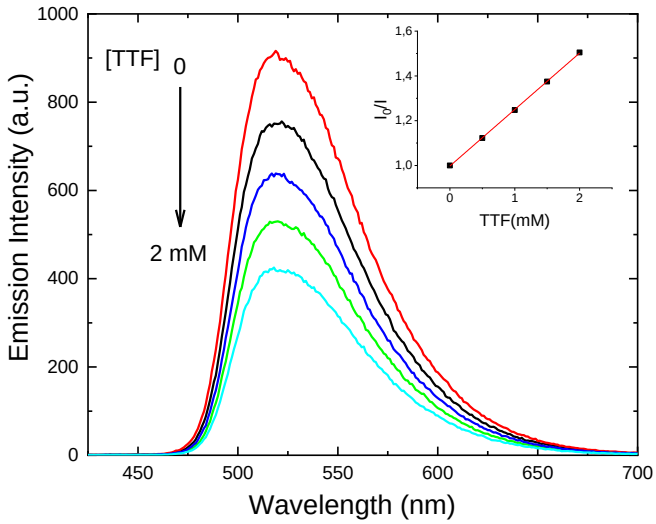

*Figure 5.5: Emission quenching measurements of *Ir(ppy)$_3$ upon TTF addition in ACN under argon atmosphere. Inset: Stern-Volmer analysis.*

Before irradiation, a CV of the solution was recorded, the potential being given *vs.* SCE electrode, using the redox potential of TTF as an internal standard. The redox waves of the catalyst are not observable on the different CVs because its concentration is too low (µM) in photochemical conditions (in typical electrochemical conditions, 0.5 to 1 mM catalyst concentration is used). Increasing the catalyst concentration to a level high enough for CV measurement would result in a very low efficiency of the photochemical reaction because of the very high absorption of the porphyrin in the visible range. The amount of photons absorbed by the sensitizer and therefore the overall reaction would be drastically lowered. As shown in Figure 5.6, the addition of catalyst (µM concentration) to the solution only changes the CV shape at the more negative potentials, where the beginning of a catalytic wave could be observed. Interestingly, even if the redox waves of the catalyst cannot be observed, its high activity toward CO_2 reduction still influences the measured current.

In order to regenerate TTF, after one electron transfer to the sensitizer, a constant potential of 0 V *vs.* SCE was applied to the photocatalytic solution, while being irradiated with visible light. This potential was chosen because it corresponds to the reduction of the TTF anion generated after the first electron transfer (see Figure 5.6). The current measured by chronoamperometry after 5 h is not stable (Figure 5.7) and the solution color changed from pale yellow to dark orange. Moreover,

no CO_2 reduction products could be detected. Actually, the change of color has been reported and is characteristic of the $TTF^{\bullet-}$ radical cation.

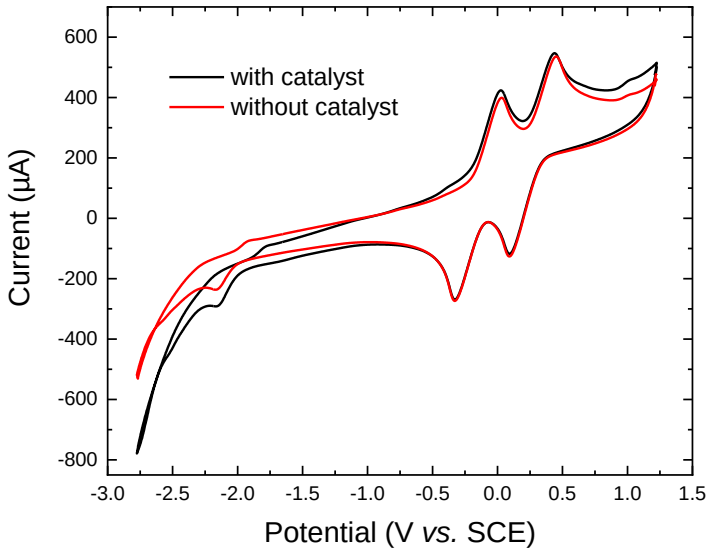

Figure 5.6: CV of a 2 mM of TTF, 200 µM of $Irppy_3$ without (black) or with (red) 10 µM of Fe-p-TMA ACN solution under CO_2 atmosphere.

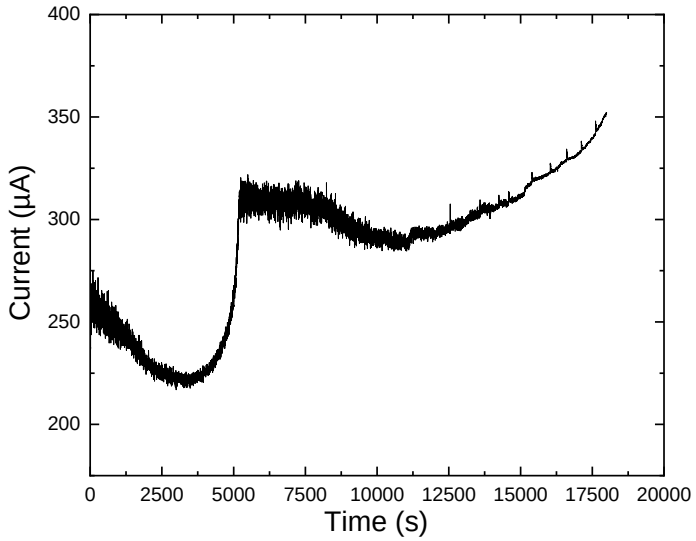

Figure 5.7: Chronoamperogram measured upon constant 0 V applied potential (see text) under CO_2 atmosphere.

A possibility is that the potential constantly holds during the whole duration of the irradiation could have a negative effect on the overall system because i) it forces TTF to be in a neutral state and ii) it does not necessarily leave enough time to the molecule to diffuse to the sensitizer in order to reduce it. To overcome this issue, the same experiment was repeated but by applying pulses of potential instead of keeping it constant. The potential was hold at 0 V for 15 min and the system

was then free to evolve hoping that the photochemical process would proceed, and the sequence was repeated every 3 h for a total 15 h.

In that configuration, the solution color did not change which indicates that TTF was mostly in it neutral state. A GC measurement of the gaseous headspace was then performed and CO was found as only product with a TON of 72, whereas, under pure photochemical conditions, the same solution gave 35 TON of CO. This first, promising result thus shows that a two-fold increase on productivity could be obtained by electro-assisting the photochemical process. This approach could be a way to enhance and to extend the lifetime of photocatalytic systems in addition to the lowering of the global energy cost, the synthesis of a molecule such has TTF being of higher cost than the electrical cost of 1 electron transfer to regenerate it.

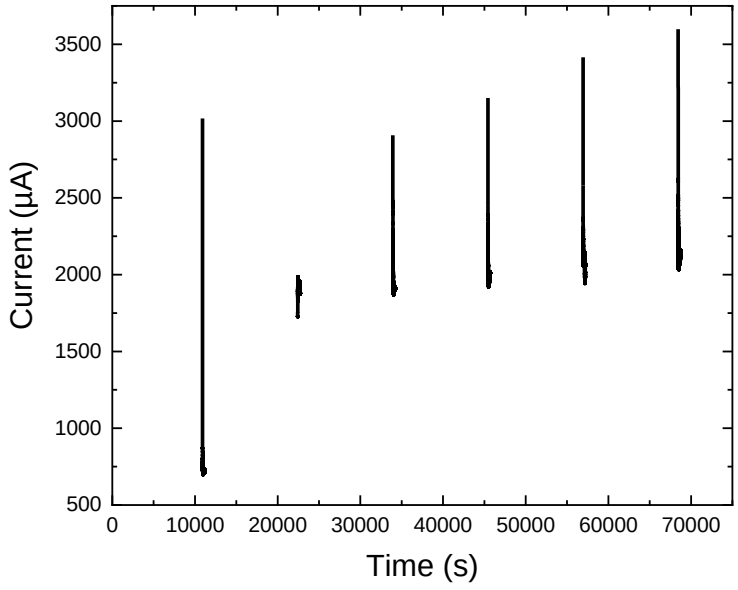

Figure 5.8: Chronoamperogram showing short pulses of potential at 0 V (see text) under visible light irradiation.

The setup that we developed also allowed us to perform electrochemical measurements on the homogeneous solution and can be used, in addition of complementary spectroscopic techniques, to better understand the behavior and the limitations of our catalytic system. As mentioned in Chapter 4, molecular oxygen has an influence on the reaction and a possible interaction, even though we did not identify it, is with the catalyst. However, due to its low concentration in solution, we cannot directly track the electrochemical signal of the porphyrin catalyst.

Identifying the rate-determining step in a catalytic system is primordial in order to enhance the performances of such system and can be a tedious task. The formation of the Fe^{II}-CO adduct and

its further reduction to CH_4 are thought to be the key steps of the process. This adduct is stable enough to be detected electrochemically: a shift in the Fe^{II}/Fe^{I} wave on the reverse (oxidation) scan under CO_2 atmosphere is indeed characteristic of such adduct. UV-Visible spectroscopy can also be used to detect the adduct as well as the various oxidation state of the porphyrin since they all have a specific optical signature. However, in our standard photochemical conditions, the catalyst absorption is fully covered by the one of the sensitizer (100 times more concentrated), making such spectroscopic measurement impossible.

We can formulate the following hypothesis: because the potential of the reduced sensitizer is very reductive (-2.19 V *vs.* SCE), all the porphyrin catalyst is maintained in a Fe^0 state and cannot undergo any other reaction than CO_2 to CO. In the presence of O_2, some of the catalyst is re-oxidized to Fe^{II}, favoring the formation of the key Fe^{II}-CO adduct on the road to methane. If this hypothesis is correct, by helping the system to build up a sufficient amount of Fe^{II} in solution, CH_4 should be detected in the gaseous headspace of the solution. The electro-assisted setup we have developed could be a useful tool to do so, *i.e.* to generate electrochemically a certain amount of Fe^{II} in solution. Before applying this strategy to our system, we have verified that our system was indeed capable of generating a large amount of the reduced Fe^{II} species. For that, a 10 µM Fe-*p*-TMA ACN solution was placed under CO_2 atmosphere at an applied potential of -0.8 V *vs.* Ag/AgCl which corresponds to the potential in between the Fe^{II}/Fe^{II} and Fe^{II}/Fe^{I} waves.

By UV-Visible spectroscopy, the optical signature was monitored and a shift in the maximum absorption have been observed. Figure 5.9 shows the progressive conversion from Fe^{III} (408 nm maximum) to Fe^{II} (428 nm maximum). The reaction is quite slow, more than 105 min been necessary to convert the majority of the catalyst, and even though a shoulder at 400 nm is still observable, suggesting that the conversion of the Fe^{III} of the porphyrin is quantitative but not total. This can be explained both by the geometry of the cell and the electrode used here: a flat carbon paper electrode immersed in a 3 mL volume at 10 µM concentration implies that even under stirring the amount of molecule reaching the active layer of the electrode is quite low. Despite this limitation, the UV-Visible spectral evolution proves the feasibility of our approach.

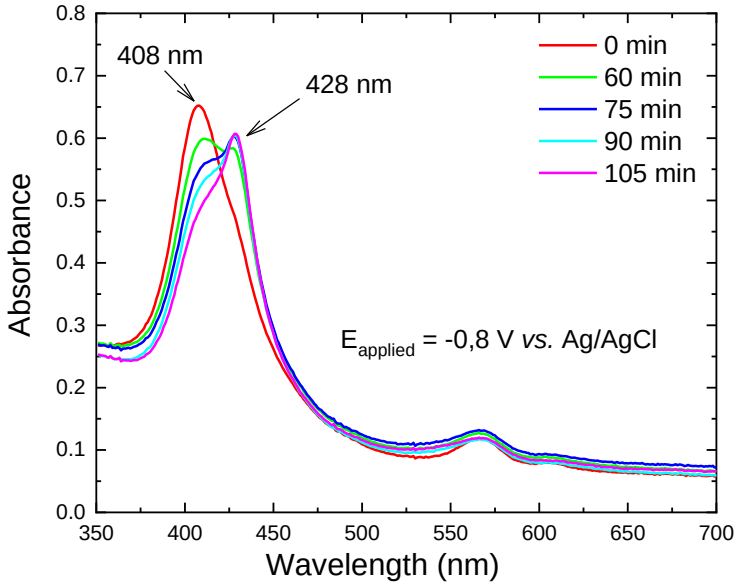

Figure 5.9: UV-Visible spectral evolution of a 10 µM Fe-p-TMA, 0.1 M $TBAPF_6$, ACN solution under CO_2 atmosphere at an applied potential -0.8 V vs. Ag/AgCl.

After this preparative electrolysis to generate Fe^{II}, the solution was saturated with CO with no potential applied and the associated spectrum was recorded (Figure 5.10). A shift toward lower wavelength (420 nm, red) as well as a sharper absorption peak, as expected by the coordination of CO to the Fe^{II} center, forming the target Fe^{II}-CO adduct. This adduct can thus be formed electrochemically, in presence of CO, in our electro-assisted photochemical setup.

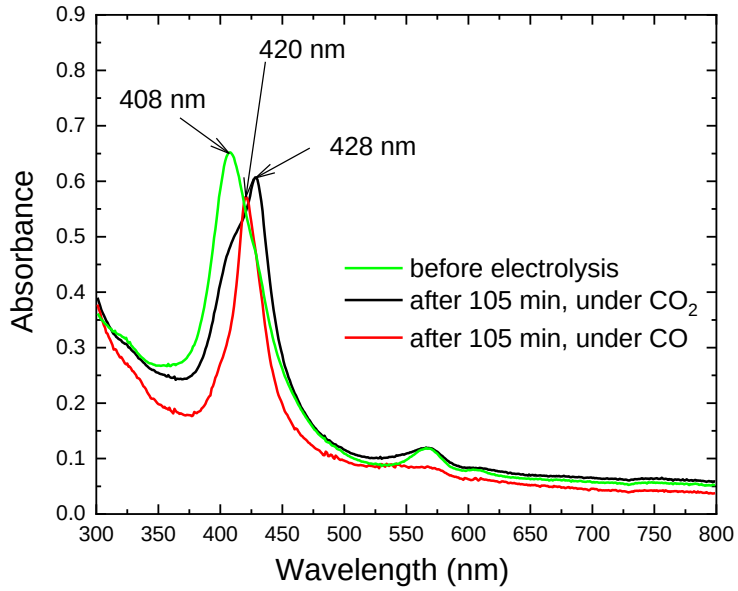

Figure 5.10: UV-Visible spectra of a 10µM Fe-p-TMA, 0.1M $TBAPF_6$, ACN solution before (green) and after 105 min at an applied potential of -0.8 V vs. Ag/AgCl under CO_2 (black) or CO (red).

However, the same issue than the one previously described for the sacrificial electron donor regeneration could be faced here: if the applied potential is held during the whole duration of the irradiation, the catalyst will then stay in vast majority in a Fe^{II} state and the reaction will not go further. So, the pulsed strategy was employed, and a potential was sequentially applied for 1 h at -0.8 V *vs.* Ag/AgCl and then the system was free to evolve for 3 h. This sequence was repeated 5 times, for a total of 15 h of irradiation (Figure 5.11) and the gaseous headspace was analyzed by GC. Two products have been detected, CO with a TON of 180 and H_2 with a TON of 10. The same experiment was performed under CO atmosphere, in order to generate sufficient amount of $Fe^{II}CO$, and only hydrogen has been detected in the gas phase. Despite our efforts, no methane could be detected, which seems to indicate that Fe^{II}-CO, albeit previously identified as a reaction intermediate, is probably not the limiting factor of the reaction and so is probably not implied in the reaction pathway with O_2.

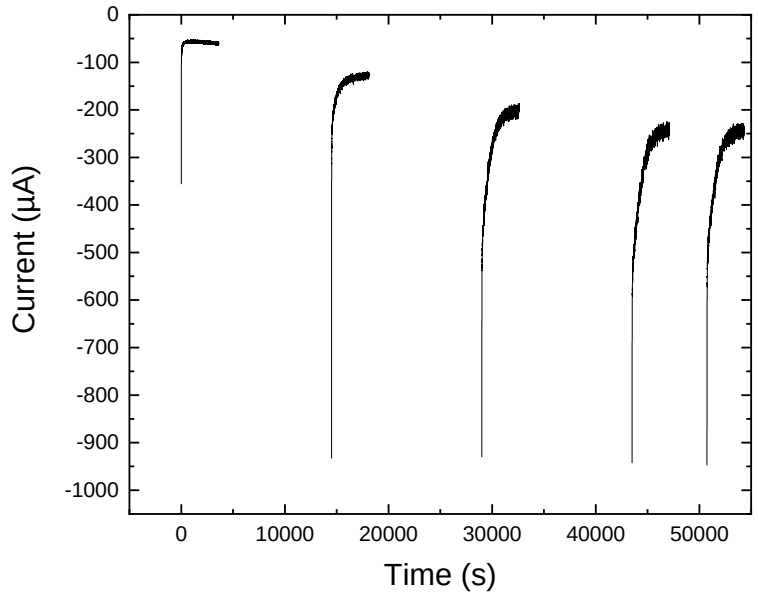

Figure 5.11: Chronoamperogram showing 1 h pulses of potential at -0.8 V (see text) under visible light irradiation.

5.3 Sub-conclusions and perspectives

Understanding the mechanism and identifying the intermediates of a catalytic process is primordial in order to optimize and then to upscale it. As seen before, the search for intermediates is tedious since their detection, either in liquid or gas phase, is not an easy task due to their low amount (if any), their probable high reactivity and therefore their short lifetime. Here we have proposed a setup combining electrochemistry and photochemistry to i) regenerate *in situ* the sacrificial electron

donor, and ii) generate the presumed key intermediate of the catalyst to investigate its importance in the overall reaction. For this, we have developed an electro-assisted photochemical setup able to performed both CVs and controlled potentials electrolysis while the solution is illuminated by a solar simulator. Even though methane was not detected, despite having tested various conditions, such combined setup opens the way to generate other possible intermediates (implying for example methanol or formaldehyde) and to investigate their behavior under irradiation.

General conclusion and perspectives of this work

In this thesis, the reduction of CO_2 was investigated in photochemical homogeneous conditions with a molecular catalyst. The catalytic system was constituted of a substituted iron porphyrin as catalyst, an iridium complex as photosensitizer, a sacrificial electron donor and a weak external acid as proton source. The main goal of our investigations was the elucidation of the reaction mechanism and the possible intermediates during the conversion CO_2 to CH_4. The resulting second objective was the optimization of the different components of the system to improve the catalysis, with a focus on the photosensitizer, currently containing a noble metal. Optimization of the photochemical cell leads to unexpected results and highlighted the role of oxygen in the CO_2 to methane reaction.

The iron porphyrin bearing four trimethylanilinium groups in para position was used in homogeneous under visible light illumination to achieve the reduction of CO_2. Previous studies from our group indeed revealed the production of methane from CO_2 and CO was identified as a reaction intermediate. In this work, we explored the possible existence of other intermediates such as formate, formaldehyde or methanol. By introducing them as starting reactant instead of CO_2, we observed that no reduction product, either liquid or gaseous, could be obtained with the first two compounds. However, when methanol was employed as starting reagent, we were able to detect the formation of methane after irradiation with visible light. Isotope labelling experiments allowed us to assert that methanol was the source of methane without ambiguity. Our catalytic system is thus able to reduce methanol into methane in photochemical conditions even if it does not formally prove that it is an intermediate between CO and CH_4.

The optimization of a process for further industrial applications requires a fine understanding of the mechanism together with the use of sustainable components. To do so, the rare metal containing iridium complex used as photosensitizer should be replaced. In this purpose, we explored two class of purely organic alternatives able to replace the iridium complex but keeping similar photophysical and redox properties. Coumarin are well known dyes being soluble in water, which constitutes an interesting point toward industrialization. In acetonitrile solution, using coumarin as photosensitizer with the iron porphyrin catalyst leaded to the formation of CO as the sole product. However, no CO_2 reduction product could be obtained in water, probably because of a strong interaction of the positively charger catalyst with the solvent and of the very short triplet state

lifetime of the coumarin. Phenoxazines were also employed in replacement of $Ir(ppy)_3$ and CO could be generated upon visible light irradiation. Having a variety of phenoxazine derivatives with slightly different structures, we were able to explore the effect of both the triplet excited state potential and the ground state oxidation potential on the catalytic performance of the system. Interestingly, no correlation was found between CO production and the driving force of the electron transfer of the catalyst activation step, whereas a clear trend was observed with the driving force of the photosensitizer regeneration step. A higher production of CO was indeed obtained with the derivative possessing the more positive oxidation potential. Therefore, it indicates that the rate determining step of the reaction is not the electron transfer from the excited state of the photosensitizer to the catalyst but the electron transfer from the electron donor to the photosensitizer to regenerate it.

By optimizing the photochemical cell, and in particular by suppressing leaks, we found that in O_2-free conditions, only CO can be obtained from CO_2 and no further reduced species, like methane, can be detected. By injecting known amounts of molecular oxygen in the solution headspace, we observed a clear correlation between the amount of generated products (CO and CH_4) and O_2 concentration. The possible effect of O_2 on each molecular partner of the system was then investigated. The iridium sensitizer did not exhibit any changes even under complete oxygen atmosphere, both its optical and electrochemical signatures remaining unchanged. The iron porphyrin catalyst, on its side, is known to be able to interact with O_2 to form either a dimer or hypervalent species, but under the strongly reductive and acidic of our typical conditions, their existence is unlikely and indeed never detected. Finally, the interaction of O_2 with triethylamine, the electron donor, was studied. Under complete O_2 atmosphere, more than 6 different oxidation products from triethylamine could be obtained upon visible light irradiation. Those products are usually generated by chemical oxidation under arch conditions such as with heated hydrogen peroxide or nitric acid. This oxidation is supposed to be due to the generation of the superoxide radical anion and then to the protonated form $HO_2^{\bullet}$ which processes a strong oxidant power. So, even if this does not constitute an absolute proof, the unexpected role of O_2 in the CO_2 to CH_4 process is thought to be located on the electron donor side. More work is ongoing to decipher this in more details.

Finally, we have developed an electrochemical setup that fits into the photochemical cell used without modification. This setup allows operando analysis such as cyclic voltammetry or control potential electrolysis while the solution is under light irradiation. This setup has been used to electrochemically prepare a specific state of the iron porphyrin catalyst, namely Fe(II), since we made the hypothesis that (one of) the limiting rate of the reaction was the formation of the $Fe^{II}CO$ adduct. By applying a constant potential to the solution, this state can be formed as confirmed by UV-Visible spectroscopy. However, no methane could be obtained from CO_2 reduction which might indicate that this oxidation state is in fact not the limiting step in the CO_2 to CH_4 photochemical reduction. Preliminary results were also obtained using this setup to regenerate the sacrificial electron donor electrochemically.

This work opens the way for a better understanding of the overall mechanism of CO_2 photochemical reduction by an iron porphyrin and it reveals the unexpected, and still unresolved, role of molecular oxygen in the process. The electro-assisted photochemical setup we developed could be used i) to better understand photochemical reactions and especially to probe possible intermediates during the reaction course and ii) to electrochemically assist the reaction by preparing key species and/or regenerating the electron donor.

References

1. *International Energy Outlook 2017*; US Energy information administration: 2017.
2. Sovacool, B. K., Valuing the greenhouse gas emissions from nuclear power: A critical survey. *Energy Policy* **2008,** *36* (8), 2950-2963.
3. Ruddiman, W. F.; He, F.; Vavrus, S. J.; Kutzbach, J. E., The early anthropogenic hypothesis: A review. *Quat. Sci. Rev.* **2020,** *240*.
4. Kayler, Z.; Janowiak, M.; Swanston, C. Global Carbon. https://www.fs.usda.gov/ccrc/topics/global-carbon.
5. Pachauri, R. K.; Meyer, L. A., Climate Change 2014 Synthesis Report. *Intergovernmental Panel on Climate Change* **2014,** *5* (1).
6. C.lngamells, J.; Lindquist, R. H., Methanol as a motor fuel or a gasoline blending component. *Society of Automotive Engineers* **1975**, 15.
7. grtgaz
8. Kabir, E.; Kumar, P.; Kumar, S.; Adelodun, A. A.; Kim, K.-H., Solar energy: Potential and future prospects. *Renew. Sust. Energ. Rev.* **2018,** *82*, 894-900.
9. Becquerel, E., Recherches sur les effets de la radiation chimique de la lumière solaire, au moyen des courants électrique. *C. R. A. S.* **1839,** *9* (145-149).
10. John F. Geisz; Myles A. Steiner; Nikhil Jain ; Kevin L. Schulte ; Ryan M. France; William E. McMahon ; Emmett E. Perl ; Friedman, D. J., Building a Six-Junction Inverted Metamorphic Concentrator Solar Cell. *IEEE J. Photovolt.* **2018,** *8* (2), 626-632.
11. IEA, Solar PV power generation in the Sustainable Development Scenario, 2000-2030, IEA, Paris
12. Mouchot, A., *La chaleur solaire et ses applications industrielles*. Gauthier-Villars: 1869.
13. EurObserv'ER *Solar thermal and concentrated solar power barometers*; 2019.
14. Pieter Janse van Vuuren; Lauren Basson; Angelo Buckley; Karin Kritzinger; Ulrich Terblanche; Manisha Gulati; Louise Scholtz *Industrial scale solar heat in South Africa opportunities in agri-processing and textiles*; WWF: 2017.
15. Deloitte *Energy storage: Tracking the technologies that will transform the power sector*; 2015.
16. Laboratory, N. R. E. https://www.nrel.gov/grid/solar-resource/assets/data/astmg173.xls.
17. Archer, D.; Eby, M.; Brovkin, V.; Ridgwell, A.; Cao, L.; Mikolajewicz, U.; Caldeira, K.; Matsumoto, K.; Munhoven, G.; Montenegro, A.; Tokos, K., Atmospheric Lifetime of Fossil Fuel Carbon Dioxide. *Annu. Rev. Earth Planet. Sci.* **2009,** *37* (1), 117-134.
18. Robert, M., Running the Clock: CO_2 Catalysis in the Age of Anthropocene. *ACS Energy Lett.* **2016,** *1* (1), 281-282.
19. Fujita, E., Photochemical carbon dioxide reduction with metal complexes. *Coord. Chem. Rev.* **1999,** *185-186*, 373-384.
20. Ceballos, B. M.; Yang, J. Y., Directing the reactivity of metal hydrides for selective CO_2 reduction. *Proc. Natl. Acad. Sci. U.S.A.* **2018,** *115* (50), 12686-12691.
21. Kortlever, R.; Shen, J.; Schouten, K. J.; Calle-Vallejo, F.; Koper, M. T., Catalysts and Reaction Pathways for the Electrochemical Reduction of Carbon Dioxide. *J. Phys. Chem. Lett.* **2015,** *6* (20), 4073-82.
22. Zheng, Y.; Vasileff, A.; Zhou, X.; Jiao, Y.; Jaroniec, M.; Qiao, S. Z., Understanding the Roadmap for Electrochemical Reduction of CO_2 to Multi-Carbon Oxygenates and Hydrocarbons on Copper-Based Catalysts. *J. Am. Chem. Soc.* **2019**.

23. Gottle, A. J.; Koper, M. T. M., Proton-coupled electron transfer in the electrocatalysis of CO2 reduction: prediction of sequential *vs.* concerted pathways using DFT. *Chem. Sci.* **2017,** *8* (1), 458-465.
24. R.Lakowicz, J., *Principles of Fluorescence spectroscopy*. Plenum Press: 1983.
25. Koike, T.; Akita, M., Visible-light radical reaction designed by Ru- and Ir-based photoredox catalysis. *Inorg. Chem. Front.* **2014,** *1* (8), 562-576.
26. Stern, O.; Volmer, M., Über die abklingzeit der fluoreszenz. *Z. Phys.* **1919,** *20*, 183-188.
27. Chen, X.; Shen, S.; Guo, L.; Mao, S. S., Semiconductor-based Photocatalytic Hydrogen Generation. *Chem. Rev.* **2010,** *110*, 6503-6570.
28. Kas, R.; Kortlever, R.; Yılmaz, H.; Koper, M. T. M.; Mul, G., Manipulating the Hydrocarbon Selectivity of Copper Nanoparticles in CO_2 Electroreduction by Process Conditions. *ChemElectroChem* **2015,** *2* (3), 354-358.
29. Boutin, E.; Wang, M.; Lin, J. C.; Mesnage, M.; Mendoza, D.; Lassalle-Kaiser, B.; Hahn, C.; Jaramillo, T. F.; Robert, M., Aqueous Electrochemical Reduction of Carbon Dioxide and Carbon Monoxide into Methanol with Cobalt Phthalocyanine. *Angew. Chem., Int. Ed.* **2019,** *58* (45), 16172-16176.
30. Rao, H.; Lim, C. H.; Bonin, J.; Miyake, G. M.; Robert, M., Visible-Light-Driven Conversion of CO_2 to CH_4 with an Organic Sensitizer and an Iron Porphyrin Catalyst. *J. Am. Chem. Soc.* **2018,** *140* (51), 17830-17834.
31. Leitenburg, C. d.; Trovarelli, A., Metal-Support Interactions in $RhCeO_2$, $RhTiO_2$, and RhNb2O5 Catalysts as Inferred from CO_2 Methanation Activity. *J. Catal.* **1995,** *156* (1), 171-174.
32. Aziz, M. A. A.; Jalil, A. A.; Triwahyono, S.; Sidik, S. M., Methanation of carbon dioxide on metal-promoted mesostructured silica nanoparticles. *Applied Cat. A* **2014,** *486*, 115-122.
33. Muroyama, H.; Tsuda, Y.; Asakoshi, T.; Masitah, H.; Okanishi, T.; Matsui, T.; Eguchi, K., Carbon dioxide methanation over Ni catalysts supported on various metal oxides. *J. Catal.* **2016,** *343*, 178-184.
34. Govorov, A. O.; Richardson, H. H., Generating heat with metal nanoparticles. *Nano Today* **2007,** *2* (1), 30-38.
35. Zhang, X.; Li, X.; Zhang, D.; Su, N. Q.; Yang, W.; Everitt, H. O.; Liu, J., Product selectivity in plasmonic photocatalysis for carbon dioxide hydrogenation. *Nat. Commun.* **2017,** *8*, 14542.
36. Cavicchioli, R., Cold-adapted archaea. *Nat. Rev. Microbiol.* **2006,** *4* (5), 331-43.
37. Blasco-Gomez, R.; Batlle-Vilanova, P.; Villano, M.; Balaguer, M. D.; Colprim, J.; Puig, S., On the Edge of Research and Technological Application: A Critical Review of Electromethanogenesis. *Int. J. Mol. Sci.* **2017,** *18* (4).
38. Royer, M. E., Réduction de l'acide carbonique en acide formique *C. R. A. S.* **1870,** *70*, 731.
39. Frese, K. W.; Leach, S., Electrochemical Reduction of Carbon Dioxide to Methane, Methanol, and CO on Ru Electrodes. *J. Electrochem. Soc.* **1985,** *132* (1), 259-260.
40. Yoshio Hori; Katsuhei Kikuchi; Suzuki, S., Production of CO and CH_4 in electrochemical reduction of CO_2 at metal electrodes in aqueous hydrogencarbonate solution. *Chem. Lett.* **1985,** *14* (11), 1695-1698.
41. Kuhl, K. P.; Cave, E. R.; Abram, D. N.; Jaramillo, T. F., New insights into the electrochemical reduction of carbon dioxide on metallic copper surfaces. *Energy Environ. Sci.* **2012,** *5* (5), 7050.
42. Zhang, T.; Verma, S.; Kim, S.; Fister, T. T.; Kenis, P. J. A.; Gewirth, A. A., Highly dispersed, single-site copper catalysts for the electroreduction of CO_2 to methane. *J. Electroanal. Chem.* **2020,** *875*.

43. Pan, H.; Barile, C. J., Electrochemical CO_2 reduction to methane with remarkably high Faradaic efficiency in the presence of a proton permeable membrane. *Energy Environ. Sci.* **2020,** *13* (10), 3567-3578.
44. Weng, Z.; Jiang, J.; Wu, Y.; Wu, Z.; Guo, X.; Materna, K. L.; Liu, W.; Batista, V. S.; Brudvig, G. W.; Wang, H., Electrochemical CO_2 Reduction to Hydrocarbons on a Heterogeneous Molecular Cu Catalyst in Aqueous Solution. *J. Am. Chem. Soc.* **2016,** *138* (26), 8076-9.
45. Shen, J.; Kortlever, R.; Kas, R.; Birdja, Y. Y.; Diaz-Morales, O.; Kwon, Y.; Ledezma-Yanez, I.; Schouten, K. J.; Mul, G.; Koper, M. T., Electrocatalytic reduction of carbon dioxide to carbon monoxide and methane at an immobilized cobalt protoporphyrin. *Nat. Commun.* **2015,** *6*, 8177.
46. Weng, Z.; Wu, Y.; Wang, M.; Jiang, J.; Yang, K.; Huo, S.; Wang, X. F.; Ma, Q.; Brudvig, G. W.; Batista, V. S.; Liang, Y.; Feng, Z.; Wang, H., Active sites of copper-complex catalytic materials for electrochemical carbon dioxide reduction. *Nat. Commun.* **2018,** *9* (1), 415.
47. Ahmed, M. E.; Adam, S.; Saha, D.; Fize, J.; Artero, V.; Dey, A.; Duboc, C., Repurposing a Bio-Inspired NiFe Hydrogenase Model for CO_2 Reduction with Selective Production of Methane as the Unique C-Based Product. *ACS Energy Lett.* **2020,** *5* (12), 3837-3842.
48. M Eisenberg; H.P. Silverman, Photo electrochemical cells. *Electrochim. Acta* **1961,** *5*, 1-12.
49. Halmann, M., Photoelectrochemical reduction of aqueous carbon dioxide on p-type gallium phosphide in liquid junction solar cells. *Nature* **1978,** *275* (1), 115-116.
50. Tooru Inoue; Akira Fujishima; Konishi, S.; Honda, K., Photoelectrocatalytic reduction of carbon dioxide in aqueous suspensions of semiconductor powders. *Nature* **1979,** *277*, 637-638.
51. Xie, S.; Zhang, Q.; Liu, G.; Wang, Y., Photocatalytic and photoelectrocatalytic reduction of CO2 using heterogeneous catalysts with controlled nanostructures. *Chem. Commun.* **2016,** *52* (1), 35-59.
52. Kočí, K.; Obalová, L.; Matějová, L.; Plachá, D.; Lacný, Z.; Jirkovský, J.; Šolcová, O., Effect of TiO2 particle size on the photocatalytic reduction of CO_2. *Applied Cat. B* **2009,** *89* (3-4), 494-502.
53. Liu, L.; Zhao, H.; Andino, J. M.; Li, Y., Photocatalytic CO_2 Reduction with H_2O on TiO_2 Nanocrystals: Comparison of Anatase, Rutile, and Brookite Polymorphs and Exploration of Surface Chemistry. *ACS Catal.* **2012,** *2* (8), 1817-1828.
54. Li, P.; Ouyang, S.; Xi, G.; Kako, T.; Ye, J., The Effects of Crystal Structure and Electronic Structure on Photocatalytic H_2 Evolution and CO_2 Reduction over Two Phases of Perovskite-Structured NaNbO3. *J. Phys. Chem. C* **2012,** *116* (14), 7621-7628.
55. Ye, L.; Mao, J.; Peng, T.; Zan, L.; Zhang, Y., Opposite photocatalytic activity orders of low-index facets of anatase TiO(2) for liquid phase dye degradation and gaseous phase CO_2 photoreduction. *Phys. Chem. Chem. Phys.* **2014,** *16* (29), 15675-80.
56. Handoko, A. D.; Tang, J., Controllable proton and CO2 photoreduction over Cu_2O with various morphologies. *Int. J. Hydrogen Energ.* **2013,** *38* (29), 13017-13022.
57. Wang, L.; Duan, S.; Jin, P.; She, H.; Huang, J.; Lei, Z.; Zhang, T.; Wang, Q., Anchored Cu(II) tetra(4-carboxylphenyl)porphyrin to P25 (TiO_2) for efficient photocatalytic ability in CO_2 reduction. *Applied Cat. B* **2018,** *239*, 599-608.
58. Roy, S.; Reisner, E., Visible-Light-Driven CO_2 Reduction by Mesoporous Carbon Nitride Modified with Polymeric Cobalt Phthalocyanine. *Angew. Chem., Int. Ed.* **2019,** *58* (35), 12180-12184.

59. Ma, B.; Chen, G.; Fave, C.; Chen, L.; Kuriki, R.; Maeda, K.; Ishitani, O.; Lau, T.-C.; Bonin, J.; Robert, M., Efficient Visible-Light-Driven CO_2 Reduction by a Cobalt Molecular Catalyst Covalently Linked to Mesoporous Carbon Nitride. *J. Am. Chem. Soc.* **2020,** *142* (13), 6188-6195.
60. Hawecker, J.; Lehn, J.-M.; Ziessel, R., Efficient photochemical reduction of CO_2 to CO by visible light irradiation of systems containing $Re(bipy)(CO)_3X$ or $Ru(bipy)_3^{2+}$–Co^{2+} combinations as homogeneous catalysts. *J. Chem. Soc., Chem. Commun.* **1983,** (9), 536-538.
61. Tinnemans, A. H. A.; Koster, T. P. M.; Thewissen, D. H. M. W.; Mackor, A., Tetraaza-macrocyclic cobalt(II) and nickel(II) complexes as electron-transfer agents in the photo(electro)chemical and electrochemical reduction of carbon dioxide. *Recl. Trav. Chim. Pays-Bas* **1984,** *103* (10), 288-295.
62. Wu, J.; Huang, Y.; Ye, W.; Li, Y., CO_2 Reduction: From the Electrochemical to Photochemical Approach. *Adv. Sci.* **2017,** *4* (11), 1700194.
63. Kumar, B.; Llorente, M.; Froehlich, J.; Dang, T.; Sathrum, A.; Kubiak, C. P., Photochemical and Photoelectrochemical Reduction of CO_2. *Annu. Rev. Phys. Chem.* **2012,** *63* (1), 541-569.
64. Yaashikaa, P. R.; Senthil Kumar, P.; Varjani, S. J.; Saravanan, A., A review on photochemical, biochemical and electrochemical transformation of CO_2 into value-added products. *J. CO2 Util.* **2019,** *33*, 131-147.
65. Sahara, G.; Ishitani, O., Efficient Photocatalysts for CO_2 Reduction. *Inorg. Chem.* **2015,** *54* (11), 5096-5104.
66. Fujita, E.; Creutz, C.; Sutin, N.; Brunschwig, B. S., Carbon dioxide activation by cobalt macrocycles: evidence of hydrogen bonding between bound CO_2 and the macrocycle in solution. *Inorg. Chem.* **1993,** *32* (12), 2657-2662.
67. Fujita, E.; Furenlid, L. R.; Renner, M. W., Direct XANES Evidence for Charge Transfer in $Co{-}CO_2$ Complexes. *J. Am. Chem. Soc.* **1997,** *119* (19), 4549-4550.
68. Matsuoka, S.; Yamamoto, K.; Ogata, T.; Kusaba, M.; Nakashima, N.; Fujita, E.; Yanagida, S., Efficient and selective electron mediation of cobalt complexes with cyclam and related macrocycles in the p-terphenyl-catalyzed photoreduction of carbon dioxide. *J. Am. Chem. Soc.* **1993,** *115* (2), 601-609.
69. Behar, D.; Dhanasekaran, T.; Neta, P.; Hosten, C. M.; Ejeh, D.; Hambright, P.; Fujita, E., Cobalt Porphyrin Catalyzed Reduction of CO_2. Radiation Chemical, Photochemical, and Electrochemical Studies. *J. Phys. Chem. A* **1998,** *102* (17), 2870-2877.
70. Dhanasekaran, T.; Grodkowski, J.; Neta, P.; Hambright, P.; Fujita, E., p-Terphenyl-Sensitized Photoreduction of CO2 with Cobalt and Iron Porphyrins. Interaction between CO and Reduced Metalloporphyrins. *J. Phys. Chem. A* **1999,** *103* (38), 7742-7748.
71. Zhang, X.; Cibian, M.; Call, A.; Yamauchi, K.; Sakai, K., Photochemical CO_2 Reduction Driven by Water-Soluble Copper(I) Photosensitizer with the Catalysis Accelerated by Multi-Electron Chargeable Cobalt Porphyrin. *ACS Catal.* **2019,** *9* (12), 11263-11273.
72. Takeda, H.; Koizumi, H.; Okamoto, K.; Ishitani, O., Photocatalytic CO2 reduction using a Mn complex as a catalyst. *Chem. Commun.* **2014,** *50* (12), 1491-3.
73. Bourrez, M.; Molton, F.; Chardon-Noblat, S.; Deronzier, A., [$Mn(bipyridyl)(CO)_3Br$]: an abundant metal carbonyl complex as efficient electrocatalyst for CO_2 reduction. *Angew. Chem., Int. Ed.* **2011,** *50* (42), 9903-6.
74. Takeda, H.; Kamiyama, H.; Okamoto, K.; Irimajiri, M.; Mizutani, T.; Koike, K.; Sekine, A.; Ishitani, O., Highly Efficient and Robust Photocatalytic Systems for CO_2 Reduction Consisting of a Cu(I) Photosensitizer and Mn(I) Catalysts. *J. Am. Chem. Soc.* **2018,** *140* (49), 17241-17254.

75. Fei, H.; Sampson, M. D.; Lee, Y.; Kubiak, C. P.; Cohen, S. M., Photocatalytic CO_2 Reduction to Formate Using a Mn(I) Molecular Catalyst in a Robust Metal-Organic Framework. *Inorg. Chem.* **2015,** *54* (14), 6821-8.
76. Takeda, H.; Ohashi, K.; Sekine, A.; Ishitani, O., Photocatalytic CO_2 Reduction Using Cu(I) Photosensitizers with a Fe(II) Catalyst. *J. Am. Chem. Soc.* **2016,** *138* (13), 4354-7.
77. Hasegawa, E.; Seida, T.; Chiba, N.; Takahashi, T.; Ikeda, H., Contrastive Photoreduction Pathways of Benzophenones Governed by Regiospecific Deprotonation of Imidazoline Radical Cations and Additive Effects. *J. Org. Chem.* **2005,** *70* (23), 9632-9635.
78. Guo, Z.; Cheng, S.; Cometto, C.; Anxolabehere-Mallart, E.; Ng, S. M.; Ko, C. C.; Liu, G.; Chen, L.; Robert, M.; Lau, T. C., Highly Efficient and Selective Photocatalytic CO_2 Reduction by Iron and Cobalt Quaterpyridine Complexes. *J. Am. Chem. Soc.* **2016,** *138* (30), 9413-6.
79. Rosas-Hernandez, A.; Alsabeh, P. G.; Barsch, E.; Junge, H.; Ludwig, R.; Beller, M., Highly active and selective photochemical reduction of CO_2 to CO using molecular-defined cyclopentadienone iron complexes. *Chem. Commun.* **2016,** *52* (54), 8393-6.
80. Rosas-Hernández, A.; Steinlechner, C.; Junge, H.; Beller, M., Earth-abundant photocatalytic systems for the visible-light-driven reduction of CO2 to CO. *Green Chem.* **2017,** *19* (10), 2356-2360.
81. Grodkowski, J.; Behar, D.; Neta, P.; Hambright, P., Iron Porphyrin-Catalyzed Reduction of CO2. Photochemical and Radiation Chemical Studies. *J. Phys. Chem. A* **1997,** *101* (3), 248-254.
82. Bonin, J.; Chaussemier, M.; Robert, M.; Routier, M., Homogeneous Photocatalytic Reduction of CO_2 to CO Using Iron(0) Porphyrin Catalysts: Mechanism and Intrinsic Limitations. *ChemCatChem* **2014,** *6* (11), 3200-3207.
83. Bonin, J.; Robert, M.; Routier, M., Selective and efficient photocatalytic CO_2 reduction to CO using visible light and an iron-based homogeneous catalyst. *J. Am. Chem. Soc.* **2014,** *136* (48), 16768-71.
84. Azcarate, I.; Costentin, C.; Robert, M.; Saveant, J. M., Through-Space Charge Interaction Substituent Effects in Molecular Catalysis Leading to the Design of the Most Efficient Catalyst of CO2-to-CO Electrochemical Conversion. *J. Am. Chem. Soc.* **2016,** *138* (51), 16639-16644.
85. Rao, H.; Schmidt, L. C.; Bonin, J.; Robert, M., Visible-light-driven methane formation from CO2 with a molecular iron catalyst. *Nature* **2017,** *548* (7665), 74-77.
86. Boutin, E.; Robert, M., Molecular Electrochemical Reduction of CO_2 beyond Two Electrons. *Trends Chem.* **2021,** *3* (5), 359-372.
87. Hammouche, M.; Lexa, D.; Saveant, J. M.; Momenteau, M., Catalysis of the electrochemical reduction of carbon dioxide by iron("0") porphyrins. *J. Electroanal. Chem.* **1988,** *249* (1-2), 347-351.
88. Nie, X.; Luo, W.; Janik, M. J.; Asthagiri, A., Reaction mechanisms of CO_2 electrochemical reduction on Cu(111) determined with density functional theory. *J. Catal.* **2014,** *312*, 108-122.
89. De, R.; Gonglach, S.; Paul, S.; Haas, M.; Sreejith, S. S.; Gerschel, P.; Apfel, U. P.; Vuong, T. H.; Rabeah, J.; Roy, S.; Schofberger, W., Electrocatalytic Reduction of CO_2 to Acetic Acid by a Molecular Manganese Corrole Complex. *Angew. Chem., Int. Ed.* **2020,** *59* (26), 10527-10534.
90. Gonglach, S.; Paul, S.; Haas, M.; Pillwein, F.; Sreejith, S. S.; Barman, S.; De, R.; Mullegger, S.; Gerschel, P.; Apfel, U. P.; Coskun, H.; Aljabour, A.; Stadler, P.; Schofberger, W.; Roy, S., Molecular cobalt corrole complex for the heterogeneous electrocatalytic reduction of carbon dioxide. *Nat. Commun.* **2019,** *10* (1), 3864.
91. Kapusta, S.; Hackerman, N., Carbon Dioxide Reduction at a Metal Phthalocyanine Catalyzed Carbon Electrode. *J. Electrochem. Soc.* **1984,** *131* (7), 1511-1514.

92. Wang, R.; Boutin, E.; Barreau, N.; Odobel, F.; Bonin, J.; Robert, M., Carbon Dioxide Reduction to Methanol with a Molecular Cobalt-Catalyst-Loaded Porous Carbon Electrode Assisted by a CIGS Photovoltaic Cell. *ChemPhotoChem* **2021,** *5* (8), 705-710.
93. Chatterjee, T.; Boutin, E.; Robert, M., Manifesto for the routine use of NMR for the liquid product analysis of aqueous CO_2 reduction: from comprehensive chemical shift data to formaldehyde quantification in water. *Dalton Trans.* **2020,** *49* (14), 4257-4265.
94. Gao, S.; Gu, B.; Jiao, X.; Sun, Y.; Zu, X.; Yang, F.; Zhu, W.; Wang, C.; Feng, Z.; Ye, B.; Xie, Y., Highly Efficient and Exceptionally Durable CO_2 Photoreduction to Methanol over Freestanding Defective Single-Unit-Cell Bismuth Vanadate Layers. *J. Am. Chem. Soc.* **2017,** *139* (9), 3438-3445.
95. Zhang, Q.; Lin, C. F.; Chen, B. Y.; Ouyang, T.; Chang, C. T., Deciphering visible light photoreductive conversion of CO_2 to formic acid and methanol using waste prepared material. *Environ. Sci. Technol.* **2015,** *49* (4), 2405-17.
96. Prier, C. K.; Rankic, D. A.; MacMillan, D. W., Visible light photoredox catalysis with transition metal complexes: applications in organic synthesis. *Chem. Rev.* **2013,** *113* (7), 5322-63.
97. Walther, R.; Fahlbusch, K.; Sievert, R.; Gottschalk, G., Formation of Trideuteromethane from Deuterated Trimethylamine or Methylamine by Methanosarcina barkeri. *J. Bacteriol.* **1981,** *148* (1), 371-373.
98. Summers, D. P.; Frese, K. W., Mechanistic Aspects of the Electrochemical Reduction of Carbon Monoxide and Methanol to Methane at Ruthenium and Copper Electrodes. *ACS Symp. Ser.* **1988,** *378*, 518-527.
99. Åkermark, B.; Eklund-Westlin, U.; Baeckström, P.; Löf, R., Photochemical, Metal-promoted Reduction of Carbon Dioxide and Formaldehyde in Aqueous Solution. *Acta Chem. Scand.* **1980,** *34* (1), 27-30.
100. DeWulf, D. W.; Jin, T.; Bard, A. J., Electrochemical and Surface Studies of Carbon Dioxide Reduction to Methane and Ethylene at Copper Electrodes in Aqueous Solutions. *J. Electrochem. Soc.* **1989,** *136* (6), 1686-1691.
101. Lehn, J.-M.; Ziessel, R., Photochemical generation of carbon monoxide and hydrogen by reduction of carbon dioxide and water under visible light irradiation. *Proc. Natl. Acad. Sci. U.S.A.* **1982,** *79* (2), 701.
102. Chang, Y. C.; Wang, C. L.; Pan, T. Y.; Hong, S. H.; Lan, C. M.; Kuo, H. H.; Lo, C. F.; Hsu, H. Y.; Lin, C. Y.; Diau, E. W., A strategy to design highly efficient porphyrin sensitizers for dye-sensitized solar cells. *Chem. Commun.* **2011,** *47* (31), 8910-2.
103. Campbell, W. M.; Jolley, K. W.; Wagner, P.; Wagner, K.; Walsh, P. J.; Gordon, K. C.; Schmidt-Mende, L.; Nazeeruddin, M. K.; Wang, Q.; Grätzel, M.; Officer, D. L., Highly Efficient Porphyrin Sensitizers for Dye-Sensitized Solar Cells. *J. Phys. Chem. C* **2007,** *111* (32), 11760-11762.
104. Li, L. L.; Diau, E. W., Porphyrin-sensitized solar cells. *Chem. Soc. Rev.* **2013,** *42* (1), 291-304.
105. Kärkäs, M. D.; Laine, T. M.; Johnston, E. V.; Akermark, B., Visible Light-Driven Water Oxidation Catalyzed by Ruthenium Complexes. In *Applied Photosynthesis - New Progress*, 2016.
106. Hewat, T. E.; Yellowlees, L. J.; Robertson, N., Neutral copper(I) dipyrrin complexes and their use as sensitizers in dye-sensitized solar cells. *Dalton Trans.* **2014,** *43* (10), 4127-36.
107. Finkenzeller, W. J.; Yersin, H., Emission of $Ir(ppy)_3$. Temperature dependence, decay dynamics, and magnetic field properties. *Chem. Phys. Lett.* **2003,** *377* (3-4), 299-305.
108. Lee, C. W.; Lu, H. P.; Lan, C. M.; Huang, Y. L.; Liang, Y. R.; Yen, W. N.; Liu, Y. C.; Lin, Y. S.; Diau, E. W.; Yeh, C. Y., Novel zinc porphyrin sensitizers for dye-sensitized solar cells:

synthesis and spectral, electrochemical, and photovoltaic properties. *Chemistry A - European Journal* **2009,** *15* (6), 1403-12.
109. Karthikeyan, S.; Lee, J. Y., Zinc-porphyrin based dyes for dye-sensitized solar cells. *J. Phys. Chem. A* **2013,** *117* (42), 10973-9.
110. He, L.-J.; Sun, Y.; Li, W.; Wang, J.; Song, M.-X.; Zhang, H.-X., Highly-efficient sensitizer with zinc porphyrin as building block: Insights from DFT calculations. *Sol. Energy* **2018,** *173*, 283-290.
111. Neves, C. M. B.; Filipe, O. M. S.; Mota, N.; Santos, S. A. O.; Silvestre, A. J. D.; Santos, E. B. H.; Neves, M.; Simoes, M. M. Q., Photodegradation of metoprolol using a porphyrin as photosensitizer under homogeneous and heterogeneous conditions. *J. Hazard. Mater.* **2019,** *370*, 13-23.
112. Yella, A.; Lee, H.-W.; Tsao Hoi, N.; Yi, C.; Chandiran Aravind, K.; Nazeeruddin, M. K.; Diau Eric, W.-G.; Yeh, C.-Y.; Zakeeruddin Shaik, M.; Grätzel, M., Porphyrin-Sensitized Solar Cells with Cobalt (II/III)–Based Redox Electrolyte Exceed 12 Percent Efficiency. *Science* **2011,** *334* (6056), 629-634.
113. Rao, H.; Bonin, J.; Robert, M., Non-sensitized selective photochemical reduction of CO_2 to CO under visible light with an iron molecular catalyst. *Chem. Commun.* **2017,** *53* (19), 2830-2833.
114. Long, G. S.; Snedeker, B.; Bartosh, K.; Werner, M. L.; Sen, A., Transition metal phthalocyanine and porphyrin complexes as catalysts for the polymerization of alkenes. *Can. J. Chem.* **2001,** *79* (5-6), 1026-1029.
115. Costa, E. S. R.; Oliveira da Silva, L.; de Andrade Bartolomeu, A.; Brocksom, T. J.; de Oliveira, K. T., Recent applications of porphyrins as photocatalysts in organic synthesis: batch and continuous flow approaches. *Beilstein J. Org. Chem.* **2020,** *16*, 917-955.
116. Zhang, J.-X.; Hu, C.-Y.; Wang, W.; Wang, H.; Bian, Z.-Y., Visible light driven reduction of CO 2 catalyzed by an abundant manganese catalyst with zinc porphyrin photosensitizer. *Applied Cat. A* **2016,** *522*, 145-151.
117. Choi, S.; Kim, C. H.; Baeg, J.-O.; Son, H.-J.; Pac, C.; Kang, S. O., Collisional Electron Transfer Route between Homogeneous Porphyrin Dye and Catalytic TiO_2/Re(I) Particles for CO_2 Reduction. *ACS Appl. Energy Mater.* **2020,** *3* (12), 11581-11596.
118. Polo, A. S.; Itokazu, M. K.; Murakami Iha, N. Y., Metal complex sensitizers in dye-sensitized solar cells. *Coord. Chem. Rev.* **2004,** *248* (13), 1343-1361.
119. Shon, J.-H.; Teets, T. S., Molecular Photosensitizers in Energy Research and Catalysis: Design Principles and Recent Developments. *ACS Energy Lett.* **2019,** *4* (2), 558-566.
120. Nyman, E. S.; Hynninen, P. H., Research advances in the use of tetrapyrrolic photosensitizers for photodynamic therapy. *Journal of Photochemistry and Photobiology B - Biology* **2004,** *73* (1), 1-28.
121. Bonnett, R., Photosensitizers of the porphyrin and phthalocyanine series for photodynamic therapy. *Chem. Soc. Rev.* **1995,** *24* (1), 19-33.
122. Ethirajan, M.; Chen, Y.; Joshi, P.; Pandey, R. K., The role of porphyrin chemistry in tumor imaging and photodynamic therapy. *Chem. Soc. Rev.* **2011,** *40* (1), 340-362.
123. Hoffmann, N., Efficient photochemical electron transfer sensitization of homogeneous organic reactions. *J. Photoch. Photobio. C* **2008,** *9* (2), 43-60.
124. Estévez-Braun, A.; González, A. G., Coumarins. *Nat. Prod. Rep.* **1997,** *14* (5), 465-475.
125. He, J.; Liu, Y.; Gao, J.; Han, L., New D-D-pi-A triphenylamine-coumarin sensitizers for dye-sensitized solar cells. *Photochem. Photobiol. Sci.* **2017,** *16* (7), 1049-1056.

126. Tasior, M.; Kim, D.; Singha, S.; Krzeszewski, M.; Ahn, K. H.; Gryko, D. T., π-Expanded coumarins: synthesis, optical properties and applications. *J. Mater. Chem. C* **2015,** *3* (7), 1421-1446.
127. Egan, D.; O'Kennedy, R.; Moran, E.; Cox, D.; Prosser, E.; Thornes, R. D., The Pharmacology, Metabolism, Analysis, and Applications of Coumarin and Coumarin-Related Compounds. *Drug Metab. Rev.* **1990,** *22* (5), 503-529.
128. Hara, K.; Sato, T.; Katoh, R.; Furube, A.; Ohga, Y.; Shinpo, A.; Suga, S.; Sayama, K.; Sugihara, H.; Arakawa, H., Molecular Design of Coumarin Dyes for Efficient Dye-Sensitized Solar Cells. *J. Phys. Chem. B* **2003,** *107* (2), 597-606.
129. Anxolabehere-Mallart, E.; Bonin, J.; Fave, C.; Robert, M., Small-molecule activation with iron porphyrins using electrons, photons and protons: some recent advances and future strategies. *Dalton Trans.* **2019,** *48* (18), 5869-5878.
130. Gualandi, A.; Rodeghiero, G.; Della Rocca, E.; Bertoni, F.; Marchini, M.; Perciaccante, R.; Jansen, T. P.; Ceroni, P.; Cozzi, P. G., Application of coumarin dyes for organic photoredox catalysis. *Chem. Commun.* **2018,** *54* (72), 10044-10047.
131. Costentin, C.; Robert, M.; Savéant, J.-M.; Tatin, A., Efficient and selective molecular catalyst for the CO_2-to-CO electrochemical conversion in water. *Proc. Natl. Acad. Sci. U.S.A.* **2015,** *112* (22), 6882-6886.
132. Ionescu, M.; Mantsch, H., Phenoxazines. In *Advances in Heterocyclic Chemistry*, Katritzky, A. R.; Boulton, A. J., Eds. Academic Press: 1967; Vol. 8, pp 83-113.
133. Lewis, G. N.; Bigeleisen, J., Photochemical Reactions of Leuco Dyes in Rigid Solvents. Quantum Efficiency of Photo-oxidation. *J. Am. Chem. Soc.* **1943,** *65* (12), 2419-2423.
134. Tian, H.; Yang, X.; Cong, J.; Chen, R.; Liu, J.; Hao, Y.; Hagfeldt, A.; Sun, L., Tuning of phenoxazine chromophores for efficient organic dye-sensitized solar cells. *Chem. Commun.* **2009,** (41), 6288-90.
135. Karlsson, K. M.; Jiang, X.; Eriksson, S. K.; Gabrielsson, E.; Rensmo, H.; Hagfeldt, A.; Sun, L., Phenoxazine dyes for dye-sensitized solar cells: relationship between molecular structure and electron lifetime. *Chem. Eur. J.* **2011,** *17* (23), 6415-24.
136. Tian, H.; Bora, I.; Jiang, X.; Gabrielsson, E.; Karlsson, K. M.; Hagfeldt, A.; Sun, L., Modifying organic phenoxazine dyes for efficient dye-sensitized solar cells. *J. Mater. Chem.* **2011,** *21* (33).
137. Tan, H.; Pan, C.; Wang, G.; Wu, Y.; Zhang, Y.; Zou, Y.; Yu, G.; Zhang, M., Phenoxazine-based organic dyes with different chromophores for dye-sensitized solar cells. *Org. Electron.* **2013,** *14* (11), 2795-2801.
138. Li, P.; Cui, Y.; Song, C.; Zhang, H., A systematic study of phenoxazine-based organic sensitizers for solar cells. *Dyes Pigm.* **2017,** *137*, 12-23.
139. Al-Ghamdi, S. N.; Al-Ghamdi, H. A.; El-Shishtawy, R. M.; Asiri, A. M., Advances in phenothiazine and phenoxazine-based electron donors for organic dye-sensitized solar cells. *Dyes Pigm.* **2021,** *194*.
140. Wang, G.; Hu, Y.; Chen, Y.; Liao, X.; Li, Z.; Chen, X.; Wang, X.; Liu, B., Effect of Multidonor and Insertion Position of a Chromophore on the Photovoltaic Properties of Phenoxazine Dyes. *ACS Omega* **2020,** *5* (35), 22621-22630.
141. McCarthy, B. G.; Pearson, R. M.; Lim, C. H.; Sartor, S. M.; Damrauer, N. H.; Miyake, G. M., Structure-Property Relationships for Tailoring Phenoxazines as Reducing Photoredox Catalysts. *J. Am. Chem. Soc.* **2018,** *140* (15), 5088-5101.
142. Bhattacherjee, A.; Sneha, M.; Lewis-Borrell, L.; Amoruso, G.; Oliver, T. A. A.; Tyler, J.; Clark, I. P.; Orr-Ewing, A. J., Singlet and Triplet Contributions to the Excited-State Activities of

Dihydrophenazine, Phenoxazine, and Phenothiazine Organocatalysts Used in Atom Transfer Radical Polymerization. *J. Am. Chem. Soc.* **2021,** *143* (9), 3613-3627.
143. Haav, K.; Saame, J.; Kütt, A.; Leito, I., Basicity of Phosphanes and Diphosphanes in Acetonitrile. *Eur. J. Org. Chem.* **2012,** *2012* (11), 2167-2172.
144. Hasegawa, E.; Takizawa, S.; Seida, T.; Yamaguchi, A.; Yamaguchi, N.; Chiba, N.; Takahashi, T.; Ikeda, H.; Akiyama, K., Photoinduced electron-transfer systems consisting of electron-donating pyrenes or anthracenes and benzimidazolines for reductive transformation of carbonyl compounds. *Tetrahedron* **2006,** *62* (27), 6581-6588.
145. Du, Y.; Yang, H.; Pearson, R. M.; Damrauer, N. H.; Lim, C.-H.; Sartor, S. M.; Ryan, M. D.; Miyake, a. G. M., Strongly Reducing, Visible-Light Organic Photoredox Catalysts as Sustainable Alternatives to Precious Metals. *Chem.-Eur. J.* **2017,** *23*, 10962–10968.
146. Pearson, R. M.; Lim, C. H.; McCarthy, B. G.; Musgrave, C. B.; Miyake, G. M., Organocatalyzed Atom Transfer Radical Polymerization Using N-Aryl Phenoxazines as Photoredox Catalysts. *J. Am. Chem. Soc.* **2016,** *138* (35), 11399-407.
147. Lakhi, K. S.; Park, D. H.; Al-Bahily, K.; Cha, W.; Viswanathan, B.; Choy, J. H.; Vinu, A., Mesoporous carbon nitrides: synthesis, functionalization, and applications. *Chem. Soc. Rev.* **2017,** *46* (1), 72-101.
148. Talapaneni, S. N.; Singh, G.; Kim, I. Y.; AlBahily, K.; Al-Muhtaseb, A. H.; Karakoti, A. S.; Tavakkoli, E.; Vinu, A., Nanostructured Carbon Nitrides for CO_2 Capture and Conversion. *Adv. Mater.* **2020,** *32* (18), e1904635.
149. Zheng, Y.; Lin, L.; Ye, X.; Guo, F.; Wang, X., Helical graphitic carbon nitrides with photocatalytic and optical activities. *Angew. Chem., Int. Ed.* **2014,** *53* (44), 11926-30.
150. Miller, T. S.; Jorge, A. B.; Suter, T. M.; Sella, A.; Cora, F.; McMillan, P. F., Carbon nitrides: synthesis and characterization of a new class of functional materials. *Phys. Chem. Chem. Phys.* **2017,** *19* (24), 15613-15638.
151. Schwinghammer, K.; Tuffy, B.; Mesch, M. B.; Wirnhier, E.; Martineau, C.; Taulelle, F.; Schnick, W.; Senker, J.; Lotsch, B. V., Triazine-based carbon nitrides for visible-light-driven hydrogen evolution. *Angew. Chem., Int. Ed.* **2013,** *52* (9), 2435-9.
152. Cometto, C.; Kuriki, R.; Chen, L.; Maeda, K.; Lau, T. C.; Ishitani, O.; Robert, M., A Carbon Nitride/Fe Quaterpyridine Catalytic System for Photostimulated CO_2-to-CO Conversion with Visible Light. *J. Am. Chem. Soc.* **2018,** *140* (24), 7437-7440.
153. Le Duff, C. S.; Lawrence, M. J.; Rodriguez, P., Role of the Adsorbed Oxygen Species in the Selective Electrochemical Reduction of CO2 to Alcohols and Carbonyls on Copper Electrodes. *Angew. Chem., Int. Ed.* **2017,** *56* (42), 12919-12924.
154. Zhang, W.; Huang, C.; Xiao, Q.; Yu, L.; Shuai, L.; An, P.; Zhang, J.; Qiu, M.; Ren, Z.; Yu, Y., Atypical Oxygen-Bearing Copper Boosts Ethylene Selectivity toward Electrocatalytic CO_2 Reduction. *J. Am. Chem. Soc.* **2020,** *142* (26), 11417-11427.
155. Collman, J. P.; Gagne, R. R.; Halbert, T. R.; Marchon, J. C.; Reed, C. A., Reversible oxygen adduct formation in ferrous complexes derived from a picket fence porphyrin. Model for oxymyoglobin. *J. Am. Chem. Soc.* **1973,** *95* (23), 7868-7870.
156. Pegis, M. L.; Martin, D. J.; Wise, C. F.; Brezny, A. C.; Johnson, S. I.; Johnson, L. E.; Kumar, N.; Raugei, S.; Mayer, J. M., Mechanism of Catalytic O_2 Reduction by Iron Tetraphenylporphyrin. *J. Am. Chem. Soc.* **2019,** *141* (20), 8315-8326.
157. Kostopoulos, N.; Achaibou, C.; Noel, J. M.; Kanoufi, F.; Robert, M.; Fave, C.; Anxolabehere-Mallart, E., Electrocatalytic O_2 Activation by Fe tetrakis(pentafluorophenyl)porphyrin in Acidic Organic Media. Evidence of High-Valent Fe Oxo Species. *Inorg. Chem.* **2020,** *59* (16), 11577-11583.

158. Sawyer, D. T.; Chiericato, G.; Angelis, C. T.; Nanni, E. J.; Tsuchiya, T., Effects of media and electrode materials on the electrochemical reduction of dioxygen. *Anal. Chem.* **1982,** *54* (11), 1720-1724.
159. Pabis, A.; Kaminski, R.; Ciepielowski, G.; Jankowski, S.; Paneth, P., Measurements of heavy-atom isotope effects using 1H NMR spectroscopy. *J. Org. Chem.* **2011,** *76* (19), 8033-5.
160. M. M. Taqui Khan; Shaukat A. Mirza; Bajaj, H. C., Oxidation of triethylamine by molecular oxygen catalyzed by Ru(III)-ion. *React. Kinet. Catal. Lett.* **1987,** *33* (1), 67-74.
161. Bai, X.; Liu, Z.; Ye, K.; Wang, Y.; Zhang, X.; Yue, H.; Tian, G.; Feng, S., The oxidation of the alpha-carbon of amines in hydrothermal condition: an alternative synthetic route of compounds containing amide bond. *Tetrahedron Lett.* **2014,** *55* (2), 319-321.
162. Ogata, Y.; Sawaki, Y.; Kuriyama, Y., The reaction of trialkylamine with nitric acid in a mixture of acetic acid and acetic anhydride. *Tetrahedron* **1968,** *24* (8), 3425-3435.
163. Davis, G. T.; Rosenblatt, D. H., Oxidations of amines VI. Platinum-catalyzed air oxidations of n-methyl tertiary amines. *Tetrahedron Lett.* **1968,** *9* (38), 4085-4086.
164. Hiroshi, T.; Teruo, Y.; Hiroo, T., Intermediates and Mechanism of Photo-Oxygenation Reaction of Triethylamine. *Bull. Chem. Soc. Jap.* **1973,** *46* (10), 3051-3055.
165. Davidson, R. S.; Trethewey, K. R., Photosensitised oxidation of amines: mechanism of oxidation of triethylamine. *J. Chem. Soc., Perkin Trans. 2* **1977,** (2), 173-178.
166. Bartholomew, R. F.; Brimage, D. R. G.; Davidson, R. S., The photosensitised oxidation of amines. Part IV. The use of aromatic hydrocarbons as sensitisers. *J. Chem. Soc. C* **1971,** (0), 3482-3484.
167. Choi, P. G.; Ohno, T.; Masui, T.; Imanaka, N., Catalytic liquid-phase oxidation of acetaldehyde to acetic acid over a Pt/CeO_2-ZrO_2-SnO_2/gamma-alumina catalyst. *J. Environ. Sci.* **2015,** *36*, 63-6.
168. Calvert, J. G.; Hanst, P. L., The mechanism of the photooxidation of acetaldehyde at room temperature. *Can. J. Chem.* **1959,** *37* (10), 1671-1679.
169. Mohamed, R. M.; Bahnemann, D. W.; Basaleh, A. S.; Qadah, R. H., Photo-catalytic destruction of acetaldehyde using cobalt, copper co-doped titania dioxide nanoparticles beneath Visible light. *Appl. Nanosci.* **2019,** *10* (3), 931-939.
170. Tamaki, Y.; Koike, K.; Morimoto, T.; Ishitani, O., Substantial improvement in the efficiency and durability of a photocatalyst for carbon dioxide reduction using a benzoimidazole derivative as an electron donor. *J. Catal.* **2013,** *304*, 22-28.
171. Marco Montalti; Alberto Credi; Luca Prodi; Gandolfi, M. T., *Handbook of Photochemistry, 3rd ed*. CRC Press: 2006.
172. Pellegrin, Y.; Odobel, F., Sacrificial electron donor reagents for solar fuel production. *C. R. Chim.* **2017,** *20* (3), 283-295.
173. Ware, W. R., Oxygen quenching of fluorescence in solution : an experimental study of the diffusion process. *J. Phys. Chem.* **1962,** *66* (3), 455-458.
174. Vasudevan, D.; Wendt, H., Electroreduction of oxygen in aprotic media. *J. Electroanal. Chem.* **1995,** *392* (1), 69-74.
175. Amao, Y.; Ishikawa, Y.; Okura, I., Green luminescent iridium(III) complex immobilized in fluoropolymer film as optical oxygen-sensing material. *Anal. Chim. Acta* **2001,** *445* (2), 177-182.
176. Bhugun, I.; Lexa, D.; Savéant, J.-M., Catalysis of the Electrochemical Reduction of Carbon Dioxide by Iron(0) Porphyrins: Synergystic Effect of Weak Brönsted Acids. *J. Am. Chem. Soc.* **1996,** *118* (7), 1769-1776.

177. Helms, J. H.; Ter Haar, L. W.; Hatfield, W. E.; Harris, D. L.; Jayaraj, K.; Toney, G. E.; Gold, A.; Mewborn, T. D.; Pemberton, J. E., Effect of meso substituents on exchange-coupling interactions in .mu.-oxo iron(III) porphyrin dimers. *Inorg. Chem.* **1986,** *25* (14), 2334-2337.
178. Kadish, K. M.; Autret, M.; Ou, Z.; Tagliatesta, P.; Boschi, T.; Fares, V., Synthesis, Structure, and Electrochemistry of an Electron Deficient μ-Oxo Porphyrin Dimer, $[(TPPBr_4)Fe]_2O$. *Inorg. Chem.* **1997,** *36* (2), 204-207.
179. Kadish, K. M.; Larson, G.; Lexa, D.; Momenteau, M., Electrochemical and spectral characterization of the reduction steps of μ-oxo-bis(iron tetraphenylporphyrin) dimer in dimethylformamide. *J. Am. Chem. Soc.* **1975,** *97* (2), 282-288.
180. Wudl, F.; Smith, G. M.; Hufnagel, E. J., Bis-1,3-dithiolium chloride: an unusually stable organic radical cation. *J. Chem. Soc., Chem. Commun.* **1970,** (21), 1453-1454.

Annexes

Chemicals

Unless otherwise noted, chemicals were used without further purification.

NaOH (99.5%), KOH (99.5%), $NaHCO_3$ (99%), KCl (99.5%), $KHCO_3$ (99.5%), NaHCOO (97%), Paraformaldehyde, L-Ascorbic acid (99+%), Tetrathialfulvalene (97%), Tris(2,2'-bipyridyl)ruthenium(II) chloride (99.95%), *fac*-(tris(2-phenylpyridine))iridium(III) (99%) were purchased from Sigma-Aldrich. NH_4PF_6 (99.5%) was purchased from Acros Organics. $TBAPF_6$ (99%) was purchased from Fluka. Free base 5,10,15,20-tetra(N,N,N-trimethyl-4-anilinium)porphyrin tetrachloride was purchased from Frontier Scientific. Phenoxazines were graciously obtained from Pr. G. Miyake at Colorado State University (USA).[141] Coumarin was graciously obtained from Pr. Pier Cozzi at Univerisity of Bologna (Italy).[130]

Acetone (99.8%), methanol (99.8%), ethanol (99.9%), ethyl acetate (99.5%), and hydrochloric acid (37%) were purchased from VWR. N,N-diethylhydroxylamine (98%) was purchased from Sigma Aldrich. Diethylamine (99+%) acetic acid (99.5%) were purchased from Alfa Aesar. Electrochemical grade acetonitrile, N, N-dimethylformamide (Acros, > 99.8%, over molecular sieves and stored under Argon atmosphere), triethylamine (TEA, Acros Organics, 99%), triethanolamine (TEOA, Sigma, >99%), and 2,2,2-trifluoroethanol (TFE, Romil Ltd., >99.5%). Ultrapure water was obtained from a Millipore filtration system. Deuterated methanol (CD_3OD), acetonitrile (CD_3CN) and trifluoroethanol (TFE-d3) were purchased from Eurisotop.

Argon (> 99.998 %), ^{12}CO (> 99.7 %), $^{12}CO_2$ (> 99.7 %), O_2 (>99.9995 %) and N_2 (>99.999%) gases were purchased from Air Liquide. CH_4 (> 99 %) was from Fluka. ^{13}CO (99 % content in atom ^{13}C) and $^{13}CO_2$ (99 % content in atom ^{13}C) were purchased from Sigma Aldrich.

Synthesis and purifications

1,3-dimethyl-2-phenyl-2,3-dihydro-1H-benzo[d]imidazole (BIH) was prepared according to literature.[77] A solution of 2-Phenylbenzimidazole (1.5 g, 7.7 mmol) was treated with 4 g of methyl iodide in 10 mL of methanol containing 0.32 g of NaOH. The reaction mixture was heated at 110 °C overnight in a Pyrex bottle. The brown crude product was decolorized by the activated carbon in hot aqueous ethanol (ethanol:H_2O, 5:1 v/v). After removal of the solvent, the product was recrystallized from absolute ethanol. The yield was over 80%. Without further purification, to a

solution of 1.7 g this product in 60 mL of CH_3OH was slowly added with 459 mg $NaBH_4$ in ice-bath. The reaction took place instantaneously to give a cloudy, white suspension. The reaction mixture was stirred vigorously for 1 h under Ar. After removal of the solvent under reduced pressure, the white solid was recrystallized from ethanol:H_2O (2:1 v/v) to give a colorless crystalline product. The yield was over 80% (0.87 g). IR (KBr) 3038 (w), 2953 (w), 2861 (w), 2801 (w), 1601 (m), 1495 (s), 1456 (m), 1368 (s), 1295 (m), 1234 (m), 1157 (m), 1121 (m), 1061 (m), 777 (m), 741 (m), 700 (m) cm-1; 1H-NMR (DMSO-d_6) δ 2.52 (s, 6 H, NCH_3), 4.88 (s, 1 H, 2-H), 6.46 (m, 2 H, 5-H), 6.64 (m, 2 H, 4-H), 7.44-7.59 (m, 5 H, phenyl); UV-vis (2-propanol-H_2O, 4:1 v/v) λ_{max} nm (log ϵ) 312 (3.82), 260 (3.70).

Iron(III) 5, 10, 15, 20-tetra(4'-N, N, N-trimethylanilinium) porphyrin (Fe-*p*-TMA)

Iron-para-trimethylanilinium porphyrin chloride (Fe-*p*-TMA) was prepared from the tetra(N,N,N-trimethyl-4-anilium) porphyrin tetrachloride purchase form Frontier Scientific. 124.5 mg free ligand were dissolved in 50 mL H_2O inside a two neck balloon and put under Argon atmosphere. Iron salt (ammonium iron(II) sulphate), was weight as 394.92 mg and it was added into the solution under Argon. Solution was degassed during 20 minutes before it was heated up to 85°C during 3 hours under Argon. After this time, reaction was stopped and leaved it to cooled down.

The obtained solution was washed with 10 equivalents NH_4PF_6 (205.38 mg) by Centrifugation at 20000 rpm during 20 minutes, and washed if necessary with more NH_4PF_6 solution until supernatant is clear. Last wash was performed with H_2O at 0°C. The obtained solution was leave to dry under vacuum overnight.

Anion exchange from PF_6 to Cl.

Product was dissolved in 5 mL solution acetone:chloroform (1:1) and centrifugated at 20000 rpm for 10 min. Supernatant is taken and 25 mL acetone are added. Solution is added to a balloon and leave it in agitation in ice bath. HCl was slowly added until a precipitated is observed. The solution was the centrifugated at 20000 rpm during 10 min. Product was then dissolved in the less amount of CH_3OH as possible (~2 mL) and excess of ethyl acetate was added until a dark red precipitate was observed. Final centrifugation was performed and product was leave to dry overnight under Argon atmosphere and vacuum.

Measurement and analysis

UV-Vis spectroscopy

UV-visible absorption measurements were done with an Agilent Technologies Cary 60. Typical spectral region ranged from 200-800 nm and the scan rate was 600 nm min^{-1}.

Solar light illumination

Newport LCS-100 solar simulator was used to mimic sunlight equipped with a 100 W Xenon lamp to produce a light corresponding to the standard AM 1.5G spectrum defined as the mean solar irradiance received by earth with a tilted angle of 38°.

The core of the photochemical cell is based on a quartz Suprasil 101-QS, 1x1 cm, 3.5 mL total volume cuvette from Hellma.

Schott long-pass filters were used to cut-off unwanted UV wavelength, both GG400 and GG420 were used in this thesis.

Fluorescence spectroscopy

Emission quenching measurements were conducted with a Cary Eclipse fluorescence spectrophotometer (Agilent Technologies), with the excitation wavelength set at 400 nm. A 1×1 cm quartz cell with four polished window equipped with screw cap was used four measurements. Oxygen was removed from solution by argon purge prior to measurement and was again purge for 5min between each addition of either catalyst or sacrificial electron donor.

Gas chromatography (GC) and mass coupled gas chromatography (GC-MS)

Gas chromatography analysis of gaseous headspace were performed with a Shimadzu GC-2010 Plus system equipped with a dielectric Barrier Discharge Ionization detector. H_2, CO and CH_4 production was quantitatively detected using a CP-CarboPlot P7 capillary column (25 m in length and 0.53 mm internal diameter). Temperature was held at 250°C for the detector and 30°C for the kakashi78oven. The carrier gas was helium flowing at 54.2 mL/min at constant pressure of 40 kPa. Injection was performed *via* a 100 µL gas-tight (Hamilton) syringe**.** Conditions allowed detection of H_2, O_2, N_2, CO, and CO_2. Calibration curves for O_2, N_2, H_2, CO, CH_4 and CO_2 were determined separately by injecting known quantities of pure gas.

GC-MS for detecting liquid products were obtained by a Shimadzu QP 20020 chromatograph equipped with a SH-Rtx-Wax column (Restek Technologies, 60 m in length and 0.25 µm of

diameter) and coupled to a mass spectrometer in positive ionization mode. The injector temperature was 230°C to allowed direct vaporization of liquid products. The carrier gas was helium with a constant flow of 53.1 mL min^{-1} with a pressure of 115.8 kPa. The temperature of the column followed a ramp from 70°C to 240°C with a rate of 10 °C min^{-1} to allow separation of products based on their boiling point. The ion source and the interface temperature of the mass spectrum was kept constant respectively at 200 and 250°C. Injection volume was 0.5 µL with a split ratio of 20.

Ionic chromatography (IC)

Ionic chromatography measurements were performed with a Thermo Scientific Dionex ICS-1100 system equipped with a Dionex ERS 500 electrolytically regenerated suppressor. All the samples were diluted 20 folds with ultrapure (MilliQ) water before analyzed through IC. Calibration curve for formate was determined separately by injecting known quantities of pure sample.

Standard electrochemical measurements

Cyclic voltammograms were obtained in a three-electrode cell by use of a Metrohm Autolab potentiostat interfaced with Nova software. The working electrode was a 3 mm diameter glassy carbon disk carefully polished with first 1 µm then 0.25 µm diamond paste (Epsil) then thoroughly rinsed in acetone before use. The counter electrode was a platinum wire and the reference electrode was an aqueous SCE electrode. All experiments were carried out either under argon or carbon dioxide atmosphere at room temperature. Ohmic drop was compensated through the positive feedback compensation method implemented in the instrument.

Homemade electro-assisted photochemical measurements were obtained in a homemade setup as described in Chapter 5. Reference electrode was Ag/AgCl leak free purchase from Alvatek. Working electrode were made from Toray Paper (Fischer Scientific TGP-H60). Cyclic voltammetry and controlled potential electrolysis were obtained using a Parstat 2273 potentiostat equipped with power source software.

Nuclear Magnetic Resonance (NMR) spectroscopy

^{1}H NMR spectrum were recorded on a Bruker Avance III 400-MHz spectrometer and were calibrated to the resonance peaks of the solvent used using Top-Spin software.

Résumé substantiel

Introduction

Depuis la fin du 19ème siècle, la concentration en dioxyde de carbone dans l'atmosphère n'a cessé d'augmenter pour atteindre aujourd'hui une concentration supérieure à 410 ppm.[1] Cette augmentation provoque un changement climatique qui ne peut être attribuée qu'à l'action de l'homme et non simplement à une variation cyclique entre différentes périodes glaciaires. La production d'énergie étant un domaine important de rejet de CO_2, il semble nécessaire d'inverser la logique actuelle faisant de CO_2 un déchet ultime pour le considérer comme un composé ressource pour la production d'énergie. Ceci permettrait de répondre, au moins en partie, aux besoins mondiaux en énergie renouvelable, fermant un cycle neutre en carbone. Cette préoccupation est au cœur du travail de thèse présenté dans ce manuscrit.

Grâce à plusieurs transferts d'électron et de proton, le CO_2 peut en effet être réduit en différents produits d'intérêt pour l'industrie et le secteur de l'énergie : le monoxyde de carbone (CO), l'acide formique (HCOOH), le formaldéhyde (HCHO), le méthanol (CH_3OH) et le méthane (CH_4). Parmi ces composés à 1 atome de carbone, les deux derniers (méthanol et méthane) sont particulièrement intéressants d'un point de vue énergétique. Tous deux peuvent en effet directement servir de carburant dans un générateur d'énergie comme un moteur à explosion. Cependant, il faut noter que le méthanol possède un pouvoir corrosif important et demande donc une modification profonde des matériaux du générateur ou du moteur afin de pouvoir être utilisé comme carburant. En revanche, le méthane est aujourd'hui un vecteur énergétique utilisé largement à l'échelle mondiale, pour des besoins industriels et domestiques. La transformation d'un véhicule à essence pour pouvoir utiliser le méthane consiste en une simple valve de pression.[2] De plus, le méthane (composé principal du gaz naturel) est le principal vecteur utilisé en 2021 pour le chauffage domestique, mais il est très majoritairement d'origine fossile même si la production de biogaz se développe. Développer un moyen de production renouvelable de méthane serait donc un moyen de participer à une production d'énergie neutre en carbone et ainsi de contribuer à limiter les émissions de CO_2.

La conversion du CO_2 en CH_4 nécessite un apport d'énergie important, énergie qui est « stockée » dans les liaisons chimiques. L'énergie solaire est la principale source d'énergie renouvelable sur Terre, avec quatre millions d'Exajoules (EJ) reçues par an sur l'ensemble du globe. On estime que 5000 EJ qui peuvent être captés, si l'on considère uniquement les terres émergées comme sites

potentiels de captage.[3] Avec environ 600 EJ de demande énergétique mondiale annuelle, l'énergie solaire est considérée aujourd'hui comme la seule source renouvelable permettant de répondre à toute ou partie de cette demande.

Le CO_2 est une petite molécule très stable de par sa géométrie linéaire qui stabilise ses différentes orbitales, et sa réduction demande donc une énergie importante. L'injection du premier électron, qui va permettre de plier la molécule et faciliter les transferts suivants, est le plus coûteux en énergie. Cette barrière d'activation peut être réduite par l'emploi d'un catalyseur qui permettra d'éviter la formation du radical $CO_2^{\bullet-}$ via la formation d'un adduit entre le CO_2 et le catalyseur en question. Parmi les nombreux catalyseurs envisageables pour la réduction du CO_2, nous nous sommes concentrés sur les catalyseurs moléculaires, et plus précisément des porphyrines de fer. Cette classe de molécule est bien connue et a été utilisée depuis les années 1980 pour la réduction électrochimique du CO_2 en CO.[4] Récemment, notre équipe du LEM a montré qu'une porphyrine fonctionnalisée avec des ligands trimethylanilinium (TMA) en position para sur les phényles permettait la production photochimique de méthane à partir de CO_2.[5] Les groupements TMA permettent une stabilisation par interaction coulombienne de l'adduit fer-CO_2 et leur caractère accepteur d'électrons permet d'avoir une surtension de catalyse plus faible qu'avec une porphyrine non fonctionnalisée.[6]

Dans un système photochimique, il est généralement nécessaire d'utiliser un photosensibilisateur, matériau ou molécule capable de capter le rayonnement lumineux et de le convertir en énergie par l'intermédiaire d'un électron promu dans un état excité. L'objectif est alors de transférer un ou plusieurs équivalents électroniques au catalyseur afin de le rendre actif pour la réduction du CO_2. Après ce transfert d'électron, le photosensibilisateur se trouve dans un état oxydé et il est régénéré par un transfert d'électron assuré par un donneur sacrificiel d'électrons. Ce processus de réduction du CO_2 peut être assistée d'une source extérieure de protons afin d'améliorer la catalyse, comme cela a déjà été montré en conditions électrochimiques. Nous avons défini, dans ce travail de thèse, un système standard pour nos expériences, composé de la porphyrine de fer modifiée (Fe-*p*-TMA) comme catalyseur, un photosensibilisateur à base d'iridium ($Ir(ppy)_3$), la triethylamine (TEA) donneur sacrificiel d'électrons et le trifluoroéthanol (TFE) comme source de protons.

L’objectif de cette thèse était de mieux comprendre le mécanisme réactionnel ainsi que les différents intermédiaires de la réduction photochimique du CO_2 en CH_4 grâce à ce système standard, afin de l’optimiser et potentiellement le développer à plus grande échelle.

Le premier chapitre de ce manuscrit présente le contexte général de production de méthane renouvelable ainsi que l’état de l’art concernant la réduction photochimique du CO_2, notamment à l’aide de catalyseur moléculaires.

Dans le second chapitre, différents composés sont étudiés comme intermédiaires potentiels entre le CO_2 et le CH_4.

Le troisième chapitre traite du remplacement du photosensibilisateur à base d’iridium par une molécule organique ainsi que son impact sur la catalyse.

Le quatrième chapitre aborde le rôle inattendu du dioxygène dans la réaction.

Enfin, le cinquième chapitre ouvre la voie à l’association entre l’électrochimie et la photochimie au sein du même système afin d’améliorer le rendement de la réaction et de permettre une analyse électrochimique du système.

Chapitre 2 - Intermédiaires potentiels dans la réduction du CO_2 en CH_4

En réduisant le CO_2 il est possible d’obtenir différentes molécules en fonction du nombre d’électrons (et de façon concomitante de protons) transférés : le monoxyde de carbone et l’acide formique avec deux électrons, le formaldéhyde avec quatre électrons, le méthanol avec six électrons et enfin le méthane lorsque le CO_2 est complétement réduit grâce à huit électrons. Le principal produit obtenu avec notre système standard est le CO, avec CH_4 et H_2 en produits secondaires. Il a été montré lors de travaux précédents que lorsque le CO_2 est remplacé par le CO comme réactif de départ, la production de CH_4 est augmentée, avec un nombre de cycles catalytiques (turnover number ou TON) passant de 31 à 87.[5] CO a ainsi été identifié comme un intermédiaire clé dans la réaction et le mécanisme réactionnel suivant a été proposé.

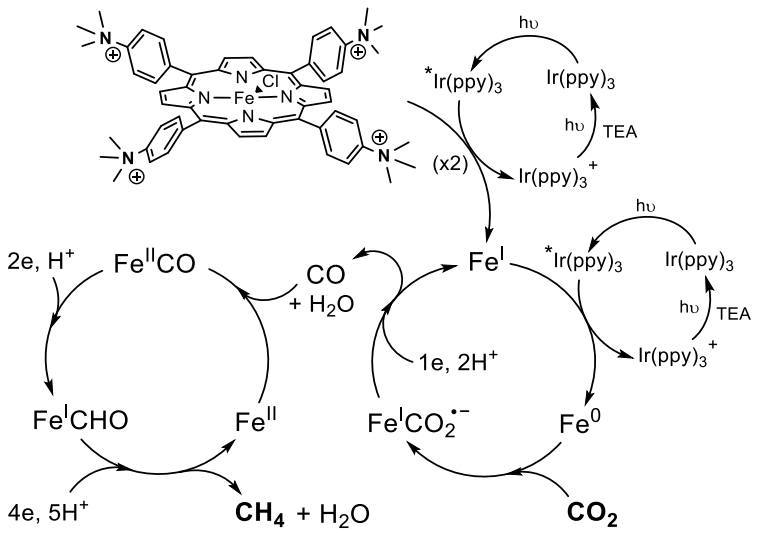

Figure 1 : Mécanisme proposé de la réduction photochimique du CO_2 par une porphyrine de fer.[5]

L'autre produit de réductions à deux électrons, l'acide formique, n'a pas été détecté en solution et lorsqu'il est introduit comme réactif de départ, sous forme d'ion formate et sous atmosphère inerte (argon), aucun produit de réduction n'a pu être détecté que ce soit en phase gazeuse ou en phase liquide, suggérant ainsi qu'il ne s'agit pas d'un intermédiaire dans notre réaction. Le même constat a pu être fait avec le formaldéhyde comme composé de départ, bien qu'il soit plus difficile de conclure clairement dans ce cas. En effet, cette molécule est instable en solution car elle polymérise rapidement et peut se trouver majoritairement sous forme paraformaldéhyde, plus difficile à réduire que le monomère. Néanmoins, aucun produit de réduction n'a là encore été détecté lorsque le formaldéhyde est utilisé comme substrat. En revanche, lorsque le méthanol est introduit dans la réaction comme composé de départ sous atmosphère inerte, du méthane a pu être observé en phase gazeuse après irradiation sous lumière visible. Afin de confirmer l'origine du méthane, nous avons réalisé des mesures avec du méthanol deutéré (CD_3OD), ce qui a conduit à l'observation de deux composés de réduction : du méthane triplement deutéré (CD_3H), suggérant que le dernier transfert de proton ne se fait pas avec une autre molécule de méthanol, sinon le composé CD_4 serait formé. Ces mesures montrent néanmoins que le méthane provient effectivement de la réduction du méthanol et que le dernier proton transféré vient probablement de l'autre source de protons présente en solution, à savoir le trifluoroéthanol. En revanche, dans la réaction originelle de réduction du CO_2, le méthanol n'a pas été détecté en phase liquide, ce qui semble l'exclure en tant qu'intermédiaire dans la réaction. Plusieurs hypothèses peuvent être formulées : soit le méthanol est produit mais est consommé rapidement, ne permettant pas son accumulation nécessaire à sa

détection, soit il ne s'agit simplement pas d'un intermédiaire mais notre système est toutefois suffisamment réducteur pour permettre sa réduction en méthane.

Chapitre 3 - Vers de nouveaux photosensibilisateurs organiques

Dans la plupart des réactions photochimiques utilisant des photosensibilisateurs moléculaires, ces derniers sont des complexes organométalliques contenant, pour la plupart, un métal précieux tel que l'iridium ou le ruthénium.[7] Afin de tendre vers un système plus durable et plus économique, il est nécessaire de remplacer ces éléments par une molécule ne contenant pas de métaux précieux, comme des molécules entièrement organiques. Parmi celles-ci, les coumarines sont des candidates intéressantes puisqu'elles présentent des propriétés physico-chimiques en adéquation avec le catalyseur employé, notamment une forte absorption dans le domaine du visible et un potentiel redox suffisamment négatif pour permettre la réduction du fer à l'état Fe^0, état actif pour la réduction du CO_2.[8] De plus, les coumarines présentent l'avantage d'être solubles dans l'eau permettant de se rapprocher encore plus d'un système durable. En partenariat avec l'équipe du Pr Pier Cozzi de l'Université de Bologne, Italie, nous avons utilisé une coumarine modifiée à la place du complexe d'iridium comme photosensibilisateur dans notre système standard. Après 68 h d'irradiation visible, du CO peut être détecté dans la phase gazeuse avec un TON de 97. Ainsi, le potentiel de réduction accessible par le catalyseur est suffisamment négatif pour déclencher la réduction du CO_2. Dans un second temps, le solvant organique a été remplacé par une solution aqueuse de bicarbonate de potassium. Malgré les différentes conditions utilisées, telles que le changement de pH, de donneur d'électrons, de donneur de protons, aucun produit ni gazeux ni liquide n'a pu être observé après irradiation. Cela peut s'expliquer par une interaction forte du solvant avec les groupements TMA chargés positivement du catalyseur, ou encore par le fait que la coumarine possède un temps de vie de l'état excité triplet faible (quelques nanosecondes), ne permettant pas un transfert d'électrons efficace par réaction bimoléculaire, donc limitée par la diffusion, entre son état excité et le catalyseur.

Une autre famille de molécules organiques, les phenoxazines, a également été étudiée comme photosensibilisateur. Ces molécules possèdent des propriétés physiques compatibles avec celles d'une sensibilisation efficace, à savoir une absorption importante de le domaine visible, un temps de vie d'état excité triplet long (plusieurs centaines de microsecondes), et un potentiel de réduction de l'état excité suffisamment négatif.[9] De plus, ce potentiel de réduction peut être modulé en

modifiant le ligand du cœur phenoxazine, nous permettant ainsi d'avoir accès à une variété importante de potentiels pour la réaction. De précédents travaux ont montré qu'au moins deux de ces molécules étaient des photosensibilisateurs efficaces pour réduire le catalyseur porphyrinique et donc de permettre la réduction du CO_2.[10] Nous avons donc étudié six dérivés phenoxazines préparés par l'équipe du Pr. G. Miyake à Colorado State University, Etats-Unis, dont le potentiel à l'état excité se situe entre -1,42 et -1,91 V *vs.* SCE. Bien qu'aucune corrélation n'a pu être mise en évidence entre ce potentiel à l'état excité et la quantité de CO produite (Figure 2, droite), une tendance très claire (Figure 2, gauche) a pu être observée entre le potentiel d'oxydation de ces molécules à l'état fondamental et la production de CO : plus ce potentiel est positif et plus le TON en CO croît. Ceci est en accord avec la théorie de Marcus qui veut que plus la différence de potentiel entre un couple donneur/accepteur d'électrons est importante, plus la réaction est favorisée. Le potentiel d'oxydation du donneur sacrificiel d'électrons utilisé ici, BIH, est de +0,33V *vs.* SCE, aussi plus celui du photosensibilisateur est haut, plus le transfert d'électron entre BIH et l'état oxydé de la phenoxazine est favorisée, permettant ainsi une régénération efficace du photosensibilisateur.

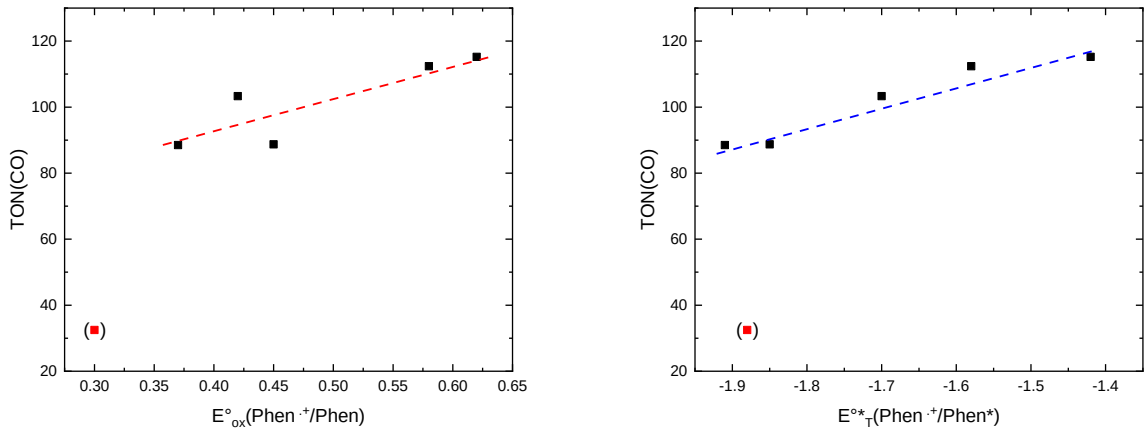

Figure 2 : TON de CO en fonction du potentiel d'oxydation (gauche) ou de réductions de l'état excité triplet (droite) des différentes phenoxazines utilisées

Ainsi, la réaction globale n'est pas régie par le potentiel de l'état excité du photosensibilisateur accessible pour activer le catalyseur, un potentiel plus réducteur ne permettant pas une production plus importante de CO comme ce qui était supposé. En revanche la régénération du photosensibilisateur dans son état fondamental semble être l'étape limitante de la réaction jusqu'à un certain point.

Chapitre 4 - L'effet inattendu du dioxygène dans la réduction du CO_2

Dans les travaux précédemment publiés par notre équipe, la cellule photochimique utilisée comme réacteur était composée d'une cellule en quartz sur laquelle était vissée un réservoir permettant d'obtenir un espace gazeux important pour les analyses par chromatographie. Cette cellule, qui présentait une étanchéité imparfaite a par la suite été modifiée pour n'être faite que d'une seule pièce de quartz, sans connecteur, afin d'assurer une bien meilleure étanchéité. Or, nous nous sommes aperçu que lorsque notre système standard était réalisé dans cette nouvelle cellule, il n'y avait pas formation de CH_4, contrairement à la cellule initiale. En introduisant volontairement de l'air (mélange O_2/N_2) dans la cellule étanche, initialement sous atmosphère de CO_2, du méthane a été obtenu après irradiation. Par la suite, des expériences ont montré que dans une cellule contenant du diazote, aucun produit de réduction n'était détecté alors que dans celle contenant du dioxygène, à la fois du CO et du CH_4 étaient présents. Ainsi, nous avons mis en évidence un rôle de O_2 dans le processus de formation du méthane. Plus la concentration en dioxygène dans la cellule était importante, plus la quantité de produits formés (CO et CH_4) l'était également. Afin d'expliquer ce phénomène, nous avons étudié l'effet de la présence de dioxygène sur les différents composés de notre système standard, individuellement. Tout d'abord, nous avons étudié la possible interaction avec le photosensibilisateur. En effet, O_2 est connu pour être un très bon quencher de fluorescence pouvant capter l'électron de l'état excité de $Ir(ppy)_3$ et générant un radical superoxyde. La structure du photosensibilisateur n'est cependant pas affectée par O_2 ni par le superoxyde, ce qui a été confirmé par des mesures de spectroscopie UV-Visible sous atmosphère d'oxygène. Par voltammétrie cyclique, la même signature électrochimique de $Ir(ppy)_3$ a été obtenue en présence et en absence d'oxygène confirmant de nouveau la stabilité de cette molécule en présence d'O_2. Nous avons donc formulé l'hypothèse que cet effet de O_2 n'impliquait pas le photosensibilisateur.

Les porphyrines de fer sont des complexes dont l'affinité avec O_2 est bien connue, et il est possible de générer des espèces hypervalentes telles que Fe^{III}O-O-H ou encore $Fe^{IV}O$ qui sont toutes les deux très réactives pour des réactions d'oxydation.11 La formation de dimères porphyriques liés par un pont oxo a également été mis en évidence en présence de dioxygène sur des porphyrines non fonctionnalisées. Il est donc en théorie possible qu'une de ces espèces soient présentes en solution lorsque O_2 est introduit dans le mélange réactionnel. En revanche, les conditions de réaction de notre système standard sont très défavorables à la création de telles espèces hypervalentes ou de pont oxo puisque ces deux espèces sont très sensibles à des pH acides et à un

potentiel fortement réducteur. Or notre système standard comprend 0.1 M de trifuoroethanol (un acide) et plusieurs espèces fortement réductrices sont produites en continu, notamment via le photosensibilisateur.[7] Ainsi, il est peu probable qu'une de ces espèces existent en solution, et elles n'ont pas d'ailleurs pu être identifiées par spectroscopie UV-Visible, même si leur implication ne peut être totalement exclue à ce stade.

Enfin, l'action de O_2 sur le donneur sacrificiel d'électrons a été évaluée. La triethylamine utilisée peut en s'oxyder en présence de dioxygène mais en l'absence de catalyseur cette réaction est lente et n'aura donc pas d'impact dans nos conditions. Ceci a été confirmé par des mesures de spectrométrie de masse d'une solution de TEA sous atmosphère O_2, après 21 h d'irradiation de lumière visible, puisque les données avant et après irradiation sont strictement identiques. En revanche, lorsque la solution réactionnelle standard est placée sous atmosphère O_2, de nombreux sous-produits peuvent être détectés par spectrométrie de masse, après irradiation de lumière visible. Parmi les molécules détectées, on retrouve des produits d'oxydation de la TEA tels que l'acétaldéhyde, le diethylhydroxylamine, le N,N-dimethylformamide ou encore l'acétamide. Ces produits sont habituellement générés par oxydation chimique de la TEA à l'aide de peroxyde d'hydrogène, un oxydant fort, ou encore d'acide nitrique. D'autres études ont montré que la TEA pouvait être oxydée photochimiquement en acétaldéhyde et en diethylamine sous irradiation UV.[12] A notre connaissance, il n'existe pas à l'heure actuelle de système photochimique capable de reproduire les effets d'une oxydation chimique en présence d'oxygène moléculaire et de lumière visible. Les mêmes produits d'oxydation ont été obtenus en l'absence de catalyseur ferrique suggérant que l'oxydation se fait via une molécule générée par interactions avec le photosensibilisateur. Comme mentionné précédemment, l'anion superoxyde peut être généré lorsqu'un électron de l'état excité du photosensibilisateur est transféré au dioxygène. Cette anion ayant un caractère réducteur, son interaction avec la TEA pour générer des produits d'oxydation est contre-intuitif. En revanche, il a été suggéré que, en présence de TEA, le superoxyde peut se protonner en radical hydroperoxyle $HO_2^{\bullet}$ possédant, lui, des propriétés fortement oxydantes.[13] Bien que l'action de ce radical n'a pas été mis en évidence dans l'oxydation de la TEA, elle peut être envisagée puisque le radical superoxyde est généré par le photosensibilisateur et qu'une importante source de protons est présente en solution (TFE). Enfin, lorsque la TEA est remplacée par l'acétaldéhyde en tant que donneur sacrificiel d'électrons en présence de O_2, de l'acide acétique a pu être détecté en phase liquide ce qui apporte une preuve supplémentaire de la présence d'une

réaction d'oxydation dans notre système, impliquant le dioxygène. Cette réaction d'oxydation photochimique de l'acétaldéhyde a déjà été rapportée dans la littérature, notamment en utilisant de l'oxyde de titane comme photocatalyseur, mais à notre connaissance aucun catalyseur moléculaire n'existe pour une telle oxydation dans des conditions ambiantes de température et de pression.14 Cette implication de O_2 dans notre réaction ne remet pas en cause les résultats précédemment publiés avec ce même système, puisqu'une attention particulière a été apportée au marquage isotopique, prouvant que les produits détectés, à savoir le CO et le CH_4, proviennent tous les deux de la réduction du CO_2, sans aucune ambiguïté. Cependant, d'autres études restent à mener pour élucider clairement le rôle de O_2 dans la conversion de CO_2 en CH_4.

Chapitre 5 - Réduction photochimique électro-assistée du CO_2

Comme nous l'avons vu, les réactions photochimiques homogènes requièrent la présence d'un donneur sacrificiel d'électrons afin de régénérer le photosensibilisateur. Comme son nom l'indique, ce donneur est sacrificiel, et donc la réaction globale est limitée par sa quantité initiale puisqu'une fois consommé, le photosensibilisateur ne peut plus être régénéré. Nous proposons ici de développer un système permettant de combiner électrochimie et photochimie pour répondre à cette problématique. Pour ce faire, nous avons développé un montage électrochimique pouvant s'adapter à la cellule photochimique utilisé précédemment. Ce montage se compose de trois électrodes : une électrode de travail en papier carbone, permettant d'avoir une surface spécifique importante, de l'ordre de 2 cm² ; une électrode de référence Ag/AgCl suffisamment fine pour être intégrée au système ; et une contre-électrode composée d'une grille de platine, séparé du compartiment de travail par un pont.

La TEA, donneur d'électrons utilisée précédemment, ne peut être utilisée ici puisque son oxydation est fortement irréversible, ce qui empêche sa régénération électrochimique. Au contraire, le tétrathiafulvalène (TTF) est une molécule capable de transférer deux électrons et dont les deux oxydations sont réversibles électrochimiquement. Cette molécule possède un potentiel de réduction plus négatif que la TEA (+0.32 V *vs.* SCE contre +0.96 V *vs.* SCE, respectivement) proche du potentiel de réduction de l'état excité de Ir(ppy)3 (+0.31 V *vs.* SCE) et un transfert d'électron efficace a pu être mis en évidence entre cet état excité et le TTF via des mesures de quenching de fluorescence. Photochimiquement, lorsque le TTF remplace la TEA comme donneur d'électrons, et que les autres paramètres sont inchangés, du CO a pu être détecté dans la phase gazeuse avec un

TON de 35 pour 21 h d'irradiation. TTF a donc été retenu comme donneur d'électron pour tester le montage photochimique électro-assistée. La présence d'une électrode permet de maintenir un potentiel appliqué durant toute la durée de l'expérience, et ainsi de régénérer le donneur en lui transférant un électron. Un potentiel constant, correspondant au potentiel de réduction du TTF oxydé a donc été appliqué pendant toute la durée de la réaction photochimique. Aucun produit de réduction du CO_2 n'a pu être détecté dans ce cas. Cela peut venir du fait que le TTF est systématiquement réduit à l'état neutre à l'électrode sans avoir le temps de diffuser pour transférer son électron au photosensibilisateur. Pour pallier à ce problème, nous avons appliqué des impulsions de potentiel d'une durée de 15 min toute les 3 heures. Une production de CO a alors été observée avec un TON de 97 après 15 h d'irradiation, multipliant donc quasiment par trois la quantité de CO produite par rapport au processus purement photochimique.

Ce montage électro/photochimique peut également nous permettre de mieux comprendre le mécanisme de la réaction et notamment d'identifier les différentes étapes et intermédiaires. Parmi ces derniers, nous savons que l'adduit $Fe^{II}CO$ doit être généré pour pouvoir, dans un second temps, subir une série de transferts d'électron et de proton menant à la production de méthane.5 Puisque chaque état d'oxydation et chaque adduit de la porphyrine de fer possèdent un spectre d'absorption spécifique, il est possible de les détecter par spectroscopie UV-Visible. En utilisant notre montage électro/photochimique, nous avons appliqué un potentiel correspondant à la réduction du Fe^{III} en Fe^{II}, sous atmosphère de CO_2, et la réaction a été suivie par spectroscopie UV-Visible. Un déplacement du maximum d'absorption correspondant à la signature du Fe^{II} a pu être observé. Lorsque CO a été introduit à la place de CO_2, le maximum d'absorption s'est de nouveau déplacé pour correspondre à la signature spectrale de l'adduit $Fe^{II}CO$. Il est donc possible, grâce à ce nouveau dispositif, de générer l'adduit $Fe^{II}CO$ en quantité suffisante pour être détecté par spectroscopie UV-Visible, en conservant la géométrie de la cellule photochimique initiale. En conditions catalytiques, sous atmosphère de CO_2, en présence de BIH comme donneur d'électrons, le potentiel correspondant à la formation du Fe^{II} a été ensuite appliqué pendant 15 min toutes les 3 h tout en irradiant la cellule de lumière visible. L'analyse de la phase gazeuse a révélé l'absence de méthane, même si du CO était présent. L'absence de méthane semble indiquer que contrairement à ce qui avait été proposé précédemment, la formation de l'adduit $Fe^{II}CO$ n'est pas davantage l'étape déterminante de la réaction de réduction du CO_2 en CH_4 par voie photochimique.

Conclusion

Ce travail de thèse, réalisé sur la réduction photochimique du CO_2 en méthane, a permis de poursuivre et approfondir des travaux précédents afin de mieux comprendre le mécanisme global de la réaction. La porphyrine de fer utilisée comme catalyseur s'est révélée capable de réduire le méthanol en méthane photochimiquement, ce qui en fait un intermédiaire potentiel menant à CH_4, bien qu'il n'ait pas été détecté in situ. Le rôle inattendu du dioxygène présent en solution a été mis en évidence puisque sa présence est nécessaire à la génération de méthane. Sous atmosphère O_2, notre système standard est capable d'oxyder la triethylamine en différents produits qui ne sont obtenus jusqu'alors que dans des conditions d'oxydation chimique. Ceci laisse à penser que c'est par l'intermédiaire du donneur sacrificiel d'électrons que O_2 intervient, les autres composés du système ayant été exclus par différentes mesures. Enfin un montage couplant électrochimie et photochimie a été développé, ouvrant ainsi la voie à une analyse plus détaillés des différents composés et intermédiaires réactionnels formés lors de la réduction photochimique du CO_2 en conditions homogènes.

1. NOAA Laboratory, https://gml.noaa.gov/ccgg/trends.
2. J. C.lngamells and R. H. Lindquist, *Society of Automotive Engineers*, 1975, 15.
3. E. Kabir, P. Kumar, S. Kumar, A. A. Adelodun and K.-H. Kim, *eRnew. Sust. Energ. Rev.*, 2018, 82, 894-900.
4. I. Bhugun, D. Lexa and J.-M. Savéant, *J. Am. Chem. Soc.*, 1996, 118, 1769-1776.
5. H. Rao, L. C. Schmidt, J. Bonin and M. Robert, *Nature*, 2017, 548, 74-77.
6. I. Azcarate, C. Costentin, M. Robert and J. M. Saveant, *J. Am. Chem. Soc*., 2016, 138, 16639-16644.
7. C. K. Prier, D. A. Rankic and D. W. MacMillan, *Chem. Rev.*, 2013, 113, 5322-5363.
8. A. Gualandi, G. Rodeghiero, E. Della Rocca, F. Bertoni, M. Marchini, R. Perciaccante, T. P. Jansen, P. Ceroni and P. G. Cozzi, *Chem. Commun.*, 2018, 54, 10044-10047.
9. Y. Du, H. Yang, R. M. Pearson, N. H. Damrauer, C.-H. Lim, S. M. Sartor, M. D. Ryan and a. G. M. Miyake, *Chem. Eur. J.*, 2017, 23, 10962–10968.
10. H. Rao, C. H. Lim, J. Bonin, G. M. Miyake and M. Robert, *J. Am. Chem. Soc.*, 2018, 140, 17830-17834.
11. N. Kostopoulos, C. Achaibou, J. M. Noel, F. Kanoufi, M. Robert, C. Fave and E. Anxolabehere-Mallart, *Inorg. Chem.*, 2020, 59, 11577-11583.
12. T. Hiroshi, Y. Teruo and T. Hiroo, *Bull. Chem. Soc. Jpn.*, 1973, 46, 3051-3055.
13. R. S. Davidson and K. R. Trethewey, *J. Chem. Soc., Perkin Trans.* 2, 1977,
14. R. M. Mohamed, D. W. Bahnemann, A. S. Basaleh and R. H. Qadah, *Appl. Nanosci.*, 2019, 10, 931-939.